Evaluation of Antennas Location on Trains for Mobile Communications

Tomás Martim Ferreira Duarte

Thesis to obtain the Master of Science Degree in

Electrical and Computer Engineering

Supervisor: Prof. Luís Manuel de Jesus Sousa Correia

Examination Committee

Chairperson: Prof. José Eduardo Charters Ribeiro da Cunha Sanguino

Supervisor: Prof. Luís Manuel de Jesus Sousa Correia

Members of Committee: Prof. Custódio José de Oliveira Peixeiro

: Eng. Fernando Manuel Lopes Santana

November 2019

I declare that this document is an original work of my own authorship and that it fulfils all the requirements of the Code of Conduct and Good Practices of the *Universidade de Lisboa*.

To my loved ones

Acknowledgements

First and above all, I would especially like to express my deepest appreciation to my supervisor, Professor Luís M. Correia, for allowing me to develop this work. During the last months, I have greatly benefited from his advice, his insightful comments and suggestions, and his extensive knowledge on mobile communications. While it was a privilege to develop a deep understanding of one of the most dynamic areas of technology, working with a brilliant mentor as Professor Correia gave me plenty of other skills which, I am sure, will be key to my future success.

I would like to express my gratitude to Thales, not only for the opportunity of studying a real-life engineering problem and adding value to its business, but particularly to some of its collaborators, Eng. Fernando Santana, Eng. Nuno Frigolet, Eng. Sérgio Rodrigues and others who greatly improved my knowledge on railway communications and gave me constructive comments. It is my vision that Engineering should be at the service of society and industry, hence, I am proud that this has happened with this work.

I have also greatly benefited from being part of GROW (Group for Research On Wireless), where I was kindly and warmly received. Both the interesting projects developed and under development, and the combined expertise of all its members provide a distinctive environment where one has the possibility to improve, grow its skills and broaden its view on the future of mobile communications. A special thanks to Magali Correia and Sérgio Domingues, my fellow master thesis colleagues, is due for their support and solidarity during the course of this work.

I also thank Professor Custódio Peixeiro and Eng. Nuno Silva for their collaboration in obtaining the necessary software for the simulation procedures on this work.

I thank Frederico Guita for his insights and useful help on developing the 3D models on AutoCAD.

To all my friends who accompanied me on this journey, such as Miguel Loff Barreto, Inês Paulino, Francisco Santos, Inês Mendes, Afonso Costa, Luís Fontes Cunha and many others. A special thanks to Zé Figueiredo, for always believing in me (sometimes more than myself), and for his support.

Finally, I owe my deepest gratitude to my family. To my mother, for showing me that the sky is the limit. To my father, for his role model and his interest and expertise in Engineering. To my brothers Lourenço and Gabriel, for their joy that cheers me up all the times. And to my grandparents, for their example and support. I am proud of who I am today, and this legacy is yours too.

Abstract

The main objective of this work was to analyse the performance of antennas on trains for mobile communications, using dedicated communication systems. The work included the design of several 3D models using AutoCAD, as well as the use of antenna models based on real equipment used in actual systems. The resulting combination of the train and antenna models was then used in the simulation of the propagation, through the CST Microwave Studio software, which takes into account antennas parameters and physical constraints imposed by the train roof. The main aspects considered concerning the placement of the antenna were roof related, essentially the longitudinal grooves, as well as the height of the antennas to the roof. The systems tested were TETRA, GSM-R, LTE-R and BBRS, with frequencies ranging from 400 MHz to 5.9 GHz. The study of the grooves impact allowed to conclude the higher frequencies suffer more severe impacts, with reductions in gain that can reach 14 dB for some angles, which was expected due to the wavelength being closer to the groove dimensions. At 400 MHz, it is recommended that the antenna is placed in close proximity to the roof, at 1 cm, while for higher frequencies the performance is improved with the increase in height to 20 cm. Depending on system requirements, a safety communications margin is recommended for some of the systems, ranging from 5 dB to 14 dB, taking into account if critical communications rely on the system.

Keywords

Railway communications, Antenna placement, Longitudinal grooves, Elevated plane.

Resumo

O objetivo desta tese foi proceder a uma análise do desempenho de antenas instaladas em comboios para comunicações móveis ferroviárias, utilizando redes móveis dedicadas. Este trabalho incluiu o desenvolvimento de vários modelos 3D do teto de um comboio, bem como o uso de modelos de antenas baseados em equipamentos reais utilizados em sistemas em funcionamento. A combinação resultante dos modelos de comboio e das antenas foi então utilizada para simular a propagação dos sinais, através do software CST Microwave Studio, que tem em consideração os parâmetros das antenas e as restrições físicas impostas pelo modelo. Os principais aspetos considerados no modelo do comboio foram as estrias longitudinais e a altura das antenas ao teto. Foram testados sistemas TETRA, GSM-R, LTE-R e BBRS, com frequências entre 400 MHz e 5.9 GHz. O estudo dos impactos das estrias permitiu concluir que as frequências mais altas sofrem maiores impactos, com reduções de ganho que atingem 14 dB em alguns ângulos, o que era esperado visto o comprimento de onda nestas frequências se situar próximo das dimensões das estrias. A 400 MHz, recomenda-se que a antena seja instalada próxima do teto do comboio, a 1 cm, enquanto que para frequências superiores o desempenho é melhorado com o aumento da altura da antena para 20 cm. Dependendo dos requisitos do sistema, recomenda-se uma margem de segurança nas comunicações para alguns dos sistemas, variando entre 5 e 14 dB, tendo em conta se há comunicações críticas a ter lugar.

Palavras-chave

Comunicações ferroviárias, Posicionamento de antenas, Estrias longitudinais, Plano terra elevado.

Table of Contents

List of Figures

List of Tables

List of Acronyms

1G	First Generation of Mobile Communications Systems
2G	Second Generation of Mobile Communications Systems
3G	Third Generation of Mobile Communications Systems
3GPP	Third Generation Partnership Project
4G	Fourth Generation of Mobile Communications Systems
5G	Fifth Generation of Mobile Communications Systems
AI	Air Interface
ARP	Allocation and Retention Priority
AuC	Authentication Centre
AV	Autonomous Vehicle
BBRS	Broad Band Radio System
BCC	Backup Control Centre
BER	Bit Error Rate
BS	Base Station
BSC	Base Station Controller
BSS	Base Station Subsystem
BTS	Base Transceiver Station
CAD	Computer-Aided Design
CDMA	Code-Division Multiple Access
CSFB	Circuit-Switched Fall Back
CST	Computer Simulation Technology
D2D	Device-to-Device
DL	Downlink
DMO	Direct Mode Operation
E-UTRAN	Evolved Universal Terrestrial Radio Access Network
EDGE	Enhanced Data rates for GSM Evolution
EIR	Equipment Identity Register
EIRENE	European Integrated Radio Enhanced Network
eMBMS	Evolved Multimedia Broadcast Multicast Services
eMLPP	Enhanced Multilevel Precedence and Pre-emption Service
EPC	Evolved Packet Core
ERTMS	European Rail Traffic Management System
ETCS	European Train Control System
ETSI	European Telecom Standards Institute

EU	European Union
FA	Functional Addressing
FD	Full Duplexing
FDD	Frequency Division Duplex
FEM	Finite Element Method
FIT	Finite Integration Technique
FNBW	First-Null Beamwidth
FRMTS	Future Railway Mobile Telecommunication System
FTBR	Front-To-Back Ratio
GCR	Group Call Register
GDP	Gross Domestic Product
GHG	Greenhouse Gases
GMSK	Gaussian Minimum Shift Keying
GPRS	General Packet Radio Service
GPS	Global Positioning System
GSM	Global System for Mobile Communications
GSM-R	Global System for Mobile Communications – Railways
HLR	Home Location Register
HPBW	Half-Power Beam Width
HSDPA	High-Speed Downlink Packet Access
HSPA+	Evolved High Speed Packet Access
HSS	Home Subscriber Server
HSUPA	High-Speed Uplink Packet Access
IMEI	International Mobile Equipment Identity
IMS	IP Multimedia Subsystem
IMT-2000	International Mobile Telephone 2000
IoT	Internet of Things
IP	Internet Protocol
IST	Instituto Superior Técnico
ITU	International Telecommunications Union
LDA	Location-Dependent Addressing
LTE	Long-Term Evolution
LTE-R	Long-Term Evolution – Railways
M2M	Machine-to-Machine
MIMO	Multiple-Input Multiple-Output
MLRL	Mesh Line Ratio Limit
MME	Mobility Management Entity
MMS	Multimedia Messaging Services

MORANE	Mobile Radio for Railway Networks in Europe
MS	Mobile Station
MSC	Mobile Switching Centre
MT	Mobile Terminals
NA	Not Applicable
NMS	Network Management System
NOMA	Non-Orthogonal Multiple Access
NSS	Network Switching Subsystem
OBU	Onboard Units
OCC	Operation Control Centre
OFDM	Orthogonal Frequency Division Multiplex
OMC	Operations and Maintenance Centre
OSS	Operational Support System
PAMR	Public Access Mobile Radio
PCRF	Policy and Charging Rules Function
PEC	Perfect Electric Conductor
PML	Perfectly Matched Layer
PMR	Private Mobile Radio
PoC	Push-to-talk Over Cellular
PPC	Pre-emptive Priority Call
QoS	Quality of Service
RB	Resource Block
RBC	Radio Block Centre
REC	Railway Emergency Call
RNC	Radio Network Controllers
RSSB	Rail Safety and Standards Board
RSSI	Radio Signal Strength Indication
SC-FDMA	Single Carrier Frequency Division Multiple Access
SDS	Short Data Service
SG-W	Serving Gateway
SIP	Session Initiation Protocol
SLL	Side Lobe Level
SMS	Short Message Service
SNR	Signal-to-Noise Ratio
SSI	Short Subscriber Identity
TDD	Time Division Duplex
TDMA	Time-Division Multiple Access
TETRA	Terrestrial Trunked Radio
TLM	Transmission-Line Matrix
TMO	Trunked Mode Operation

TRAU	Transcoder Rate Adaptation Unit
UIC	Union Internationale des Chemins de Fer
UL	Uplink
UMTS	Universal Mobile Telecommunication Service
UN	United Nations
USIM	Universal Mobile Telecommunications Subscriber Identity Module
VBS	Voice Broadcast Calls
VGCS	Voice Group Call Service
VLR	Visitor Location Register
VoLTE	Voice over LTE
VR	Virtual Reality
VSWR	Voltage Standing Wave Ratio

List of Symbols

α_{3dB}	Half-Power Beam Width
Γ	Reflection coefficient
$\Delta G(\theta,\phi)$	Gain difference in the point defined by coordinates θ and ϕ
$\overline{\Delta G(\theta,\phi)}$	Average gain difference
η	Intrinsic impedance of the medium
Θ_{3dB}	Interval of angles in which at least half of the power for the main lobe is radiated on the system
θ	Angle between the positive half of Z-axis and the observation point
θ_{max}	Main lobe direction
$\theta_{3dB-/+}$	Minimum/maximum angle in which the main lobe radiates with at least half of the maximum gain of the radiation pattern
λ	Wavelength
φ	Angle between the positive half of X-axis and the observation point projected on XOY plane
$D(\theta,\varphi)$	Directivity
D_{SBF}	Smallest box face diagonal in the meshing grid
d_g	Distance between the longitudinal grooves
$E(r,\theta,\varphi)$	Far zone electric field intensity
E_θ^V	Electric field for a vertical dipole at the θ direction
E_θ^0	Far zone electric field intensity at the θ direction
E_φ^0	Far zone electric field intensity at the φ direction
E_{back}	Electric field of the backward lobe
E_{max}	Maximum electric field of the main lobe
E_{SL}	Maximum electric field of the first side lobe
G	Gain (IEEE)
$G_{realised}$	Realised gain
h	Antenna height
h_p	Elevated ground plane height
h_g	Longitudinal groove height
I_0	Maximum current fed to the antenna
k	Free space wave number
l	Largest geometrical dimension of the antenna
l_p	Elevated ground plane length

M_{LL}	Lower mesh limit
M_{LW}	Mesh lines per wavelength
M_{MS}	Maximum mesh step
N_L^V	Number of lobes of the vertical dipole
P_{in}	Input power
P_{rad}	Total radiated power
r	Distance between the antenna and the observation point
S_{LL}	Side lobe level
w_p	Elevated ground plane width
w_g	Longitudinal groove width
Z_0	Characteristic impedance of the transmission line
Z_{in}	Antenna input impedance

List of Software

Autodesk AutoCAD 2019 for Mac	Model development
CST Microwave Studio	Electromagnetic simulation
Microsoft Excel for Mac	Results post-processing, calculations
Microsoft PowerPoint for Mac	Image editing
Microsoft Word for Mac	Word processing
Paintbrush	Image editing
VMware Fusion 8	Virtual machine monitor

Chapter 1

Introduction

This chapter gives a brief overview of the work, detailing the evolution of communication technology, explaining the relevance of train transportation in modern societies, highlighting why mobile communication systems play a crucial role in railway networks and how train antennas' location is of utmost importance for performance. At the end, the work structure is provided.

1.1 Railway transportation and mobile communications

Telecommunication essentially consists of any transmission or reception of signs, signals, writings, images or sounds by wire, radio, optical or other electromagnetic systems [ITUT16]. Playing a crucial role in modern societies, telecommunication systems have been developing throughout the centuries and are now part of the everyday life of the vast majority of the world's growing population.

During the 1980s, a growing trend for digital communications was the lead for the development of a digital network with a maximum data rate of 2.4 kbps, following previous analogue systems, such as the First Generation of Mobile Communication System (1G). In the early 1990s, the Second Generation of Mobile Communications Systems (2G) was launched with increased security – featuring encrypted communications – and, in addition to voice, new services, such as text messages know as Short Message Service (SMS) and Multimedia Messaging Service (MMS). Several standards emerged from 2G, the most common being the Global System for Mobile Communications (GSM), which was the first widely adopted standard, allowing for international roaming to become universal. GSM uses Time Division Multiple Access (TDMA), allowing up to 8 calls per radio channel in the 900 and 1800 MHz bands, initially using only circuit switching, being capable of data transmission up to 9.6 kbps [Corr18].

As of today, GSM is still the global standard for mobile communications, currently used in 193 countries. Since it was first introduced, the GSM technology suffered major improvements, such as the General Packet Radio Service extension (GPRS), that allows GSM to operate in both the circuit- and packet-switching domains. Later, GPRS networks started using the 8-PSK modulation, an evolution called Enhanced Data rates for GSM Evolution (EDGE), improving data rates up to 59.2 kbps [MiKu15].

The next big step in mobile communications was called the Third Generation of Mobile Communications Systems (3G), being the evolution of previous 2G-systems, with backwards compatibility, but featuring a wide range of worldwide standards defined by the International Telecommunications Union (ITU), called International Mobile Telephone 2000 Standard (IMT-2000). The aim was to finally allow seamless roaming across the world [ITUT11].

By this time, the Third Generation Partnership Project (3GPP) was created, as an effort of several standards organisations, and from it resulted the Universal Mobile Telecommunication Service (UMTS), with up to 284 kbps of downlink (DL) data rate. In this period (early 2000s), the internet was aggressively expanding, and in Europe, UMTS led the 3G transition [MiKu15]. Several protocols were developed for the initial 3G architecture, such as the High-Speed Downlink Packet Access (HSDPA), the High-Speed Uplink Packet Access (HSUPA), or the Evolved High-Speed Packet Access (HSPA+). This last one was introduced in 3GPP Release 7, and was further developed, reaching peak DL data rates up to 40 Mbps, and uplink (UL) ones over 11 Mbps [GGBS09].

The increasing demand of higher data rates for the new mobile applications, such as Multimedia Online Gaming, mobile TV, Web 2.0 or streaming content, has motivated 3GPP to work on a new standard in mobile network technology, which was called the Long-Term Evolution (LTE). LTE standards set aggressive performance requirements that would allow co-existence with older technologies while significantly improving data rates: peak data rate for DL was required to reach 100 Mbps, with UL reaching 50 Mbps. LTE supports only packet-switching, therefore requiring carriers to re-engineer their voice call network [LTEM07]. In 2018, more than 35% of the world's mobile users rely on 4G LTE as their primary technology, a ratio that is expected to double, reaching over 60% by 2025 [GSMA17].

The push for data rates of the order of many Gbps has been increasing due to the aggressive growth in video traffic and ultra-high definition video streaming, as well as a rapid expansion of Internet of Things (IoT) applications. To answer these needs, the next generation, called Fifth Generation of Mobile Communications Systems (5G), is expected to be deployed around 2020 featuring new physical layer technologies such as widely deployed Multiple-Input Multiple-Output (MIMO), Non-Orthogonal Multiple Access (NOMA) at a later stage, Full Duplexing (FD), Device-to-Device (D2D) and Machine-to-Machine (M2M) communications.

5G is expected to reach peak data rates of 10 Gbps, with very low latency, high reliability, relaying functionalities between users and better coverage. This new standard will bring improvements in a wide range of technologies that rely on mobile, such as Virtual Reality (VR), Smart City applications, emergency communications, cell automation, Autonomous Vehicle (AV) control and High-Speed train communications, with the system being developed to work at speeds up to 500 km/h [TELC18].

All this evolution was fuelled by the ever-growing popularity of mobile technology. During 2017 the number of unique mobile phone subscribers peaked at 5 billion. It is expected that by 2020 almost 75% of the world's population will be connected by phone. Mobile has a greater reach than any other technology, and devices are increasingly relying on data as over 80% of terminals are used to access mobile internet [GSMA17]. Mobile communications are hence crucial for future technological evolutions, and the railway industry is no exception, as it will be shown.

The transport sector is one of the main contributors to Greenhouse Gases (GHG), mainly due to its 90% dependency on oil-powered vehicles. Hence, in order to improve efficiency of transport systems in Europe, the European Union (EU) Mobility and Transport committee has set a number of goals to achieve by 2050: to cut road freight, shifting to efficient rail corridors; to complete a European high-speed rail network; to connect all core airports and seaports to the rail network [ECMT11].

In fact, in the last decade, passenger rail transport in Europe has been recording a year-on-year market share increase over other means of transportation, with an average 1.5% annual growth on demand. With more than 9 billion train trips taking place annually across the EU, efficient networks are critical to achieve the aforementioned goals [VoLo17]. Railways were among the first industries to rely on communication technology for its operation. Throughout the years, trains adapted to innovative technologies and even led to the development of dedicated networks to fulfil the industry needs.

In fact, by the end of the XX century, member states of the EU decided to develop a dedicated European Rail Traffic Management System (ERTMS) for rail standards all across Europe, assuring railways business competitiveness and operational efficiency. As a result, 32 countries partnered with the worldwide railway organisation, the Union Internationale des Chemins de Fer (UIC), on the specification of a European standard for train control and communication systems. The goal was to eliminate conflicting rail operation rules and to define common homologation standards regarding traffic organisation, rail gauge, electrification systems and communication systems.

The ERTMS project was also developed by industry players, as it was fundamental to assure common standards in the different countries' networks but also interoperability among equipment from different suppliers [ERTM18a]. Key industry manufacturers signed several Memorandum of Understandings from 2005 to 2016, on the cooperation for the deployment of the ERTMS and stating their long-term commitment to the project [ERTM18d]. ERTMS features several sub-standards, from which the most relevant for this work is GSM-R: a radio system designed to provide voice and data communications between the track and the train. This technology was developed based on regular GSM, with the inherent economies of scale of such decision, but has specific frequencies [GSMR11]. GSM-R specifications were finalised by 2000, as a result of the European Integrated Radio Enhanced Network (EIRENE) and the Mobile Radio for Railway Networks in Europe (MORANE) protocols. The main goal for developing these standards – an initiative under the ERTMS project – was to facilitate the interoperability between different countries, allowing for a true European-scale rail network [GSMR18].

Operation of GSM-R (and other similar systems) to rail communications takes place just like regular GSM networks: trains are the moving users, featuring antennas on rolling stock's roof, which communicate with base station masts placed close to the railway. These are featured with highly directional antennas to cover only track areas, reducing interference.

As GSM-R became the world standard for train communications, Terrestrial Trunked Radio (TETRA), another private mobile communication network, has become popular with underground rail services (subway, tramway systems), while it is also commonly used by government agencies and emergency services. TETRA relies on lower frequencies, which allow for longer range cutting infrastructure costs (less equipment needed to assure same coverage). As a drawback, data transfer achieves a lower data rate. TETRA network architecture was first developed by ETSI and standardised with its Release 1, published in 1996. Release 2 was issued by ETSI circa 2005, answering the need to enhance technologies to better satisfy user requirements and ensure longevity [ETSI07].

BBRS, on the other hand, is a mobile communication solution provided by Thales and other integrator companies, with the main goal of allowing transmission and reception of data between railway infrastructures and the rolling stock. In opposition to other systems, BBRS is focused on data transmission from its core, and therefore is the best suited solution to data transmission of non-critical management systems such as Closed-Circuit Television (CCTV) and others [THAL18].

Just like mobile subscribers, railway operators are also in need of higher data rates and more capacity for train communications. Therefore, although GSM-R is expected to remain operational at least until 2030 [HUAW15], it is slowly being replaced by similar version of LTE networks: LTE-R. Some countries have already deployed pioneer LTE-R networks, such as China and Korea, but the architecture is not standardised by ETSI yet. Industry groups, standards organisations and operators have been partnering to reach agreement on the specifications for LTE [KRNA18], as UIC officially launched the Future Railway Mobile Telecommunication System (FRMTS) project in 2013 [FFCa16].

1.2 Motivation

The increasing complexity of safety and control systems in railways, combined with the desire to provide more services to passengers, has created the need in the rail industry for the proper development of an onboard connected environment. As said before, this has been made possible by using dedicated networks, such as TETRA and GSM-R, featuring rolling stock mounted antennas and trackside antennas, which work as Base Stations (BS) for these systems, receiving operational and locational data from trains, relaying this information to the control centre. Placed at regular intervals, the goal is to provide a continuous wireless link between train and the control centre.

Rolling stock mounted antennas are the Mobile Terminals (MT), as they move with the train. They are expected to send data regarding speed, operator awareness, brake and engine performance, and sometimes security services, such as real-time video surveillance of passenger carriages [MPAN15]. Typically, antennas on trains are mounted on front cars' roofs (for example locomotives), as it can be seen in Figure 1.1, in order to facilitate the Line of Sight path to the BS.

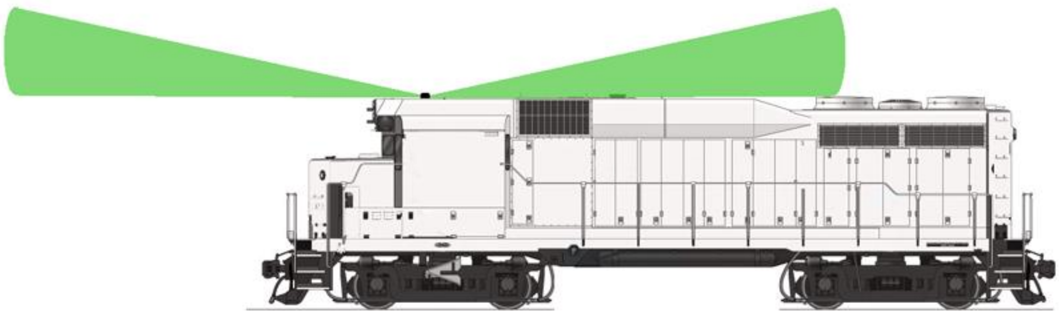

Figure 1.1 5 GHz Bi-Directional Antenna Single Feed (extracted from [MPAN17]).

The standardisation of internet connectivity for passenger Wi-Fi and the increasing digitalisation of the rail industry makes antenna performance a critical matter for train to ground connectivity. As future technologies will probably rely on both lower and higher frequencies than traditional radio systems, and since data rate needs will for sure increase, efficient rooftop antenna placing is a crucial problem that needs to be addressed. The increasing popularity of high-speed networks, with speeds that can reach 500 km/h, also imply that railway communications must be capable to adapt to this increase in speed.

As rolling stock is being fitted with a growing number of antennas to support customer and operational communications, the physical size constraints of the rooftop mean that antennas are often installed in close proximity of other train equipment and even other antennas. Interference and disturbance of Line of Sight paths due to absorption, reflection or multi-path distortions give rise to technical conflicts that have the potential to limit the performance of the radio system [Darl17].

The goal of this work is to analyse the performance of antennas mounted on trains for mobile communications, evaluating the influence of their position on the train roof, bearing in mind other relevant factors affecting performance. Roof design and additional equipment in proximity to the antenna (such as A/C units) are some of the factors analysed. Several common antennas in the industry are tested using simulation software Computer Simulation Technology (CST) Microwave Studio.

The majority of previous works on performance of antennas mounted in vehicles never focused specifically on train-fitted antennas; having explained the crucial importance of antenna placing for performance, this work intends to clearly develop a model for design criteria for the deployment of antennas on trains, taking the antenna position within the train into account. This work focused on TETRA, GSM-R, LTE-R and BBRS-based systems.

1.3 Contents

This thesis is composed of 5 chapters and additional annexes.

Chapter 1 focuses on the evolution of mobile communications, detailing the different historical milestones that shaped what mobile is today, followed by a railway industry description and future analysis. The motivation for this work is presented, explaining the importance of antenna location for performance in railway communication systems, and the thesis structure is described. Chapter 2 includes the fundamental concepts for the matter comprehension, more specifically, a theoretical background on the technologies (TETRA, GSM-R, LTE-R and BBRS), railway communications system architecture and finally a definition of the main parameters affecting the performance. By the end of this chapter, the state of the art of this thesis is presented. Chapter 3 provides a model overview for the work developed, showing also the analytical models upon which it is based. An explanation of the simulation program used (CST) and the functions used is also included, as well as sections on surrounding environments for antennas and monopoles performance. Chapter 4 presents the scenarios considered for simulations as well as the results from the three approaches developed in this work, with both quantitative and qualitative results analysis. Chapter 5 includes the conclusions of this work, namely the most important results, the recommendations to the industry and future developments that should be considered to further enrich this field. Annex A provides a comprehensive comparison of the technical aspects of each of the four communication technologies studied. Annexes B to E feature datasheets of commonly used antennas for the different systems. Annex F presents the 3D far-field views of the $\lambda/4$ test monopoles (isolated antennas). Annex G shows the 3D far-field views of the test antennas with a flat surface. Finally, Annexes H to J show relevant the complete range of 2D far-field results obtained from simulations.

Chapter 2

Fundamental Concepts

This chapter provides an overview of the fundamental concepts required to understand railway communication systems, namely the system architecture, technical specifications of TETRA, GSM-R, LTE-R and BBRS, and main parameters affecting performance. At the end of the chapter, the state of the art of the work is presented, detailing the approaches taken and the innovative aspects of the methods used, with remark to the conclusions drawn.

2.1 TETRA

In this section, the basic aspects of TETRA are shown, providing an overview of its architecture and features.

2.1.1 Network architecture

TETRA, as a digital trunked mobile radio standard developed to satisfy the needs of Professional Mobile Radio networks, is used mainly by official entities and governments. It features a set of standards developed by ETSI.

Although the system's main function is one-to-many communications (in opposition to commercial mobile telecommunication networks), some one-to-one telephone type of calls can be made. TETRA has many handy features, for example, it has centralised call control so that priority calls can be put through and other calls can be queued. It features also direct push-to-talk, voice encryption and relay mode. TETRA additionally enables privacy and confidentiality thanks to built-in encryption features. It offers a high voice quality and a fully digital solution, hence combining the benefits of digital radio with the advantages of a Private Mobile Radio (PMR) system [HYTE18].

Typical TETRA configurations feature a network of BSs and MTs, just like a commercial mobile cellular communications network. As it is analysed in the next section, TETRA usually rely on much lower frequency bands than other communication systems, hence allowing increased coverage by each BS.

TETRA network architecture standards are featured in ETSI Release 1, dividing the network into two main interfaces, as seen in Figure 2.1:

- Switching and Management Infrastructure (SwMI), consisting of all the equipment and sub-systems that comprise the network, including switches and BSs;
- Inter-System Interface (ISI), making possible that infrastructures supplied by different manufacturers interoperate with each other, while also allowing interoperability with other networks.

The SwMI is the core component of the TETRA network, comprising all switching equipment, BSs, management and service provision elements. It features the MT and Line Station (LS) terminals, the Direct Mode Mobile Stations, a Gateway, the Network Management Unit (NMU) and the physical TETRA network, including all BSs. Internal nodes of the SwMI are not standardised in order to allow manufacturers to develop the most cost-beneficial solutions.

The BS network is connected to the SwMI via landline or microwave links, and in some systems redundant connections are assured through star or ring configurations. The system allows for seamless handover, provided that there is sufficient overlapping coverage of the two adjacent BSs. To manage resource allocation, priority queues are used. Pre-emptive services are also supported.

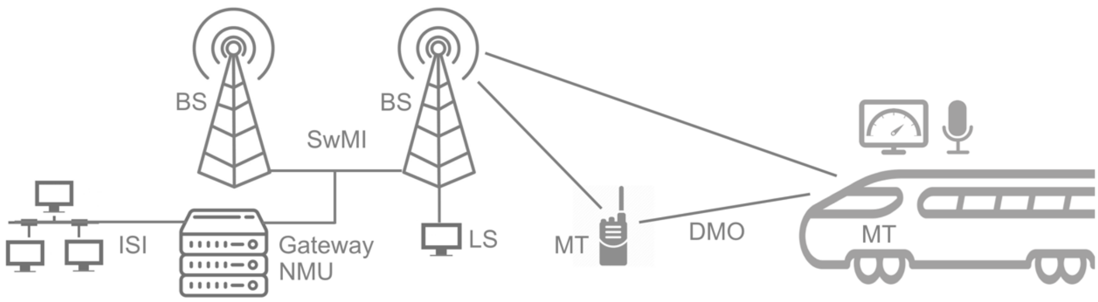

Figure 2.1 TETRA-based Railway Communication Network.

As a mission-critical communication system, TETRA ensures that operations can run smoothly in all situations, not just guaranteeing service reliability and cost effectiveness. Therefore, its deployment for Railway Communication Networks allows operators to handle voice and packet data transmissions safely and featuring a wide range of dedicated functionalities.

Including a built-in PMR voice call functionality, essential to railway operation, but also DMO capabilities which can work in Local Mode (without need for BS communication, in case the network is down) and Priority Calls, TETRA provides fast and consistent voice call setup even over wide area connections. Narrow and wideband packet data services allow for basic status messaging, location information and other vital data to be transmitted [Salk06].

Direct Mode Operation (DMO) is one of TETRA's core features, allowing for connected radio terminals to communicate directly with each other independently from the SwMI, which is the regular Trunked Mode Operation (TMO). It helps to get additional capacity outside the TMO network for localised work activities, major accidents or periodic events. In DMO, it is also possible to install a temporary auxiliary repeater that would work as BS for local communications, through a mobile radio vehicle, for instance.

Release 2 for TETRA incorporates the High-Speed Data enhancement, featuring services such as TMO Range Extension, Adaptive Multiple Rate and Mixed Excitation Liner Predictive enhanced voice codecs and Enhanced Data Service [ETSI07].

2.1.2 Radio interface

The system's radio interface consists of the layer between the BS and the MT, called Air Interface in the TETRA architecture. The system was designed to operate in both the 400 MHz and 800 MHz bands, though with lower frequencies coverage increases substantially. Specific TETRA bands defined by ETSI are the 380-400, 410-430, 450-470 and 800 MHz bands, with railway applications focusing mostly in the 400 MHz one. Indeed, most countries have dedicated frequencies for TETRA use in the 400 MHz, divided in bands for emergency/governmental services and civil applications. In France, for example, TETRA has allocated the 380-400 MHz band for emergency services and the 410-430 MHz band for civil use. In The Netherlands, emergency services relying on TETRA use the 380-386.50 MHz and 390-396.50 MHz pairs for emergency operations, whilst the 410-430 MHz band is available for civil use

[ElCC18]. In Germany and Norway the technology is only used for emergency services, with Germany having a 10 MHz band for TMO and a dedicated 4 MHz band for DMO use [AARO18], and Norway having several frequency pairs in the region of the 400 MHz but also a higher band between 870-876 MHz for specific applications [NKOM14].

The radio system uses TDMA with 4 time slots in one radio carrier and 25 kHz spacing between carriers. This configuration allows for the optimal solution to balance cost of equipment with service availability and reliability. As a TDMA-standard technology, several users share the same frequency, with speech and data being multiplexed into time slots. All four different time slots in one carrier bear different channels, so there can be as many as four different calls on one 25 kHz wide carrier frequency. The maximum number of carriers for one BS is eight, adding up to 32 time slots. The control channel is responsible for signalling, as information is broadcasted through it to all MTs, who get informed to go to a specific traffic channel for a connection. In the opposite direction, MTs willing to connect request so to the SwMI through the control channel.

For modulation, TETRA uses $\pi/_4$ Differential Quadrature Phase-Shift Keying, resulting in a frame structure of 17.65 frames per second, with 18 000 symbols per second, 255 symbols per slot and 4 slots per frame. In DL, all slots are usually filled with a burst even if idle, however of the 18 frames per second, only 17 are used for traffic, with the 18th being reserved for signalling, Short Data Service messages or synchronisation [TCCA18].

Although data can only be transmitted at 7.2 kbps for a single channel, it is possible to increase this data rate combining up to 4 time slots reaching a 28.8 kbps maximum. Expanding channel bandwidth can allow for higher data rates, however many countries have been opting for relying on TETRA for mostly voice and signalling traffic using other, more powerful networks for data transfer [Leit09].

Overall, TETRA combines the features of digital cellular, mobile radio, wireless data and paging with increased coverage requiring less infrastructure, fast call set-up, high security and quality communications. It is therefore a good option for railway operators in opposition to dedicated PMR, as the wide support from industry and official standards entities will ensure technology development and support over the next years.

2.2 GSM-R

In this section, the basic aspects of GSM-R are shown, providing an overview of the system architecture and features.

2.2.1 Network Architecture

GSM-R was standardised by the European Telecom Standards Institute (ETSI) and is supported by the GSM Association Group, the association of GSM equipment suppliers [GSMR12].

The GSM-R architecture is divided in three main components, as can be seen in Figure 2.2:

- The Base Station Subsystem (BSS), which is the section responsible for handling traffic and signalling between MTs and the network;
- The Network Switching Subsystem (NSS), the component that handles mobility management, tracking the MT location and allowing mobile services to be provided to users;
- The Operational Support System (OSS), computerised-systems working in the background of the network, supporting management functions such as network inventory, service provisioning, network configuration and fault management.

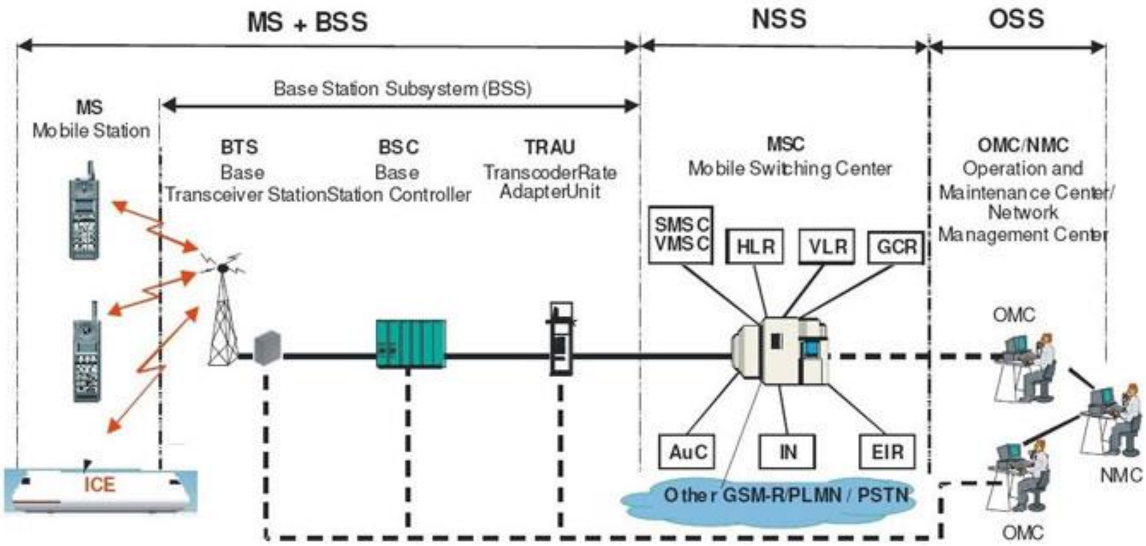

Figure 2.2 GSM-R Network Architecture diagram (extracted from [Kraf17]).

On the user side of the system, there is the Mobile Station (MS), which are the mobile transceivers installed on trains but also other terminals that rely on the GSM-R network, for example, railway track workers for maintenance, or security and emergency services. Mobile users can be reached by means of functional numbering and Location-Dependent Addressing (LDA), which is an addressing method that requires information on the location of the MS in order to forward the call to the correct called party [MiZh00]. The system supports both voice and radio transmission.

GSM-R features four fundamental components [Kraf17]:

- Enhanced Multilevel Precedence and Pre-emption Service (eMLPP), providing different levels of precedence for call set-up and handover, ensuring priority connections for priority users and emergency services [3GPP01];
- Functional Addressing, a feature that allows calling users by their functional number, which identifies both functions and applications, instead of the number of the MT [GSMR12];

- Location-Dependent Addressing, a routing system to call the most appropriate train controller regarding the current train position, using a short-code number [Kraf17];
- Railway Emergency Call (REC), a call with the highest possible priority.

Figure 2.2 shows that the trackside mounted antennas are the Base Transceiver Stations (BTS), containing the equipment for transmitting and receiving signals, antennas and encrypting equipment. For sectorised cells, the BS might have several transceivers, allowing it to serve different frequencies/sectors, but GSM-R usually has a single cell for the track area, so the BTS has several transceivers working at different frequencies, to maximise capacity.

The BTS is controlled by a parent Base Station Controller (BSC), a small unit frequently incorporated in the transceiver, providing operations and maintenance connection to the Network Management System (NMS), managing the operation of transceivers as well as software handling and alarm correction. The BTS is responsible for the allocation of radio channels as well as handover control. The last component of the BSS is the Transcoder Rate Adaptation Unit (TRAU), responsible for coding and decoding the voice channel, as well as adapting to the user data transmission rate. It might be installed in the Mobile-services Switching Centre (MSC) or in the Base Station Controller installation.

The Network Switching Subsystem (NSS), also called the core network, is responsible for call out and mobility management functions between MTs in the network and those with the control centre. The main component of the NSS is the Mobile Switching Centre (MSC), in which the switching of calls between users is performed, but also registration, authentication, location updating, handovers and call routing. The switching system includes several functional elements: the Home Location Register (HLR), a database used for storage and management of network subscribers' info such as profile, location and activity status; the Visitor Location Register (VLR), another database, but in this case a temporary one storing information about active subscribers in the network, reducing the number of times the HLR is accessed; the Authentication Centre (AuC), a protected database used to authenticate and cipher the radio channel, shielding the system against fraud; the Equipment Identity Register (EIR), one extra database containing a list of all valid mobile equipment in the network, as each MS carries an International Mobile Equipment Identity (IMEI) number and each user has a unique USIM card used for its identification in the network; the SMS-C which handles incoming SMS; the VMS-C which handles voice mail system and finally the Group Call Register (GCR), a management database for voice group or broadcast calls in the area controlled by the associated MSC [ETSI96].

Finally, in the background of the whole network lies the Operational Support System (OSS), supporting the network configuration and management tasks. It consists of the Operations and Maintenance Centre (OMC), which is connected to all equipment in the switching system and to the BSC. The OMC performs administration and commercial operation such as subscription monitoring, billing and statistics, as well as security management, network configuration, operation and performance management, and maintenance tasks. Sometimes, the AUC and EIR infrastructure are placed as part of the OSS, whereas traditionally these network elements belong to the NSS [ETSI96].

2.2.2 Radio Interface

The radio interface for GSM-R consists of the information flow taking place between the train MT and the BS. GSM-R has been assigned by ETSI a 4 MHz bandwidth between 876-880 MHz for UL and 921-925 MHz for DL. This band is called the GSM-R band or the UIC band. The UIC has also defined the possibility of having an additional band to increase channel availability, called the E-GSM-R band, consisting of frequencies usually reserved for governmental and defence use, hence when the GSM-R band is insufficient for railway communication needs in a certain area, the regulator might allow for the use of extra frequencies, provided their availability [SEPU17]. The frequency distribution can be seen in Figure 2.3.

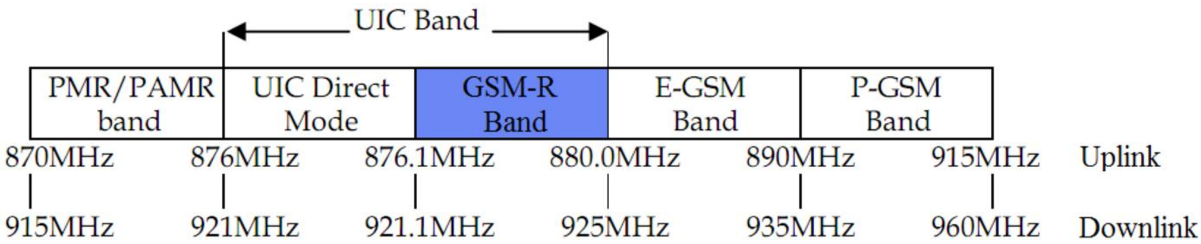

Figure 2.3 Frequency allocation for GSM-R (extracted from [SEPU17]).

Like public GSM, in GSM-R each carrier takes 200 kHz of band, which allows for 19 pairs of carriers in the specified bandwidth with an extra 100 kHz in the bottom of the band reserved for Direct Mode, which enables the direct communication between MTs in the network over short distances.

GSM-R is recommended to have a 400-600 kHz lower guard band and a 200 kHz upper guard band to avoid interference with systems operating at neighbouring frequencies.

GSM-R relies on Gaussian Minimum Shift Keying (GMSK) modulation and operates in TDMA, dividing each carrier in 8 time slots and allocating to each channel a specific time slot. Each TDMA frame has 4.615 ms with the 8 time slots of 0.577 ms each, including information bits and safety guard spaces on bottom and top ends [Corr18].

GSM-R offers voice services up to 22.8 kbps with a transmission rate of 9.6 kbps per time slot, and data connections with data rates up to 236.8 kbps combining four time slots, using EDGE [WILL18].

2.3 LTE-R

In what follows, the already know aspects of LTE-R are presented, providing an overview of what is expected from the system when it is fully developed, as well as the services it is expected to provide.

2.3.1 Network architecture

As the first fully packet-switched IP-based mobile communication standard release from 3GPP, LTE architecture implies that both data and voice communication are packet based. Furthermore, LTE introduces a simplified backbone network called Evolved Packet Core (EPC), requiring less equipment than previous standards, such as GSM, as there is no need for switching units.

The LTE-R architecture is divided into two main components, as seen in Figure 2.4:

- The Evolved Universal Terrestrial Radio Access Network (E-UTRAN) layer, the equivalent to the Base Station Subsystem in GSM, featuring the BS communicating with trains;
- The EPC, the main component of the network, which communicates with packet data networks outside LTE-R, such as the internet, private corporate networks or the IP multimedia subsystem.

LTE-R, just like commercial LTE, assigns network resources to users and applications depending on data rate demands in the specific moment. The IP Multimedia Subsystem (IMS) is the technology proposed to support multimedia services in future LTE-R, and is expected to allow voice calls to be easily combined with other sessions, like video streaming or conferencing. This will occur by means of the Session Initiation Protocol (SIP), a signalling protocol used for setting up, modifying and terminating two-party or multi-party sessions consisting of one or several media streams. SIP addresses are used to find the user's network location, in order to reach them anywhere [CMAF13].

As seen in Figure 2.4, the proposed LTE-R architecture (3GPP Release 12 [3GPP15]) is backward compatible with GSM-R. The network features a core network of EPC and a radio access network of E-UTRAN to transmit and receive signal from Onboard Units (OBU).

Starting from the MT, the OBU block features the necessary equipment for railway communications of voice and data, but also functional equipment of the European Train Control System (ETCS), which is analysed in further detail in the following sections. The LTE-R architecture has also planned the installation of small cells in passenger cars, for example femtocell access points, that will improve indoor coverage for passenger use [CMAF13].

Then, the equivalent of the Base Station Subsystem in GSM is the E-UTRAN layer in LTE. Although it contains the BSs, which are called NodeBs, but there is no Radio Network Controllers (RNC). UTRAN equipment connects through four different interfaces: the Iu interface is an external one, connecting the RNC to the core network (to the EPC), the Uu interface is also external, but connecting Node B with the OBU. Iub and Iur are both internal interfaces, with Iub connecting Node B to the RNC and Iur connecting two different RNC with each other. NodeB BSs are interconnected by means of the X2 interface, while they are connected to the EPC by means of the S1 interface, through S1-MME (connection to the Mobility Management Entity – MME) and S1-U (connection to the Serving Gateway – S-GW) [DNXi08], as featured in Figure 2.4.

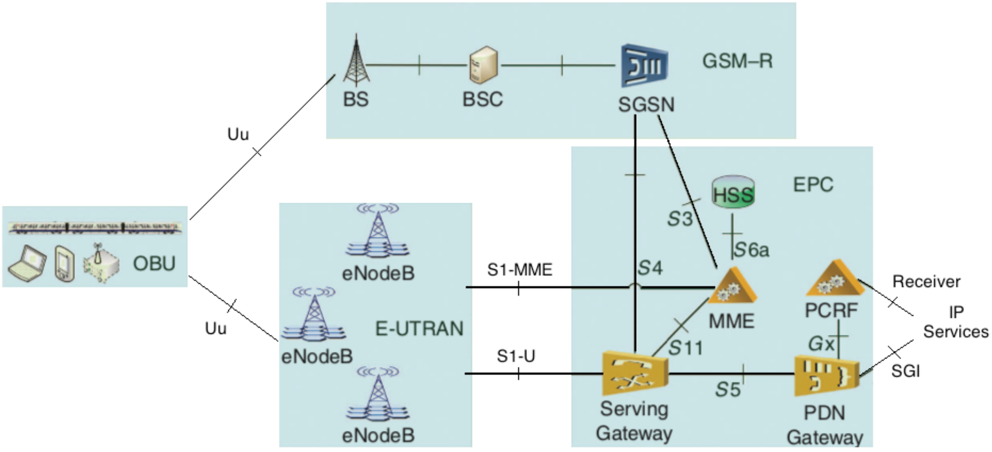

Figure 2.4 Network Architecture of LTE-R (adapted from [HAWG16]).

Finally, there is the EPC, featuring several components: the MME, the key control-node for the IP-based access network, responsible for idle mode of user equipment, for choosing the S-GW for a new device connection and for handling the connection to older technologies (depicted in Figure 2.4 is the connection of the MME to the SGSN, with a GSM-R backup network); the PDN Gateway, which provides packet screening and filtering for each user and allows connection with non-3GPP technologies such as legacy railway communication systems; the Home Subscriber Server (HSS), a central database focused on user and subscription information, replacing MSC of GSM-R components HLR and AuC; the SGW, responsible for serving the several connections inside the EPC and to its exterior; and finally, the Policy and Charging Rules Function (PCRF), aggregating information to and from the network and operational support systems in order to determine policy rules in the network, such as user priority, being also crucial for voice calls, through Voice over LTE (VoLTE) operation [CMAF13].

Since voice is a crucial service in a Railway Communication System, voice service over IP in LTE networks is key for the success of LTE-R as a reliable alternative to GSM-R. While Circuit-Switched Fall Back (CSFB) is a possibility to address the problem, IMS-based solution VoLTE would allow the LTE-R network to operate without the need for GSM-R to backup voice calls. CSFB technology consists of a forced handover of voice calls required to the LTE network to a 2G or 3G network. For successful operation, it would need a fully operating GSM-R parallel network to handle voice communications, with LTE-R band being used only for data. Furthermore, VoLTE has six times more voice capacity than traditional GSM, and strict call setup time requirements for critical railway services might exclude a CSFB-based approach to voice communications [CMAF13].

2.3.2 Radio interface

The radio interface for LTE-R consists of the transmission of information between the MTs placed in the train (OBU) and the E-UTRAN interface BSs.

LTE standards and infrastructure have great spectrum flexibility, allowing for carrier bandwidths ranging from 1.4 MHz up to 20 MHz, and frequency bands from 700 MHz up to 2.7 GHz. This enables responsible entities to make the choice of frequencies that will have the least interference problems, according to systems in parallel use [Nohr18]. In order to allow the transmission of bidirectional information, each frequency band is standardised to use full duplex systems. Some of the bands rely on Time Division Duplex (TDD), ideal for asymmetric systems, while other bands operate with Frequency Division Duplex (FDD), better for symmetric systems.

The smallest division of resources LTE has is called a Resource Block (RB), which is 180 kHz wide and lasts for a timeslot of 0.5 ms. For standard LTE, an RB comprises 12 subcarriers at a 15 kHz spacing. The number of supported RBs depends on the transmission bandwidth. Since LTE is designed to operate with channel bandwidths from 1.4 MHz to 20 MHz, the maximum number of RBs supported varies from 6 to 100, respectively.

Currently, although most commercial LTE networks use higher frequency bands, usually higher than 1 GHz, Portuguese operators use both the 900 MHz and the 1.8 GHz bands for LTE services [ANAC18]. Preliminary planning in Europe led to an agreement for the possible working bands of LTE-R: 400 MHz, 790-960 MHz, 1.7-2.2 GHz, 2.5-2.7 GHz. Since upper bands have higher bandwidths available, they allow higher data rates. However, coverage in higher frequency bands is substantially reduced, increasing the costs for network deployment, as a higher BS density is required. Due to high propagation loss and more severe fading, LTE-R cell radius for a system operating in 2.6 GHz would need to be less than 2 km in order to comply with strict Signal to Noise Ratio (SNR) and Bit Error Ratio (BER) requirements defined for High-Speed Railway operation [HAWG16]. This said, lower frequency bands are the most interesting for operators, having been adopted in pioneer LTE-R systems. In South Korea, the deployment of the world’s first LTE-R network in a new High-Speed Railway was done using the 700 MHz band (UL 718-728 MHz and DL 773-783 MHz) and a bandwidth of 10 MHz [KRNA18], while in China LTE-R systems are being deployed using the 450-470 MHz band.

UL and DL do not present the same requirements, since energy consumption is a critical issue for MTs and the RF power amplifier that transmits the radio signal through the antenna is the component with the higher power. Signals with high peak to average ratio and requiring linear amplification need RF power amplifiers that do not guarantee a near constant power level when operating, therefore Orthogonal Frequency Division Multiple Access (OFDMA) is used only for DL in LTE networks, while for UL a different concept is used for the access technique. Although still a form of OFDM, the implementation is called Single Carrier Frequency Division Multiple Access (SC-FDMA), which features the lowest peak-to-average ratio of single-carrier systems, while it still reduces interference impact and allows for a flexible subcarrier frequency allocation like OFDM [Pool18].

LTE-R systems are being developed to meet powerful requirements in terms of capacity, so it is possible to expect from the next-generation mobile communications network for railways data rates aligned with commercial LTE. DL speeds of up to 100 Mbps and UL reaching 50 Mbps (theoretical maximum) will fulfil the railway operators’ needs in terms of capacity.

2.4 BBRS

In this section, an overview of this Thales solution for railway mobile communications is provided.

2.4.1 Network architecture

Similar to TETRA, GSM-R and LTE-R, communication systems operating BBRS rely on BSs installed along the railway, providing RF transmission for equipped rolling stock operating in the line. These MTs usually operate a continuous data stream as the applications require so.

BBRS features parameter-based handover, therefore allowing seamless handover between BSs based on Radio Signal Strength Indication (RSSI), data-rate, quality of the connection, or other parameters specified by users. BBRS is based on Wi-Fi (IEEE 802.11n 2x2).

An overview of the network architecture for BBRS is shown in Figure 2.5.

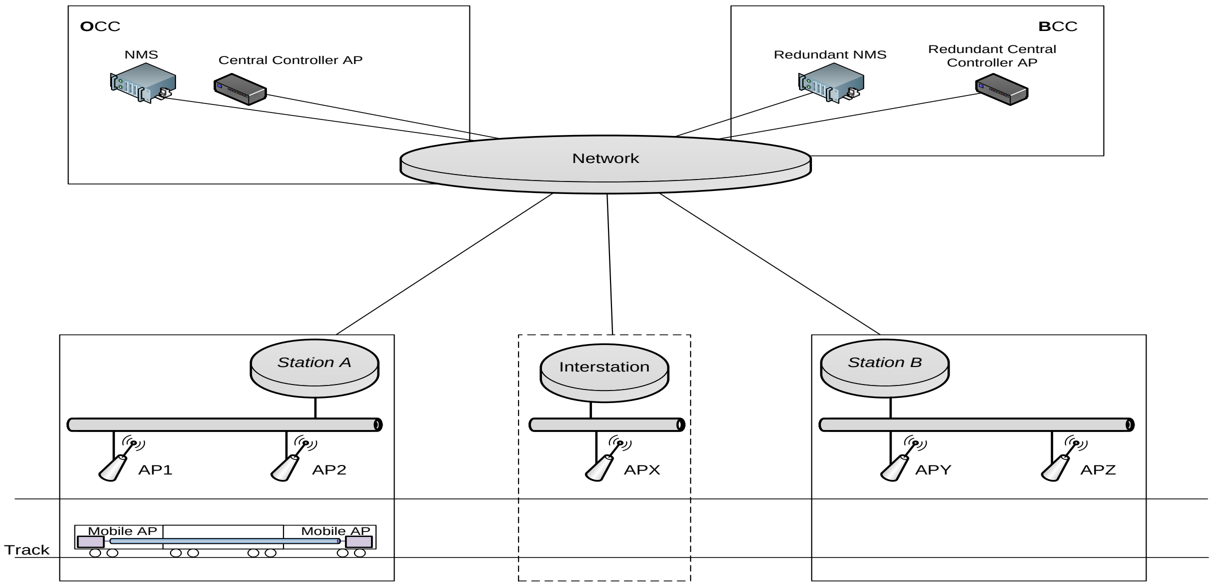

Figure 2.5 BBRS Network Architecture (extracted from [THAL18]).

As seen in Figure 2.5, the BBRS comprises several network elements, similarly to other railway communication networks. The backbone of the architecture features the Operation Control Centre (OCC), the core of the network functions, and the Backup Control Centre (BCC), which is used as redundancy for increased stability guarantee. The general architecture includes the elements described as follows:

- Network Management System (NMS): responsible for managing the network, it monitors all functions, enabling access to mesh configurations and individual node settings, identifying roaming and handover, detecting possible errors or faults, regulating traffic prioritisation, adjusting radio power controls and assuring security measures. It is located in the OCC with a redundant other placed in the BCC;

- S-GWs: are responsible for managing mobility and traffic among the static nodes of a specific mesh. They are also located at the OCC, but placed as redundancy on the BCC;
- Mobility Controller: with a primary goal of controlling the mobility of all system meshes and anticipate handover needs, it is placed at the OCC and also at the BCC;
- Static Mesh Nodes: several sets of two directional antennas located along the track, responsible for providing the adequate coverage, which are the BSs;
- Mobile Mesh Nodes: installed on the rolling stock, these provide the radio link with the Static Mesh Nodes.

2.4.2 Radio Interface

Since BBRS connection is assured through Wi-Fi, it allows bidirectional data packet transmission, using the Internet Protocol (IP), and typically operating in the 2.4 GHz or the 5 GHz bands. The system was designed [THAL18] to work with the standard Wi-Fi frequencies 2.405-2.495 GHz and 5.150-5.825 GHz as well as the higher, non-standard frequencies 5.825-5.925 GHz, the latter being the most common for several applications.

BBRS uses OFDM as the transmitting data method and MIMO, using two transmitting antennas and two receiving antennas. Channels are spaced 5 MHz from each other and can be 20 or 40 MHz wide (achievable with the combination of primary and secondary channels). Since a 20 MHz band features 52 usable subcarriers, increasing the channel capacity to 40 MHz yields an ever higher increase in subcarriers, since the band guard does not need to be doubled as well. Although 40 MHz channels can operate up to 108 subcarriers, most BBRS applications rely on 20 MHz channels.

BBRS is prepared to operate with several modulation schemes, such as BPSK, QPSK, 16-QAM and 64-QAM, and was designed to operate with train speeds up to 250 km/h with a maximum data rate of 125 Mbps. However, a more commonly used value is 70 Mbps, the measured value that assures the required Quality of Service.

Concerning the railway environment, BS antennas are usually located at 5 m height and are no farther than 1 km from each other. This leads to an increased BS density, much higher than in the other mobile communication technologies under study, but needed due to the high frequency resulting in higher propagation losses. On urban environments BS placement is even more strict, sometimes requiring the distance between BSs to lower to 300 m. MT antennas are located on top of the rolling stock, usually at the front and back of the trains, on top of the operator cabin.

BBRS features, additionally, seamless handover capabilities with a maximum delay of 100 ms, allowing high mobility along the entire track, as well as an integrated remote graphical network management and encrypted links to increased system safety.

2.5 Railway Communications

In this section, a description of the most relevant parameters for railway communications is provided, focusing on specific requirements for railway operations, for instance the integration of ERTMS systems, and also looking at typical railway scenarios and performance parameters.

2.5.1 Requirements

ERTMS features three different sub-systems: an interoperable safety and control system – the European Train Control System (ETCS), a radio system supporting cab signalling for driving without line side signals (currently GSM-R is the standard), and an international traffic management system.
Regarding the ETCS, the system offers various functional configuration options that allow for a staged introduction of the standard, or an adaptation to the use of specific rail corridor. These configuration options were standardised as ERTMS Levels and range from 0 to 3, as follows [ERTM18b]:

- **Level 0**: in this case, the rail corridor has not successfully deployed the minimum ETCS equipment to allow for the usage of the system. Without it, train drivers have to look at trackside signals in order to comply with speed limits and other signalling. The train's maximum speed is determined by onboard sensors' information based on the operational limits of the rolling stock;
- **ERTMS Level 1**: designed as an add-on to conventional lines equipped with lineside signals and train detectors. In this level, there is communication from the track to the train, through the use of dedicated eurobalises, devices placed in close proximity to trackside signals, operating a digital radio beacon system and connected to the train control centre. In Level 1, the train speed is permanently analysed by ETCS onboard equipment, which also calculates the maximum speed and braking points, taking into account the information obtained from the eurobalises as well as track and train specifications;
- **ERTMS Level 2**: featuring continuous radio communications between the train and the Radio Block Centre (RBC), railways operating this level of the system do not require lineside signals. The train receives a continuous stream of data featuring line-specific data and signals status on the route ahead and returns information on position and speed to the control centre. Eurobalises are still placed in the locations where physical signals used to be, but are only used to transmit fixed messages such as location, gradient and speed limits. This level allows the train to reach its maximum or optimal speed, while maintaining a safe braking distance factor. With permanent communication of trains with control centres, it is also possible to increase capacity due to reduced headways (safety distance between two trains operating in the same track, in the same direction), and infrastructure/maintenance costs are cut due to the lack of trackside signals;
- **ERTMS Level 3**: still in specification development phase, level 3 will further increase the system's potential, introducing a moving block technology with the primary goal of optimising the distance and speed between trains. In this level, the radio communication system will be used to control the train's movements, while the eurobalises will have the purpose of determining the train's position. The track will no longer be divided into fixed blocks, since the

train's position will be controlled as a distance to the next and previous train in the same track.

Currently, ERTMS Level 1 already brings significand advantages over traditional railway operation systems, allowing for High-Speed travel. However, ERTMS Level 2 allows for substantial line capacity increase by enabling higher operational speeds. In a near future, ERTMS Level 3 will further step up the benefits of this technology. Therefore, as railways operating at Levels 2 and 3 rely heavily in the radio communication systems, it is critical to guarantee the best possible connectivity between trackside-mounted BSs and train MTs, proving once again the importance of the present work.

The mobile communication network defined for ERTMS application is GSM-R, standardised by ETSI based on the EIRENE and MORANE protocols [ERTM18a]. To allow for the correct system operation, a number of system services are required, as listed on Table 2.1.

Table 2.1 System services required for ERTMS/ETCS (adapted from [GSMR15a]).

Voice services	
Point-to-point voice calls	Public emergency calls
Broadcast voice calls	Group voice calls
Multi-party voice calls	
Data services	
Text message bearer service	Bearer service for general data applications
Bearer service for automatic fax	Bearer service for train control applications
Call related services	
Multi-level priority and pre-emption	Advanced call handling (hold, transfer, queue)
Auto answer service	Barring incoming or outgoing calls
Call supervisory indications	Charging information
Railway specific applications	
Functional addressing by train, engine, coach number or functional number	
Call specific users depending on location	Multiple driver communications on same train
Railway operational emergency calls	Shunting operation mode (link assurance signal)
Railway specific features	
Set-up of urgent or frequent calls through single keystroke or similar	
Display of functional identity of other party	Fast and guaranteed call set-up
Support for train speeds up to 500km/h	Automatic and manual test modes
Control over mobile network selection	Control over system configuration

Due to the expected increase in cross-border railway connections, as rail transport is getting more competitive for both passengers and cargo, it is now crucial to guarantee a common railway management system for the whole region. Therefore, one can predict that ERTMS standards will be fitted in many new rail corridors in the upcoming years, as well as retrofitted in existing ones, since ERTMS allows upgrades from one level to another [ERTM18b].

The decision to install a specific ERTMS Level in a particular line has to take into account several factors such as the existence of other signalling systems in the line, the possibility of equipping the line with GSM-R, the maximum speed allowed, future predicted capacity upgrades or needs, among others. Concerning the radio communication system, it is crucial to know the line profile to understand the surrounding terrain details, as well as existing communication systems that might create interference. The higher the Level installed, the more benefits the system can offer to operators.

On the other hand, Quality of Service (QoS) mechanisms have to ensure the eMLPP functionalities. While commercial networks manage different QoS policies according to traffic, GSM-R, being a mission-critical network, has to ensure QoS for real-time applications as it is needed for resource management. For seamless railway operations, strict latency requirements are essential. EIRENE specifications state that connection establishment error ratio over one train line should be less than 1% per hour and 99% of ETCS data must have a maximum latency lower than 0.5 s. Table 2.2 shows a summary of the main GSM-R QoS parameters, with their availability requirements shown in brackets [FFCa16].

Table 2.2 GSM-R QoS parameters (extracted from [FFCa16]).

Requirements	Value
Connection establishment delay of mobile originated calls	$<$ 8.5 s (95%) $\leq$ 10 s (100%)
Connection establishment error ratio	$< 10^{-2}$ (100%)
Connection loss rate	$< 10^{-2}$/h (100%)
Maximum end-to-end transfer delay (of 30 byte data block)	$<$ 0.5 s (99%)
Transmission interference period	$<$ 0.8 s (95%) $<$ 1 s (99%)
Error-free period	$>$ 20 s (95%) $>$ 7 s (99%)
Network registration delay	$\leq$ 30 s (95%) $\leq$ 35 s (99%) $\leq$ 40 s (100%)
Call setup time	$\leq$ 10 s (100%)
Emergency call set up time	$\leq$ 2 s (100%)
Duration of transmission failures	$<$ 1 s (99%)

Since the ERTMS standards were designed to ensure high speed train operations, one of the biggest concerns is the high switching failure rate during handover processes. As trains move at higher speeds, they will be constantly moving out of the current cell and requiring switching for the next one. Small overlap areas and the Doppler frequency shift, combined with group switching situations (several trains moving in the same track, requesting to switch BSs at the same time) could lead to high switching failure. However, since trains move along the railway and do not change directions often, it is easier for the system to predict handovers and accommodate the switching equipment to these needs. If the system management software has information on the train speed and direction, it is also possible to compensate for the Doppler shift.

Just like other mission-critical systems, two of the main requirements for railway communications in general, and therefore for GSM-R in particular, are coverage and interference ones. EIRENE specifications for GSM-R clarify that coverage is defined as the field strength at the antenna on the roof of a train, at a height of 4 m above the track. An isotropic antenna with a gain of 0 dBi is assumed, as well as the use of the standard defined frequencies for the GSM-R technology [GSMR15b], resulting in the following coverage minimum values:

- Coverage probability of 95% based on a coverage level of -95 dBm, for voice and non-safety critical data;
- Coverage probability of 95% based on a coverage level of -95 dBm on lines with ERTMS levels 2 or 3, for speeds lower than or equal to 220 km/h;
- Coverage probability of 95% based on a coverage level between -95 and -92 dBm on lines with ERTMS levels 2 or 3, for speeds between 220 and 280 km/h.
- Coverage probability of 95% based on a coverage level of -92 dBm on lines with ERTMS levels 2 or 3, for speeds above 280 km/h;

The specified coverage probability means that, with a probability value of at least 95% in each location interval (with a standard length of 100 m), the measured coverage level shall be greater than or equal to the figures stated. It also considers a maximum total loss of 6 dB between antenna and receiver inputs in the MT installed in the train, in order to ensure that the level at the input of the receiver will never be lower than the reference sensitivity level of the receiver.

2.5.2 Technical/services comparison

In order to better understand the differences among the systems in study, Table A.1, in Annex 1, summarises infrastructure, radio interface and performance aspects of TETRA, GSM-R, LTE-R and BBRS, providing also an overview of the offered dedicated railway communication services.

Frequency choices are quite flexible for all systems, and the trend in new railway communication projects has been to try to rely on lower frequencies (sometimes recently made available due to deactivation of legacy radio systems) in order to reduce infrastructure cost.

The biggest differences among these technologies lie in the architecture: while GSM-R and TETRA are circuit-switch based, LTE-R is being based on LTE standards and therefore will be packet-switched based and BBRS is also packet-switched, since it is based on Wi-Fi. This means LTE-R and BBRS are less suited to voice communications, a critical feature in railway communication systems. However, it also allows for improved performance in data transmission, which is believed to be fundamental in the development of railway communication systems capable of providing new services both to operations management and passenger information and entertainment. BBRS, for instance, is used mostly for video transmission, a service that requires much higher data-rates and lower latency.

It is important to note that LTE-R is still not standardised by ETSI, therefore some technical characteristics might be changed. Nevertheless, the core architecture is based on commercial LTE parameters, which are the specifications LTE-R pioneer systems already deployed are using.

2.5.3 Railway scenarios

As with any communication system, signal propagation in railway communications is highly influenced by the surrounding environment, as environments generally introduce multipath effects causing fading and channel time dispersion. Since distinct propagation environments have different path loss and multipath effects, it becomes crucial to analyse the performance of the system with the adequate propagation model for each scenario.

Developing different propagation models in order to better adapt to each environment scenario allows not only to better predict how the propagation will occur in a given location, but also to improve cell planning for railway communication systems, assuring a superior level of performance while cutting infrastructure cost to the minimum necessary to fulfil requirements.

Regular cellular planning methods usually rely on three basic types of environment classification: rural, suburban, and urban. These scenarios have different parameters for multipath loss and fading, as several models have been developed based on them.

However, railways feature several specific characteristics, such as the unusual handover rate due to high mobility, or the particular structures in the railway environment. For radio propagation purposes, it is then possible to classify railway scenarios based in the type of line, taking into account the usual trains operating in each environment, and also to analyse the impact on radio propagation characteristics of the specific railway structures such as cuttings (cuts in uneven land to create an artificial valley to allow building a railway), embankments (railways are raised onto an embankment made of compacted soil to avoid a change in level required by the terrain), viaducts, tunnels or large station buildings [AHZG12].

In Table 2.3, it is possible to compare the different line types that can be found in railways. There are very different railway scenarios, therefore being crucial to analyse the railway not as a whole but as several subsections in order to correctly project and run a radio communication network that fulfils the operators' needs [FFCa16].

Table 2.3 Main characteristics of the different line types (adapted from [FFCa16]).

Characteristics	Urban	Suburban	Inter-city	High Speed
Maximum Speed (km/h)	≤ 70	$]\,70;160\,]$	$]\,160;250\,]$	≥ 250
Line length (km)	≤ 20	$]\,20;100\,]$	$]\,100;250\,]$	≥ 250
Parallel tracks	$1-2$	2	$2-3$	$2-4$
Rolling stock usage type	Single	Similar	Mixed	Very mixed
Train stations	$1-5$	$6-20$	$21-50$	$50+$
Operators	1	2	$3-5$	$6+$
Passengers (1000s/km of line)	< 100	$[\,100;200\,[$	$[\,200;500\,[$	≥ 500
Range of services	Single service	Small diversity	Multiple variances	Extremely varied

In addition to the urban, suburban and rural typical scenarios, the specific structures and environment scenarios that can be found in railways can be defined as follows [AHZG12]:

- **Viaducts**: one of the most common scenarios, as High-Speed Railways can be made up of more than 85% of it. These are long bridge-like structures carrying a railway across a valley or uneven ground, usually with a height of 10 to 30 m. BS antennas are placed 20 to 30 m over the surface of the viaduct, with few scatter areas being higher than it;
- **Cuttings**: a technique used to pass or cut through large obstacles such as hills or uneven ground, it is also often used in High-Speed Railway construction. Cross bridges built over the cuttings lead to non-line-of-sight propagation over short distances and diffraction;
- **Tunnels**: artificial underground passage, usually built through mountains or under densely populated areas, tunnel lengths vary from several hundred metres to dozens of kilometres. Generally, two main BSs are placed at the beginning and at the end of the tunnel in High-Speed Railways, featuring additional BSs inside the tunnel if needed;
- **Railway stations**: facilities where trains stop to load and unload passengers, generally consisting of a platform next to the tracks and facilities providing passenger services. Inside stations, trains run at reduced speeds and people walk at around 3 to 5 km/h;
- **Water**: railway in close proximity of rivers, lakes or sea areas, with the consequent expected reflection creating multipath propagation resulting in interference, phase shifting and fading;
- **Mountain**: railway built in a valley surrounded by mountains, with peaks, hanging valleys and valley steps being responsible for multipath propagation;
- **Desert**: railway going through a mostly flat dry land, with strong atmospheric duct formation resulting in unexpected reflections and diffraction of the transmitted radio waves, as the refractive index of the atmosphere can change dramatically;
- **Combination scenarios**: combining two of the types featured above, the more common schemes are a merge of tunnels with viaducts (a), and combining cutting sections with rural landscape (b) due to depth of the cutting changing frequently. These frequent changes of the

propagation scenario greatly increase the severity of fading, resulting in poor communication quality, while posing challenges to coverage estimation as multipath effects vary a lot.

From this scenario definition, the work of [AHZG12] defined modelling parameters for the different situations, resulting in predicted values for path loss and standard deviation of shadowing, performing simulations for regular GSM-R operating at 930 MHz. These results can be seen in Table 2.4.

Table 2.4 Predicted values of modelling parameters for GSM-R (adapted from [AHZG12]).

Scenario	Path loss [dB]	Standard deviation of shadowing [dB]	Fast fading distribution
Viaduct	2-4	3-4	Rice
Cutting	2.5-4	3-5	Rice
Tunnel	1.8-3	5-8	Rice
Station	3-5	3-5	Rice/Rayleigh
Water	2-4	2-3	Rice
Urban	4-7	3-5	Rice
Suburban	3-5	2-3	Rice
Rural	2-5	2-3	Rice
Mountain	3-7	2-6	Rice/Rayleigh
Desert	2-4	2-3	Rice
Combination (a)	3-7	5-8	Rice
Combination (b)	3-7	5-8	Rice

The analysed scenarios take into account only the train-to-infrastructure link, as it is the critical point of the railway communication system for this work, but scenarios for other radio wave transmissions on trains could be analysed, such as: inter-car connections, which might be done using wireless communication; intra-car wireless connections to provide broadband internet to passengers and train information systems; and inside station propagation, taking into account the different technologies in use in the premises.

Regarding BS placing, while for inter-city and high speed train lines most of the railway path is probably flat and straight, this is not true for urban and suburban scenarios, where dense neighbourhoods and the need of connecting several locations of interest apart from each other create the need of a very dense network featuring lots of curved sections and tunnels/viaducts.

As mentioned in earlier sections, for typical inter-city and high speed rail lines, BSs are placed along the track featuring highly directive antennas, covering both directions of the line. However, for urban and sub-urban scenarios, due to the aforementioned features, BS placing might achieve better results if done away from the tracks, for instance, in an elevated area nearby, or in a close building.

Due to this, for urban and suburban scenarios it is crucial to address the location of BSs in the line the train is operating to successfully install and adjust the antenna's tilt and azimuth in order to provide the best possible coverage.

2.5.4 Performance parameters

In a mobile communication system, it is crucial to select the most suitable technology in the planning and development phase, in order to achieve the highest possible level of performance of the system. Cell planning has to take into account QoS parameters to guarantee that the required services are adequately provided, while also reducing infrastructure costs to the minimum. Therefore, it is extremely important to define which are the key performance parameters to consider.

The main wireless performance metrics are as follows [SDey11]:

- **Coverage**: it is the range of a wireless link to reliably connect devices, the primary driver being the link budget. This parameter is affected by BS and MT parameters such as transmit power, antenna gain and receiver sensitivity, which is analysed further ahead in this section;
- **Capacity**: it consists of the amount of data from device endpoints a BS can simultaneously serve, and might refer to the single-link throughput from a single endpoint to a gateway or to the total capacity of the gateway to serve several MTs. Some systems with low single-link capacity might provide a high capacity using good multiple-access schemes, and therefore total capacity is the key metric. Coverage and capacity are the two most important parameters in cellular planning and there is a trade-off between the two, as the goal is to provide coverage for as many devices as possible without compromising capacity. Since railway communication systems are mission-critical, data-rates are one of the most important parameters;
- **Latency**: the delay that occurs due to the time it takes a signal to travel from one point to another throughout the whole system, i.e., takes into account the time needed for the information to flow from the emitting device to the radiating antenna, the free space delay and finally the time needed to go from the receiving antenna to the network core. Since it is not possible for the information to go faster than the speed of light, there's no such thing as zero latency in a communication system. Nevertheless, even though new 5G wireless networks are being designed to keep latency to a minimum (below 10 ms, down to about 1 ms), most railway communication systems rely on GSM-based technology and therefore might experience latencies up to 1000 ms, compromising the reliability, especially for systems deployed in high-speed railway networks;
- **Coexistence**: a guarantee of the network performance even with interfering systems operating along, only possible to achieve analysing not only neighbouring networks already in use but also expected frequency links to be deployed in the future as well as unlicensed bands, where transmitters are hardly regulated and traffic patterns are unpredictable;
- **Security**: mobile communication networks, making use of the air to transmit the information, are especially vulnerable to attacks from cyber criminals. Since railway communication systems

are mission-critical networks, it is even more important to make sure the network is strong, using a comprehensive defence in-depth strategy including prevention, detection and recovery mechanisms, relying on proven security algorithms.

In addition to the listed parameters, to pursue a successful and efficient network planning, it is also important to bear in mind the terrain scenarios, described in the previous section, and signal estimation models, which need to take into account the radio signal characteristics.

In order to analyse different options for antenna placing on train cars' roofs, it is important to define which parameters should be taken into account to evaluate the several options. For this work, the most relevant parameters are antennas' ones, as it is the performance of the antenna that is the main purpose of the study. The main antenna parameters relevant for this work are [Bala16]:

- **Radiation pattern**: the radiation pattern is usually defined for the far field of the antenna, and can focus on the magnitude of the electric/magnetic fields (field patterns) or the square of the magnitude of the electric or magnetic field (power patterns), often being normalised with respect to its maximum value. The more common scale is dB, and spherical coordinates (θ, ϕ) are used, where ϕ is the azimuth of the antenna (horizontal) and θ is the co-elevation (vertical). Both BS and MT antennas' radiation patterns are extremely important for the problem under study, since railway mobile communication systems are designed to provide coverage along the tracks and many times feature highly directive antennas. In Figure 2.6, a radiation pattern featuring the most common coordinate system for antennas can be seen.
- **Beamwidth**: consisting of the angular separation between two identical points on opposite sides of the pattern maximum, antenna patterns have several beamwidths. Usually, two beamwidths are considered: the Half-Power Beam Width (HPBW), which refers to the angle between the two directions in which the radiation intensity is half of the main beamwidth (3 dB difference), and the First-Null Beam Width (FNBW), which is the angular separation between the first nulls in both sides of the major lobe, as seen in Figure 2.6. Side lobes can also provide information on the transmission losses, and for this analysis the Side Lobe Level (SLL) is the key parameter, stating the difference between the maximum value of the major lobe and the biggest minor lobe peak value. For highly directive antennas, the Front-to-Back Ratio (FTBR) is used to provide information on the backward radiated power, comparing it to the major lobe.
- **Directivity**: it is the dimensionless ratio of the radiation intensity in a given direction to the radiation intensity averaged over all directions. While for isotropic antennas one can conclude that the directivity is unity, for all other cases it is possible to express it as a function of ϕ (azimuth) and θ (co-elevation).
- **Efficiency**: a measure of the electrical efficiency with which a radio antenna converts the radio-frequency power accepted at its terminals into radiated power. For receiving antennas, it describes the proportion of the radio wave's power intercepted by the antenna which is actually delivered as an electrical signal.

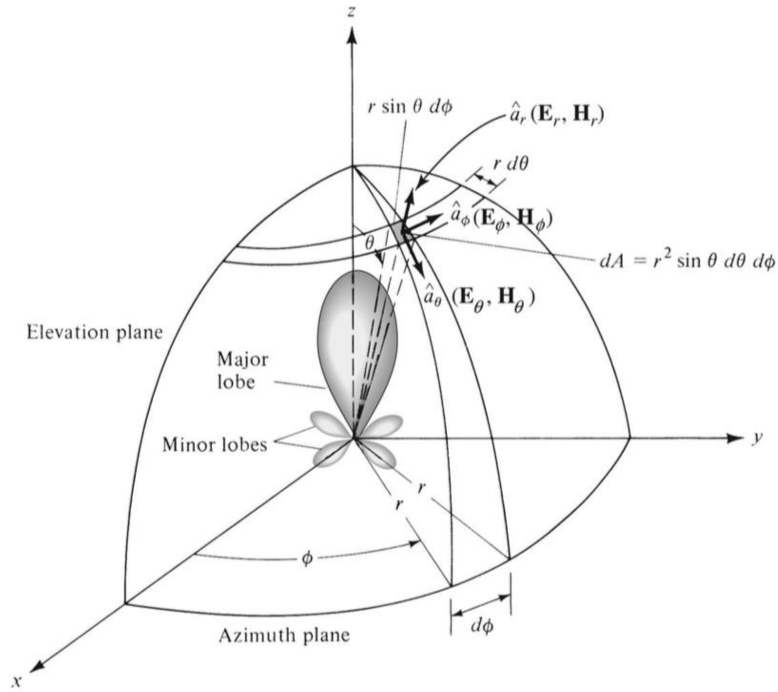

Figure 2.6 Coordinate system for antenna analysis (extracted from [Bala16]).

- **Gain**: closely related to directivity, it is a measure that takes into account the efficiency of the antenna as well as its directional capabilities, defined as the ratio of the radiation intensity, in a given direction, to the radiation intensity that would be obtained if the power accepted by the antenna were radiated isotropically.
- **Polarisation**: as the property of an electromagnetic wave describing the time-varying direction and relative magnitude of the electric-field vector, the polarisation is then the curve traced by the end point of the vector representing the instantaneous electric field, and may be classified as linear (vertical or horizontal), circular (left or right) or elliptical (left or right). To achieve the highest efficiency, the wave and the antenna's polarisations must match, otherwise the coupling efficiency (or polarisation loss) may be up to 20 dB (coupling loss for a right-hand circular polarised wave reception at a left-hand circular polarised antenna, for example).
- **Input impedance**: it is the impedance presented by an antenna at its terminals, with no load attached. It is very important to match the antenna's input impedance with the transmission line impedance, otherwise impedance mismatch will occur, leading to transmission losses. The antenna's input impedance is generally a function of frequency, hence the antenna will be matched to the interconnecting transmission line and other associated equipment only within a bandwidth. If the working frequencies change, the mismatch loss might increase.
- **Bandwidth**: the range of frequencies, on either side of a centre frequency (usually the resonance frequency for a dipole), where the antenna characteristics are within an acceptable value of those at the centre frequency. This parameter divides antennas in two groups: broadband antennas, where the bandwidth is usually expressed as the ratio of the upper-to-lower frequencies; and narrowband antennas, where the bandwidth is expressed as percentage of the frequency difference over the centre frequency.

All this said, one can conclude that antennas feature a range of parameters that must be taken into account while planning and designing railway communication systems, with the operating frequencies influencing also the choice and performance of the physical equipment.

2.6 Antennas for railway communications

As the core element for any mobile communication system, train antennas might be of different types, depending on the operating frequency and services needed. The different antenna types affect the parameters listed in the previous section.

The location where the antenna is mounted and its design play a critical role on the total performance of the system. Train antennas are mounted on the roof and connected to the radio units installed on the interior of the train cabin [Mich14].

As seen in the previous section, one of the most important parameters of antennas is their bandwidth. For railway communication antennas, this parameter divides train antennas in two distinct groups:

- **Narrowband antennas**, explicitly designed to support a specific frequency band and a single functionality, being easier to design as the corresponding gain and directivity are targeted to the specific system they are operating for;
- **Broadband antennas**, merging different technology needs in one single antenna, multi-band antennas might feature Wi-Fi, UMTS, GSM, UMTS, GPS and LTE technologies.

Since there is limited space on the roof of the train and the installation and support for each unique antenna would be complex and unpractical, multiband antennas are becoming more and more popular. Other advantages of a broadband-antenna solution include the reduction of rooftop clutter, the support to MIMO solutions, and the simplification of installation and repair procedures without compromising the integrity of the carriage where the antenna is placed.

On the other hand, broadband antennas might not offer the same performance as narrowband ones. Therefore, a compromise between supporting spectrum and performance needs to be achieved so that it can support all radio systems.

Broadband antennas can include several radiating elements, one for each radio, under one single radome (protective cover made of plastic or other material). For each element a separate connector is used, allowing each element to have each own specific gain and radiation patter fitted for each radio technology and isolating the different systems. However, this solution increases the complexity of the installation, both at the antenna level but also on the interior of the train.

The other option for broadband antennas is to contain only one radiating element and one connector to support the whole frequency spectrum of the radios, having as main advantage the simplified installation and maintenance process. On the other hand, this configuration requires a multiplexer close to the location of the radio units, and lacks isolation between the different systems sharing the antenna. The most common solution for trains, using this scheme, is a combination of a GPS patch antenna element with a mobile antenna element under the same radome, as can be seen in Figure 2.7.

Figure 2.7 Combined GPS and mobile antenna (extracted from [Mich14]).

Manufacturers have been designing antennas using this scheme. In Europe, for instance, GSM-R antennas featuring support to other bands are the primary choice for railway operators [Mich14].

An example of a common broadband antenna used in the railway industry is the Kathrein 741009, whose datasheet is in Annex C.

Given that usually BS placement along railway tracks includes two sectorised antennas per site and that trains usually operate with two antennas, one in each end, one must understand which are the important angles of attack to consider in the radiation patterns. Issues affecting the gain of the train antenna in a direction that is not relevant for its communication with the BS do not present significant problems, while those interfering in the main beam in which the connection takes place should be taken into account.

Analysing Figure 2.6, and considering a train moving along the xx axis, one can conclude that:

- The **elevation plane** depicts the elevation angle between the train and the BS. Therefore having a co-elevation of $\theta = 0º$ means the antenna is perpendicularly above the train, whereas with $\theta = 90º$ it has the same altitude of the train antenna, being probably located in the far horizon in front of the train and with $\theta = 270º$ one has the same case but with the BS in the back of the train;
- The **azimuth plane** portrays the orientation angle between the train and the BS in relation to the ground, that is, seen from above. Given that, an angle of $\phi = 0º$ means the BS is exactly in the left trackside of the train antenna, while by analogy an angle of $\phi = 180º$ means the BS is exactly in the right trackside of the train antenna. For $\phi = 90º$ the BS is in the far, front side of the train, while with $\phi = 270º$ the BS is in the far back.

All this said, not all angles are relevant. In the elevation plane one should only consider angles in the two upper quadrants as it is unlikely that the BS antenna is located significantly lower than the height of the train antenna. Still in the elevation plane, the critical scope is $\theta \in [45, 90]°$, since as seen most trains have one antenna in each end, which means it is only relevant to evaluate performance to the front of the train direction. Moreover, when the BS is in close proximity of the train, there will probably be enough power to still achieve QoS parameters, and this is why the study has to focus on the mentioned angle interval. In the azimuth plane, and due to this same argument, it is not relevant to consider the case when the train is passing through the BS, and only the running direction angle should be taken into account. Therefore, the critical scope is $\phi \in [80, 100]°$. These angles are in accordance to the angles used in [Ribe18].

2.7 CST software overview

In order to develop a model and simulate the behaviour of different antenna configurations, to fulfil the primary goal of delivering a model for design criteria for the deployment of antennas on trains for mobile communications, the software used was Computer Simulation Technology (CST) Microwave Studio [CSTS19].This software is a high-performance 3D electromagnetic analysis tool, created to design, analyse and optimise electromagnetic components and systems.

Working with the full electromagnetic spectrum, CST features field solvers for several domain applications, all across a single user interface. As the solvers can be coupled to perform hybrid simulations, it is possible to analyse the performance of complex systems, made of multiple components, in an efficient and straightforward way.

CST is a popular tool to analyse performance, efficiency and installed performance of antennas and other radio equipment, electromagnetic compatibility and interference, exposure of the human body to fields, electromagnetic effects in motors and generators as well as thermal effects in high-power devices. For this work’s problem, CST is extremely useful as a way to simulate the behaviour of antennas on train rooftops, taking into account the influence of the roof material and shape on the propagation of the radio waves supporting the mobile communication systems in study.

The program includes a range of tools, such as low and high frequency simulations, thermal and mechanical analysis, system assembly and modelling, and also board, package and cable simulations. Since the goal of this work is to assess the performance of train-mounted antennas, and these use frequencies in the order of the hundreds of MHz or GHz, the main tool to be used will be the high frequency simulation functionality.

The program includes additionally several solvers for the electromagnetic simulation problem, such as:

- The transmission line matrix (TLM) solver, which uses the time domain solving method, and is suited for complex structures as it includes simplification techniques;
- The transient solver, based on the finite integration technique (FIT), being a general purpose time domain solver it is appropriate to broadband simulations of radiated emissions and susceptibility, and therefore is the main solver used for the simulations in this work;

- The frequency domain solver, based on the finite element method (FEM), commonly used to simulated conducted emissions, as its design includes a special meshing engine allowing for complex boards to be simulated faster than conventional methods;
- The cable harness solver, focused on simulation cables in complex environments, using a bidirectional coupling between the cable harness solver and the time domain solvers.

The transient solver is the most appropriate for this work [Ribe18]. The finite integration technique is a consistent discretisation scheme for Maxwell's equations in their integral form, which uses the resulting matrix equations of the discretised fields for numerical simulations, allowing to simulate real-world electromagnetic field problems with complex geometries.

This technique, based upon the usage of integral balances, allows to prove stability and conservation properties of the discrete fields without any prior calculations. The formulation has algebraic properties that make it possible to develop long-term stable numerical time integration schemes or accurate eigenvalue solvers, instead of using complex, time-consuming processes that would lead approximately to the same solution. The first discretisation step of this method consists of the restriction of the electromagnetic field problem to a bounded space region, as most electromagnetic radiation is open-wide and can be observed very far away. The next step consists of the decomposition of the computation domain of integration, which is usually the two-dimensional $\mathbb{R}^2$, into a locally finite number of simpler cells which may be, for instance, hexagons. This decomposition serves as computational grid [Debe19].

Due to this architecture of the FIT method, it is crucial to define the best mesh for the problem, one that should achieve the best trade-off between result accuracy and simulation time. The computational resources are limited and therefore the number of cells the solver is going to be applied to is very important. To simplify the process of mesh creation, CST features an "Automatic Mesh Generation with an Expert System" feature that is an automatic mesh generator that develops the optimised mesh structure for each problem based on the identification of key features of the region and structure.

As discussed, the FIT technique is CST's approach to solve the problem with simulation boundary conditions for the space in which the electromagnetic radiation is propagating. However, several other boundary conditions need to be set in order to allow for the simulator to work. For the high frequency mode, CST has seven boundary conditions: electric (simulates a perfect electric conductor, setting to zero each of the tangential electric fields and normal magnetic fluxes); magnetic (simulates a perfect magnetic conductor, setting all tangential magnetic fields and normal electric fluxes to zero); open PML (simulates free space, allowing the waves to pass the boundary with little reflection, known as perfectly matched layer (PML)); open added space (similar to the open PML boundary but with extra added space for far-field calculation); periodic (links two opposite boundaries simulating a periodical wave expansion in that direction); conducting wall (simulates a lossy conducting wall); unit cell (a two-dimensional periodicity may be set, instead of the direction of the coordinates axes).

Last but not least, in order to achieve relevant results, it is fundamental to simulate the scenario using a model whose dimensions are at the scale of the wavelength of the radiation or bigger. Given that the lowest frequency in these systems is around 400 MHz (see Annex A), that gives λ = 0.75 m. Any section of the model in study should have this as minimum dimension for each of its sides, in order to validate the results for all the systems.

2.8 State of the art

In this section, the state of the art for this work is presented. Since the scope is antenna placing on train roofs for mobile communications, relevant sources for this include works focusing on antennas in train roofs, but also cars and other vehicles with metallic roofs.

Kathrein, a widely recognised antenna manufacturer, offers an installation guide for antennas on trains and buses. In [Kath02], a set of guidelines are included, such as antenna placement in a metallic surface to work as a ground plane, or its proper grounding, as the antenna's voltage cannot exceed 60 V and it might be working close to catenary systems with tens of kV. Mounting position, sealing, painting, as well as the minimum distances to obstacles and other antennas are also defined.

Antonics, another antenna manufacturer, also provides an installation guide for outdoor train and bus antenna placing. In [Anto18], the company mentions the ground plane issue as well, including minimum and recommended ground plane diameters for several different operating frequencies besides sealing and other suggested installation procedures to achieve the best possible results. The document includes additionally instructions to install GPS-amplifier devices attached to train antennas.

More generally, [PRRB11] provides an insight on distributed microstrip patch antennas mounted on a moving platform, featuring near omnidirectional antennas with high gain. By analysing the far field radiation patterns of patch antennas mounted on moving platforms, this paper investigates the optimal location for the antennas, as well as how changing the number of antennas, their position and orientation affects the overall system performance. The paper includes a number of simulations to evaluate the different options, focusing on 900 MHz technology (but including simulations for 1 GHz, 1.7 GHz and 2.5 GHz) and using a car-like vehicle model.

In [Pals13], the influence of conducting environments on antenna radiation patterns is studied, using as a model a vehicle structure with the antenna located in the back end of the vehicle roof. This master thesis dissertation analyses the influence in the radiation pattern of corners and edges in the car roof, as well as the curved plane effect. The analysed antenna is a telephone antenna, connected to the car. The simulations were performed using CST, first with the antenna placed in simple square and curved planes, and then in the full body of a sample vehicle.

In [RuTa17], simulations are performed to determine good practices for antenna design and placement in cars. The work takes into account the need of using the same antenna for different technologies and services, as cars are fitted with an increasing number of driving-aid and entertainment systems (GPS and GSM, for example). This conference paper focuses on the numerical techniques available used for the design of antennas, such as time domain, frequency domain and integral equation techniques.

In order to provide an easier way to analyse high-speed railway communications performance, [PuWa09] relies on integrative modelling techniques to develop a model to associate the field parameters in free space propagation with the circuit parameters at the antenna terminal. Parameters taken into account include the influence of the locomotive, steel rails, earth plane, conducting wire for power supply and others. The paper features the analysis of nine monopole train antennas.

Focusing on another very important issue for antenna placing on train roofs, [DFHR13] gives an insight of how railway power supply catenary systems and train pantographs produce electromagnetic interferences to the surrounding environment, in particular to mobile communication antennas. The work features a train simulation model and several antenna designs. The model deploys a GSM-R 900 MHz antenna in the roof of a high speed train carriage operating a dual-voltage pantograph system (for both 3 kV DC and 25 kV AC power supply). The results include simulations of the antenna reception for different placement sites closer or farther from the pantograph in the roof of the train (1 m to 20 m). This research paper also relied on CST software for the model development.

In order to provide good practice solutions for safe and effective optimisation of train antenna design and installation practices, Siemens Mobility UK developed a study for the Rail Safety and Standards Board (RSSB). In a report [Will09], the study of the impact on the performance of the several different types of antennas takes into account the various types of train roofs and items mounted on it, such as air conditioning units, strengthening bars, roof curvature and pantographs. The different technologies/services are divided in three groups: Group A (GSM-R voice), Group B (GSM-R circuit-switched data and GPRS) and Group C (GSM-public and UMTS 900). The report provides a summary of the minimum spacing needed between antennas and isolation of transceivers in order to provide the required minimum standards for the different technologies.

Finally, in [Ribe18], a related previous work was developed by André Ribeiro, a student from Instituto Superior Técnico (IST) developing his master thesis in the same area. In this dissertation, the main objective was to pursue an analysis of antenna performance for different railway communication systems, studying the influence of the surrounding environment on them. The work focused in GSM-R, LTE-R and the higher band BBRS, and was carried under the development of a train plus antenna model based on CST, which considered antennas parameters and physical limitations of surrounding environments. The main topics of this work were the study of the curved surface in train roofs impact on propagation, as well as the presence of air conditioning and ventilation units obstructing the radiation path. The results are safety distances for antenna placement in train roofs featuring these two characteristics.

Chapter 3

Models and Simulator

In this chapter, the methodology used to approach the problem is presented. Key Performance Indicators for antennas are defined, as well as other relevant aspects having direct effect on simulations. Used antenna models and surrounding environments for antennas deployment are also analysed in detail.

3.1 Model overview

Having studied the fundamental features of the most commonly used technologies in railway communications (TETRA, GSM-R, LTE-R and BBRS), as well as the main aspects of railway communications systems and networks, a model to address the problem is defined in this section.

Following the establishment of scenarios for the usage analysis, a model for design criteria for the deployment of antennas on trains was developed. This model takes the main characteristics of the problem in study into account, i.e. the influence of the defined metrics on the overall performance of the antenna on the train roof. These are the environment parameters.

Information provided from Thales related to their ongoing projects on mobile communications in railway networks helped defining the main issues to address, which are:

- **Longitudinal grooves**: many rolling stock manufacturers fit train carriages with longitudinal metallic grooved surfaces for increased strength and durability. While they do not impact significantly on the carriage weight, when fitted in the roof of the train they might affect the radiation propagation of antennas placed there. Scattering might generate destructive interference and other multipath phenomenon degrading overall antenna performance. In Figure 3.1, an example of this design can be seen.

Figure 3.1 Longitudinal grooves on rolling stock roof (adapted from [Teoh09]).

- **Variation of antenna height**: a metallic support structure might be fitted on top of the train roof to accommodate the installation of mobile communication antennas, which in these situations are no longer mounted directly on the train roof. With a smaller ground plane, and in presence of one extra metallic structure, the performance upgrade from improved line-of-sight might be jeopardised by multipath reflection and other side effects. In Figure 3.2, an example of this application can be seen.

Bearing these in mind, other surrounding environment factors may be taken into account, such as roof shape (curve or irregular) as well as other equipment fitted that might affect line-of-sight propagation.

Figure 3.2 Elevated ground plane for antenna placement (adapted from [Sour13]).

Additionally, antenna-specific parameters also need to be considered, as performance is affected by them. Most relevant parameters for the problem under study include electrical specifications, such as working bandwidth (which varies with the used technology), antenna gain and polarisation type as well as physical specifications (antenna dimensions).

With the input parameters defined, the model relies on the following software to process data:

- **Antenna Magus**: software tool designed for the antenna design and modelling process, which helped in the development of working 3D models of the antennas under study [SIMU19];
- **CST Microwave Studio**: a tool for 3D electromagnetic simulation of high frequency components, enabling fast and accurate analysis of antennas, which was used for the antenna placement model through the use of the transient solver, one of the available solvers [CSTS19].

In Figure 3.3, the followed methodology is shown, defining the critical input parameters, how calculations/simulations are performed and the output key performance indicators.

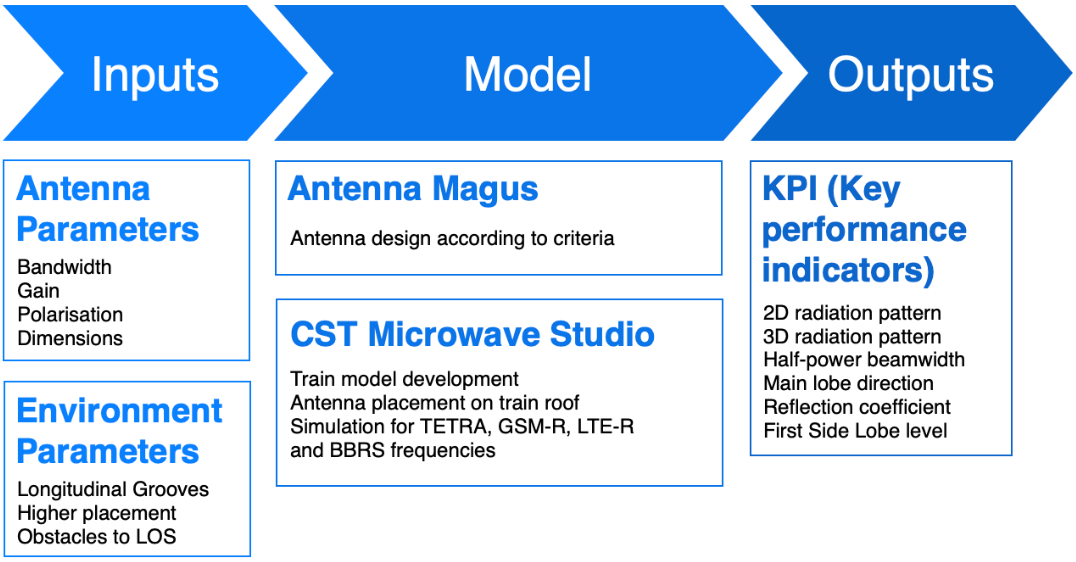

Figure 3.3 Model Configuration.

This said, the model consists of the development, through Antenna Magus, of a working 3D model of the antenna one is planning to fit in a given train, to operate a specific railway communication system, followed by its placement in several locations on the model of the train carriage and subsequent simulation using CST Microwave Studio software.

The results provided by the software include the 2D and 3D radiation patterns, the Half-Power Beam Width, the reflection coefficient and the first side lobe level. With these properties, it is possible to evaluate how changes in the positioning of the antenna affect the overall system performance, as well as to measure the impact of the grooved surface and the higher placement using a metallic structure.

3.2 Analytical models

In this section the relevant technical aspects affecting antennas' performance are defined, with special attention to the image theory technique used to depict the operating environment of antennas placed on train roofs, as well as the vertical and horizontal electric dipole models.

3.2.1 Image Theory

The behaviour of antennas over infinite ground planes is of interest for the performance analysis of antennas, since these are usually designed to make use of the ground plane. Similarly, train roofs can serve as ground planes for antennas, especially thanks to the metallic properties of the materials they are commonly made of [SHum19].

To analyse the performance of antennas fitted near infinite conductor planes, and given that they generate reflections, virtual sources are introduced to account for these reflections, which act as virtual antennas placed as a reflected image of the real ones, forming an equivalent system. For analysis purposes, the equivalent system gives the same radiated field on and above the conductor as the actual system itself. However, it is important to note that above the conductor, the equivalent system does not give an accurate estimate of the radiated field in the real situation. This is not an issue, since the field above the conductor is not relevant for the problem under study.

The image theory method has been developed to study the performance of antennas in close proximity to near conductor planes acting like a perfect reflector. Although metals usually absorb a small part of incident radiation, they are usually considered Perfect Electric Conductors (PEC). This is a classification attributed to surfaces that exhibit ideal electric conducting properties, satisfying the electromagnetic boundary conditions. Electric conductivities of PEC are on the order of 10^7 to 10^9 S/m and considering metals PEC is a good approximation for most electrical characteristics, especially when using metal surfaces as ground planes for antennas applications [Bala16]. In Figure 3.4, a vertical electric dipole is placed above and infinite, flat, PEC surface.

This method consists mainly in a geometrical technique to calculate the radiation pattern of an antenna placed near a PEC, since it is almost identical to the pattern if instead of the reflective ground plane a second, similar antenna was placed right under the real one. This second apparent source of radio waves is the image antenna, which is used in calculating electric and magnetic field vectors, and electromagnetic fields emitted by the real antenna. Each charge and current in the real antenna has a correspondent one in the image antenna. In Figure 3.4 this becomes clear as the real propagating waves (both direct and reflected ones) are depicted with a solid line while the virtual waves, used to ease the reflection calculations, are depicted with a dashed line.

In order to form an image and to validate results from the image theory method, the ground plane surface must have dimensions of at least a quarter-wavelength of the waves radiating from the antenna. Since the lowest frequency under study is around 400 MHz (lowest ETSI-standardised TETRA band) one has a model application limit of 0.1875 m. Therefore, no problems arise with boundary conditions in the application of the image theory method to the problem under study given the antenna is placed at least 20 cm from the edge of the train roof [SHum19].

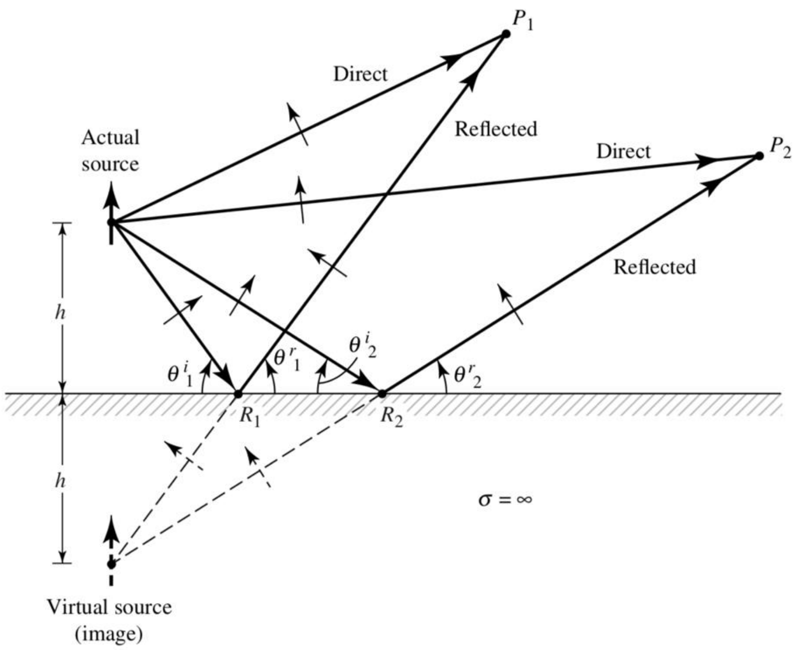

Figure 3.4 Vertical electric dipole above an infinite, flat, PEC (extracted from [Bala16]).

However, the image theory method is limited to far-field, due to the higher complexity needed to compute near field behaviour of real and image antenna propagation. The far-field region is given by [Bala16]:

$$r_{[\mathrm{m}]} > \frac{2l^2{}_{[\mathrm{m}]}}{\lambda_{[\mathrm{m}]}} \tag{3.1}$$

where:

- l is the largest geometrical dimension of the antenna;
- λ is the wavelength of the waves radiated by the antenna;
- r is the distance between the antenna and the observation point.

3.2.2 Vertical electric dipole

In a vertical electric dipole, both the real and the image antennas have vertical polarisation, with the same direction, as seen in Figure 3.4 with the arrows representing both sources.

The total electric field is equal to the product of the field of a single source positioned symmetrically about the origin and the array factor, which is a function of the antenna's largest dimension (h) and the observation angle (θ), which is:

$$E^V_{\theta\,[\mathrm{V/m}]} \cong j\eta_{[\Omega]} \frac{k_{[\mathrm{m}^{-1}]} l_{[\mathrm{m}]} I_{0\,[\mathrm{A}]} e^{-jk_{[\mathrm{m}^{-1}]} r_{[\mathrm{m}]}}}{4\pi\, r_{[\mathrm{m}]}} \sin\theta \left[2\cos\left(k_{[\mathrm{m}^{-1}]} l_{[\mathrm{m}]} \cos\theta\right)\right], \quad l \geq 0 \tag{3.2}$$

where:

- η is the impedance (120π [Ω] for free space);
- k is the free space wave number;
- I_0 is the maximum current in the antenna;
- θ is the angle between the positive half of the Z-axis and the observation point;
- h is the antenna height.

The array factor provides a relation between the radiation pattern and the antenna height, which is within brackets in (3.2). This factor has a direct effect on the electric field form and amplitude.

The shape and amplitude of the field depends also on the positioning of the element relative to the ground. For $h > \lambda/4$, minor lobes are formed, in addition to the major ones, with its number increasing the higher the element is placed. In general, the number of lobes can be given by the closest integer to [Bala16]:

$$N_L^V \cong \frac{2h_{[\mathrm{m}]}}{\lambda_{[\mathrm{m}]}} + 1 \tag{3.3}$$

The radiated power of the vertical electrical dipole can be written as [Bala16]:

$$P_{rad} = \pi\eta \left|\frac{I_0 l}{\lambda}\right|^2 \left[\frac{1}{3} - \frac{\cos(2kh)}{(2kh)^2} + \frac{\sin(2kh)}{(2kh)^3}\right]. \tag{3.4}$$

As $kh \rightarrow \infty$ (antenna height increases to move away from the ground plane) the radiated power is equal to that of an isolated element, which makes sense, since the reflected radiation (calculated through the virtual source) becomes less intense until it is approximately zero.

3.2.3 Antennas placed on irregular surfaces

In order to evaluate the impact of the longitudinal grooves on the antenna propagation, a research on available models was pursued. The goal was to find a relevant propagation model that could be adapted to the specific conditions in study, as seen in Figure 3.1.

There is a wide range of propagation models applicable to a wide range of circumstances, such as Free Space, Plane Earth, Obstruction by a Knife Edge, Urban and Suburban. However, these theoretical models are approximations to reality, since they do not account for all factors influencing propagation and are designed to easily allow changes in parameters [Corr18].

Furthermore, most propagation models focus on long distance propagation, assuming that antennas are positioned in a correct way. Due to this, these models usually do not account for the influence of the antenna's close environment, which is the focus of the problem under study.

For the strengthening bars configuration, the longitudinal grooves in close proximity with the MT antenna generate destructive interference due to multiple reflections. Scattering from rough surfaces, also known as Rayleigh Scattering [Nord13], was the theoretical approach studied taken.

The Rayleigh Condition defines basically two heights for the reflection and analyses the difference in angle between specular and diffuse reflection components. The simplified model for this phenomenon takes into account the statistical distribution characterising the terrain height, considering 1st order scattering (low roughness surfaces) and the condition that the wavelength is much smaller than the roughness characteristic dimensions [Fern18].

Since the lowest frequency in study comes from the lowest bands of TETRA, at around 400 MHz, that gives a wavelength of 0.75 m. The longitudinal grooves present in most trains are considerably smaller than this. Even the higher frequency bands in study (BBRS, 5.9 GHz) have a wavelength in the order of 5 cm, within the order of magnitude of the groove dimensions. Therefore, one cannot use the Rayleigh simplified model to determine the two reflection components on the antenna's propagation on train roofs.

Another option is to consider the roof a Frequency Selective Surface (FSS). These are surfaces typically flat and made of composite material, designed to be transparent in some frequency bands while reflecting, absorbing or diffracting others. To perform the frequency filtering, these surfaces absorb some radiation using specific lossy materials or resonant structures, while diffracting, reflecting or interfering with other frequencies, through grating or using a guided-mode resonance.

There are several types of FSS, with the different configurations allowing these materials to be used in a wide range of applications, such as antenna radomes, dichroic reflectors, artificial magnetic conductor or waveguide applications [KiCh06].

Since train's strengthening bars usually follow a periodic layout, one can consider the said configuration a Frequency Selective Surface. FSS response to radiation varies a lot with surface geometry, electric properties of the material and the spacing between unit cells. However, the wide majority of the work developed in this field focuses in developing FSS to filter or diffract a specific source of radiation, with no prior work found on the impact of a metallic FSS on a radiation source, since these filters are usually made of dielectric materials.

This said, no theoretical approach on the impact of metallic longitudinal grooves in mobile communication antennas was found, and therefore this work focuses on the simulation of this phenomena in order to understand its impact on the antenna propagation.

3.2.4 Antennas placed on elevated ground planes

To understand the impact of the height of the antenna's ground plane, it is important to analyse what does this distance affect in terms of the antenna behaviour and propagation performance. While improving Line of Sight propagation from the train to the trackside mounted antennas, placing the antenna in an elevated plane does mean that the ground plane for the antenna becomes this higher plane, instead of the whole train roof.

Monopole antennas are very popular in mobile communication systems due to their size reduction over equivalent dipole designs, and also their increased directivity. However, monopole antennas require an effective ground plane to work properly. This type of antennas requires usually a ground plane with a diameter on the order of $\lambda/2$ to perform well, with the transmission loss increasing substantially if the diameter of the ground plane is reduced to below $\lambda/10$ [LiRL05].

Theoretically, the performance of monopole antennas placed on infinite, metallic ground planes is independent of it. However, for finite ground planes, the surface acts also as a radiator, with some of the current fed to the antenna being radiated by the metal ground plane. In fact, the current distribution on the ground plane affects the bandwidth, gain and radiation pattern of the antenna [WeCY10].

Measurements and simulations performed in a range of frequencies from 2 to 12 GHz [WeCY10] allow to conclude one should expect that:

- Antennas with larger ground plane sizes operate with higher efficiency;
- The width of the ground plane affects the efficiency more than the length;
- Increasing the length of the ground plane reduces the lower cut-off frequency of the antenna, meaning the antenna's effective bandwidth increases.

It is expected that the antennas behave similarly for frequencies slightly lower than the range tested in [WeCY10]. Also noteworthy is that simulation and measurement results were in good agreement for most of the parameters the mentioned conference paper focuses on.

Taking all this into account, the following sections include a detailed analysis of the antennas in study, and using the operating frequencies for each technology, it is possible to define minimum physical dimensions for the ground plane of the working monopole antenna. Additionally, most antenna's Original Equipment Manufacturers (OEM) provide on each antenna's datasheet the information if a ground plane is needed and its size, in the device placement instructions.

3.3 CST simulation tool

As seen in Section 2.7, CST is a powerful simulation tool that features a variety of simulation options and a wide range of solvers available. Since the goal of this thesis is to evaluate antennas performance operating at frequencies that range from several hundred MHz up to a few GHz, the relevant tool is the high frequency simulation [CSTS19].

As explained in detail in [Ribe18], the most adequate application area for the problem under study is the MW & RF & Optical. This area features also several different workflows from which the most appropriate is the antennas option, since the study focuses on antenna propagation. In the category of antennas, an additional range of options is available, allowing for the study of several types of antennas including waveguide, planar, wire, and reflector antennas. However, for this work, the relevant type of antennas in study is the wire antennas since this category includes monopoles, the most common type used in railway communications.

CST has also six different solvers, as mentioned before, and the most adequate for the problem under study are the time domain, the frequency domain and the integral equation solvers, as explained in [Ribe18]. These are the solvers that provide the best understanding of the electromagnetic field behaviour of structures like the ones this work focuses on, with the designated frequencies.

The best solver for this problem happens to be the transient solver, which is based in a hexahedral mesh and is capable of showing the broadband frequency domain effects through the scattering S-matrix. Using this matrix eases the process of understanding the performance of the antennas in study, as it is a useful tool to express a wide range of parameters of interest, such as gain, return loss, voltage standing wave ratio (VSWR) or reflection coefficient [Bala16]. The transient solver is also a good option due to its ability to simulate several frequencies in a single run, which eases the process of testing several wanted frequencies for the technologies in study.

In order to perform the desired simulations, CST requires the creation of a mesh to the problem, which consists of the definition of the geometric domain for the simulation. When performing numerical solutions of Maxwell's equations in electromagnetic simulations, it is well known that the quality and type of mesh used for discretising the model are the key factors for the accuracy of the results but also for the simulation speed. Therefore, it is crucial to choose the meshing technique that offers the best trade-off between speed, accuracy and memory requirements.

While the definition of the mesh can be made manually, that process is highly time consuming, and CST features two different automatic mesh creation options: one is the "Automatic Mesh Generation with an Expert System", in which the program identifies the relevant features of the models in which the simulation is taking place, defining a mesh that provides the best trade-off between simulation time and result accuracy; the other is the "Adaptive Mesh Refinement", which involves the creation of an initial mesh and subsequent refinement through local estimation procedures.

The size of the mesh cells is also conditioned by numerical dispersion. This phenomenon consists of each frequency component propagating at a slightly different velocity in the mesh, due to the space discretisation of the problem. In order to minimise this effect, providing a guarantee that the defined mesh works well for all frequencies, the shortest wavelength of interest must be spatially sampled at a rate of at least 10 mesh cells per wavelength. Since the highest frequency is 5.9 GHz (BBRS Wi-Fi non-standard frequency), that gives a minimum wavelength of 0.05 m and a resulting maximum mesh cell size of 5 mm. This parameter is calculated automatically by CST through the Lines per Wavelength (M_{LW}) setting, at the Mesh Properties menu, which should be kept at 10, minimum.

On the other hand, the smallest mesh size is the main constraint for the Maximum Mesh Step (M_{MS}), which is the speed at which the signal is propagated in the computational volume. The higher the time step, the best results. However, the time step cannot be increased indefinitely, since it must be small enough to ensure stability of the simulation. The minimum number of mesh cells across the diagonal of the smallest face of the box bounding the computational volume is defined by the Lower Mesh Limit (M_{LL}) setting, being particularly important for electrically small problems, since in these the Lines per Wavelength setting does not have a good control over the mesh.

The relationship between the M_{LL} and the M_{MS} is given by:

$$M_{MS} = \frac{D_{SBF}\sqrt{3}}{M_{LL}} \tag{3.5}$$

where:

- D_{SBF} is the smallest box face diagonal allowed in the meshing grid.

The ratio between the largest and the smallest mesh cells in the computational volume is defined by the Mesh Line Ratio Limit ($MLRL$) parameter. Since the largest mesh cell is already determined by the shortest wavelength and the M_{LW} parameter, increasing $MLRL$ results in a decrease of the size of the minimum mesh cell, resulting in smaller structural features in the model being properly meshed, but also increasing the total number of mesh cells. As a result, the simulation time will be higher, therefore this option should be used only if meshing small features is absolutely necessary. For the problem under study, since the goal is to analyse the overall performance of the system, there is no need to reduce the size of the minimum mesh cell too much as it is not useful to determine more in detail the level of radiation in specific points of the meshing grid.

Instead of defining the $MLRL$ parameter, it is possible to specify the Smallest Mesh Step, to define the smallest feature size in the model that needs to be meshed [CSTS19]. Regarding the mesh, the used input parameters consist of defining the mesh type (hexahedral), the number of cells per wavelength near and far from the model as well as the minimum cell size for the adaptive mesh creation.

Using the monopole layout designed by [Ribe18] the antenna input parameters include the frequency centre, its height and diameter, as well as the ground plane dimensions to simulate the reference antenna performance (width, length, metal thickness).

To analyse the performance of mobile communication systems, one should look at the antennas performance through a number of parameters. First, the radiation intensity, which is related to the far-zone electric field of an antenna [Bala16]:

$$U(\theta,\varphi)_{[\mathrm{W}]} = \frac{r_{[\mathrm{m}]}^2}{2\eta_{[\Omega]}} \left|E(r,\theta,\varphi)_{[\mathrm{V/m}]}\right|^2 \cong \frac{r^2}{2\eta}\left[\left|E_\theta^O(\theta,\varphi)\right|^2 + \left|E_\varphi^O(\theta,\varphi)\right|^2\right] \tag{3.6}$$

where:

- $E(r,\theta,\varphi)$ is the far-zone electric field intensity of the antenna;
- E_θ^O and E_φ^O are the far-zone electric field components of the antenna.

While the directivity of the antenna is a measure that describes only its directional properties, and is therefore defined by the radiation pattern, the gain of the antenna in a given direction is defined as the "ratio of the intensity, in a given direction, to the radiation intensity that would be obtained if the power accepted by the antenna were radiated isotropically" [Bala16]. The gain is given by:

$$G_{[\mathrm{dBi}]} = 10\ log_{10}\left(4\pi\frac{U(\theta,\varphi_{[\mathrm{W}]})}{P_{in_{[\mathrm{W}]}}}\right) \tag{3.7}$$

where:

- P_{in} is the total input accepted power by the antenna.

To analyse an antenna's performance, other parameters can be taken into account. One of which is the input impedance, defined as "the impedance presented by an antenna at its terminals". The input impedance of an antenna depends on many factors, such as its geometry, its method of excitation and its proximity to surrounding objects. However, if the antenna is well-adapted when mounted on the train's rooftop, impedance losses will not change, and thus this parameter is not of interest for this work.

Concerning the beamwidth properties, the Half-Power Beam Width helps characterise the antenna's directivity, and is commonly analysed in terms of the electric field, considering [Bala16]:

$$E_{\alpha_{3dB}[\mathrm{V/m}]} = \frac{E_{max[\mathrm{V/m}]}}{\sqrt{2}} \quad , \quad \theta = \frac{\alpha_{3dB}}{2} \tag{3.8}$$

where:

- E_{max} is the maximum electric field of the main lobe (with $\theta = 0$ as the maximum lobe direction).

Additionally, to understand if the antenna is well adapted, one can analyse its reflection coefficient, Γ:

$$\Gamma = \frac{Z_{in} - Z_0}{Z_{in} + Z_0} \tag{3.9}$$

where:

- Z_{in} is the antenna input impedance;
- Z_0 is the characteristic impedance of the transmission line connecting to the antenna.

This coefficient is also the S_{11} element of the antenna scattering matrix (or **S**-matrix), which relates the outgoing and incoming waves of a given *n*-port network.

3.4 Isolated antenna performance

Since most antennas placed on trains for mobile communications are monopoles, this works focuses on simulating monopoles performance under the specific conditions described previously. In this section, the simulation approach for the problem is detailed, featuring the antennas technical aspects description, and how the model is going to be analysed concerning its results.

In order to perform the desired simulations for the different systems, the first step is to define the antennas used in the simulations. Since the focus of the simulations are single-band antennas, one can choose specific ones for each system:

- For simulations using the TETRA system, the frequency chosen was 400 MHz and a monopole antenna based on the Kathrein 702021 (datasheet is in Annex B) antenna is used;
- Regarding GSM-R simulations, simulations are performed using 900 MHz frequency, and a monopole based on the Kathrein 741009 (datasheet is in Annex C) antenna is used;
- For LTE-R simulations, 2.6 GHz is the used frequency, and the model of a monopole based on the Kathrein 87010010 (datasheet is in Annex D) antenna is used;
- Finally, for simulations of the BBRS Wi-Fi system, 5.9 GHz is the chosen frequency, using a monopole antenna design based on the Kathrein 87010022 (datasheet is in Annex E).

Based on a common monopole layout design by [Ribe18], the specific parameters of the aforementioned antennas were defined in CST in order to test the different monopole configurations to see if they perform as expected from a theoretical point of view, as follows.

By analysing the datasheets in the Annexes, all four monopole antennas have an input impedance $Z_0 = 50\,\Omega$. The gain is said to be 0 dBi taking the quarter-wave antenna as the reference, and theoretically the quarter-wave monopole should have a gain similar to twice the half-wave dipole (3 dB greater gain). Since a half-wave dipole has a gain of 2.19 dBi, the equivalent quarter-wave monopole is expected to radiate with a gain of 5.19 dBi. In Table 3.1 the sizing of the monopoles for each system can be seen. The base is the quarter-wavelength antenna, with tuning to achieve reasonable results.

For all simulations, the ground plane was initially sized with 500 mm length/width, since it is the minimum size defined in the datasheets of all the antennas in which the monopoles were based. For the three higher bands, it is possible to achieve reasonable gains, as shown in Table 3.1; in these bands, the matching also worked well with such a ground plane, with S_{11} values below -10 dB. However, for the 400 MHz band, the gain with a ground plane of 500 mm length/width is extremely low (1.8 dBi) while the S_{11} is significantly above -10 dB.

To solve this problem with the 400 MHz band, several simulations were performed increasing the monopole size, but even considering a height of more than 300 mm it is not possible to achieve reasonable gains. The only way to achieve the impedance match needed to validate the antenna is to tune it with a bigger ground plane. With a ground plane of 2000 mm length/wide, it is possible to achieve reasonable figures for the antenna gain and S_{11} parameter, as seen in Table 3.1.

The maximum and minimum frequency were considered 1.4 and 0.6 times the operating frequency.

As explained before, the chosen solver is the transient solver, using a hexahedral mesh with 20 cells per wavelength in the antenna near field and 10 cells per wavelength in the far field, adding two additional mesh groups near the monopole itself and its feeding port. The bounding box for the mesh is defined to be sized with the base being the ground plane. The simulation boundary conditions are set to be open added space, adding extra space for far-field calculation compared to open PML. In this case, the meshing conditions applied result in 249 969 mesh cells, with a simulation time of 5 minutes and 10 seconds, using a 2018 MacBook Pro with a 3.1 GHz Intel Core i5 processor in a VMWare Virtual Machine software running Windows 10 N with 4 processor cores and 5 GB of RAM memory allocated.

For 400 MHz, one tried to simulate the same scenario with a higher number of cells per wavelength (40 near/20 far from model), but results do not change significantly, while simulation time increased almost six-fold to 28 minutes and 23 seconds.

Table 3.1 Simulated gains of the monopoles tested for the different systems.

Communication technology	**TETRA**	**GSM-R**	**LTE-R**	**BBRS**
Monopole height [mm]	165	77	27	12
Operating frequency (f) [MHz]	400	900	2600	5900
Simulated gain [dBi]	5.5	4.3	5.2	5.1
Difference to reference [dB]	+0.32	-0.89	+0.03	-0.04
Reflection coefficient (S_{11}) [dB]	-13.4	-55.9	-20.6	-17.1

The gain of the simulated antennas is close to the theoretical value, as seen in Table 3.1. Since all the tests were performed with an appropriate ground plane, the behaviour of the simulated model is very close to the theoretical performance. One also compared the simulated gain results with the simulated directivity, and it was possible to conclude they are almost identical, meaning the model depicts a lossless antenna [Bala16]. The small differences observed, in some cases a higher than expected gain, in others lower, is due to simulation approximations and the monopole design itself. In Annex F, it is possible to see the 3D far-field radiation patterns of all frequencies.

3.5 Train model

Having the antennas for each of the frequencies in study, one needs to develop an accurate but simple train model that can be imported to CST to test the overall system performance with the antennas. Concerning the grooved roof, to characterise the rolling stock roof grooves, three dimensions are relevant: groove height h_g, groove width w_g and the distance between grooves d_g (perpendicular to the length), as in Figure 3.5.

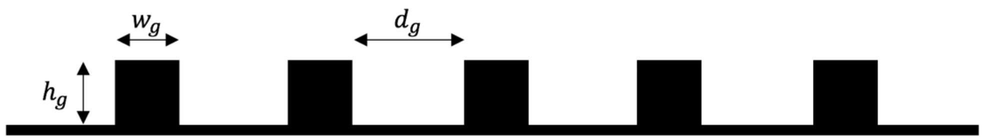

Figure 3.5 Longitudinal grooves in train section - cross section.

To analyse the impact caused by placing the antenna in this auxiliary structure, the dimensions of the structure are relevant (elevated ground plane width w_p and length l_p) as well as its height regarding the train roof h_p as in Figure 3.6. The antenna is placed at the centre. In the simulations, since the platform supports are most likely made of a dielectric material, these are not be fitted, therefore the antenna and its ground plane are placed to a specific height regarding the roof, with no support.

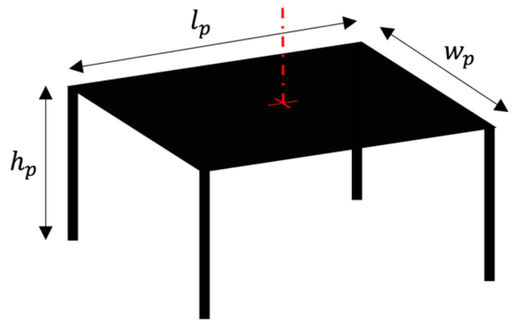

Figure 3.6 Elevated ground plane for antenna placement on train roof.

To validate the design of the grooves accurately, a wide research was done on the topic, however it was not possible to find relevant information on the dimensions of the strengthening bars on train rolling stock. To solve this problem, measurements were made to base the models on factual data. The measurements were performed on the 18th of March 2019 on the Santa Apolónia railway station, with the results shown in Table 3.2.

Table 3.2 Rolling stock longitudinal grooves measurements.

Sorefame/Corail Intercity 1st class car		
Side	Lateral panels	Roof panels
Groove width w_g [mm]	40	12
Distance between grooves d_g [mm]	35	20
Groove height h_g [mm]	11	23
Sorefame UTE class 2200		
Groove width w_g [mm]	21	
Distance between grooves d_g [mm]	21	
Groove height h_g [mm]	13	

The dimensions were measured according to the model depicted in Figure 3.5. The rolling stock measured was a Sorefame/Corail Intercity 1st class car, which features two different grooving patterns, as seen in

Figure 3.7 (a). In Figure 3.7 (b) the longitudinal grooves in a power train plus carriage Sorefame UTE tripe unit class 2200 can be seen, as well as the GSM-R antenna fitted on the roof of the first car, directly placed above the grooved roof surface.

Since the computational resources were limited, in order to be possible to simulate the behaviour of different antennas, and specially for the higher frequencies, a simplification of the train was made, focusing only on the front power unit's roof, a grooved box surface, as seen in Figure 3.8. This model features a width of 3.5 m, 4 m of length and 0.340 m of height, which is enough to evaluate the impact of the grooved surface. In order to study the impact of a grooved surface in a curved roof, one designed a curved, grooved model similar to the one depicted in Figure 3.8, with similar dimensions but with a curved surface, depicted in Figure 3.9. To compare with the flat ground propagation, a rectangular box of PEC was defined, with approximately the same dimensions.

a) Sorefame Intercity car b) Sorefame UTE 2200

Figure 3.7 Rolling stock longitudinal grooves measured, March 2019.

Both models feature grooves sized to sit in the middle of the range of measurements that were made, with width w_g = 15 mm, height h_g = 25 mm and distance between them d_g = 15 mm.

The increase in the size of the model would not offer significant advantages for the evaluation of the antenna performance in these specific conditions, since the goal is to assess the impact of grooving patterns in the propagation, in the close proximity of the antenna. Using a complete model of a train unit would allow to understand the impact of the whole rolling stock piece in the radiation pattern, but that result would not be relevant, since simulating 3 or 4 m farther from the antenna placement location would include not only the train design pieces but also the surrounding scenario [Ribe18].

Since the goal of this thesis is to evaluate the impact of the grooving surfaces on the overall system performance, the simplified model of the grooved roof is enough to compare it with a reference roof scenario, with no grooves. Increasing the size of the model would result on a higher mesh needed and increase substantially the simulation time.

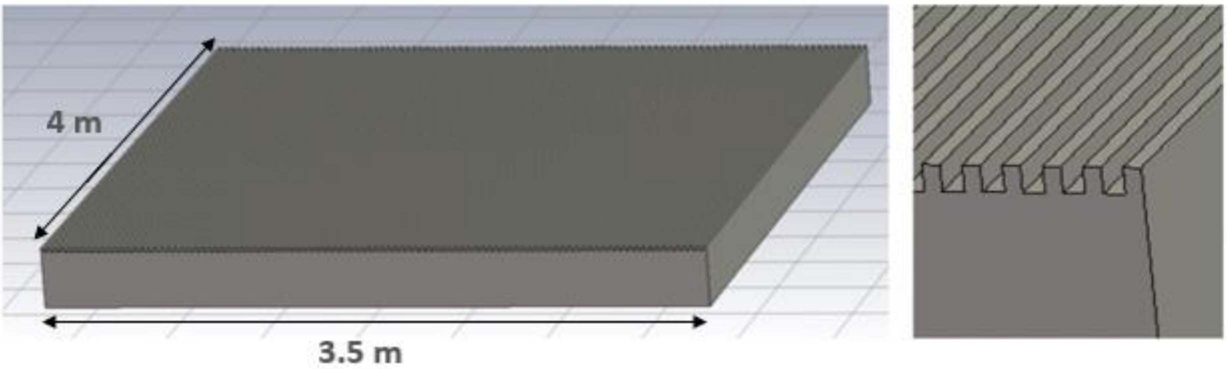

a) Model overview b) Surface detail

Figure 3.8 Straight grooved train model.

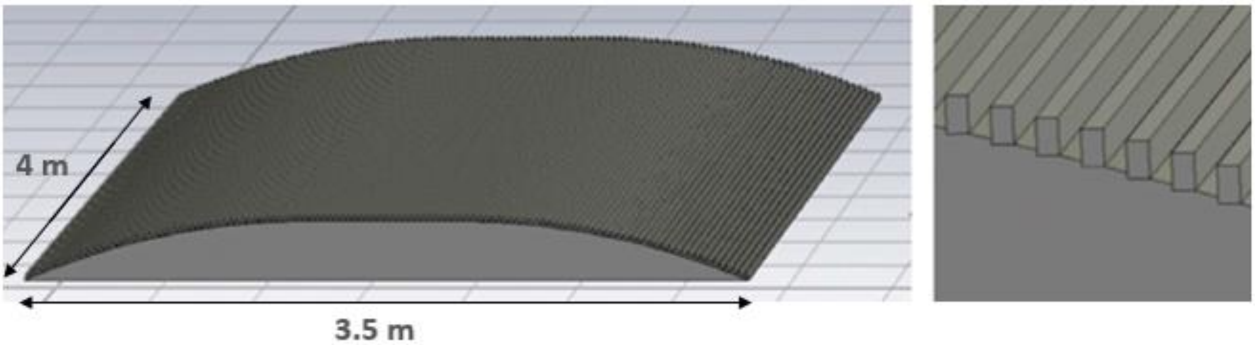

a) Model overview b) Surface detail

Figure 3.9 Curved grooved train model.

3.6 Key Performance Indicators (KPI)

Having the 3D models for simulation and the monopoles, it is important to define the KPIs that help in addressing the main topics of this work. As it is possible to see in Figure 3.3, several performance indicators are set, and the performance analysis is mostly based on these:

- The **2D radiation patterns** provided by CST allow a comprehensive analysis of the far-field power radiated by the antenna, and can be presented in a 2D graph with θ and ϕ coordinates but also in polar coordinates, allowing different cuts for both elevation and azimuth planes, with the possibility to have the data points extracted to develop further quantitative analyses;
- The **3D radiation pattern** is also generated by CST and allows a qualitative overview of the global changes introduced by each of the scenarios under simulation, indicating the gain;
- The **half-power beam width** along with the **main lobe direction** and the **side lobe level** allow to understand the directivity of the antenna in the specific scenario, which is important since not all angles matter equally for the performance of the overall system;

- The **reflection coefficient** is an important measure of how well-adapted the antenna is.

From the main lobe direction (θ_{max}) and half-power beam width (α_{3dB}) metrics, it is possible to compute the minimum ($\theta_{3dB-[°]}$) and the maximum ($\theta_{3dB+[°]}$) angles in which the main lobe radiates with at least half of the gain through:

$$\theta_{3dB-[°]} = \theta_{max\,[°]} - \frac{\alpha_{3dB\,[°]}}{2} \quad (3.10)$$

$$\theta_{3dB+[°]} = \theta_{max\,[°]} + \frac{\alpha_{3dB\,[°]}}{2} \quad (3.11)$$

With these two angles the interval in which at least half of the gain is radiated, Θ_{3dB}, is defined:

$$\Theta_{3dB\,[°]} = \left[\theta_{3dB-[°]}; \theta_{3dB+[°]}\right] \quad (3.12)$$

This measure is useful to assess if the grooved surfaces change the radiation pattern in a way that impacts severely the radiation in the window of relevant angles defined in Section 2.6.

In order to understand the impacts caused by the surfaces in more detail, the far-field polar plots are exported from CST in both planes $\theta = 90°$ and $\phi = 90°$, and the far-field gains for the two grooved surfaces compared in the relevant angle window. The angles acquired to compute the attenuations are depicted in green in Figure 3.10, as well as the defined relevant angles.

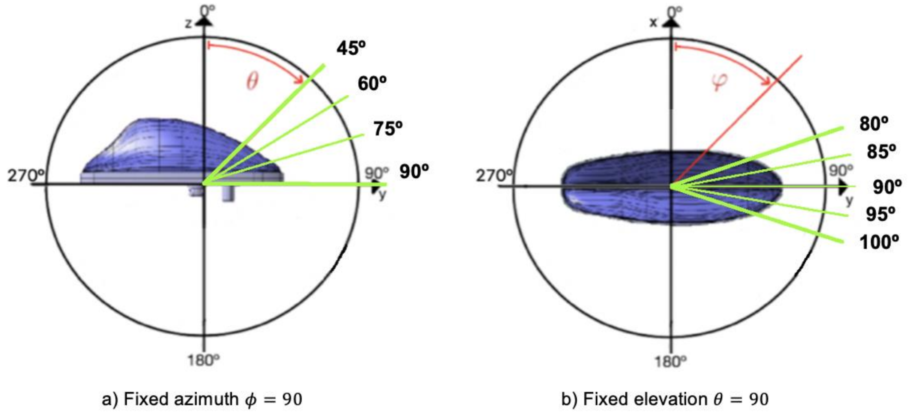

Figure 3.10 Relevant angle window and acquisition angles for both planes.

These are the angles in which is relevant to assess the impact of the grooved surfaces, since these are the most critical angles for the performance of the system in a railway context, in most scenarios. The resulting gain difference is given by the following expression:

$$\Delta G_{[\mathrm{dB}]}(\theta,\phi) = G_{gro_{[\mathrm{dBi}]}}(\theta,\phi) - G_{fla_{[\mathrm{dBi}]}}(\theta,\phi) \quad (3.13)$$

where:

- G_{gro} is the gain for the grooved surface (straight or curved), acquired from the CST polar plot far-field result for a specific co-elevation and azimuth angle pair;
- G_{fla} is the gain for the flat surface acquired from the CST polar plot far-field result for a specific co-elevation and azimuth angle pair.

Furthermore, with the angles acquired from the polar plots a mean attenuation can also be computed, through the following general expression:

$$\overline{\Delta G_{[\mathrm{dB}]}(\theta,\phi)} = \frac{1}{N_{ang}} \sum_{n=1}^{N_{ang}} \Delta G_{n_{[\mathrm{dB}]}}(\theta,\phi) \tag{3.14}$$

where:

- N_{ang} is the number of angles used for the sampling;
- $\Delta G_{n_{[\mathrm{dBi}]}}(\theta,\phi)$ is the gain difference for the angle n.

Using the results from CST, a mean gain difference can be calculated for $\phi = 90°$ (46 angles):

$$\overline{\Delta G_{[\mathrm{dB}]}(\theta,\phi = 90°)} \quad , \quad N_{ang} = 46 \tag{3.15}$$

Similarly, the resulting gain difference for a fixed co-elevation of $\theta = 90°$ (21 angles) is given by:

$$\overline{\Delta G_{[\mathrm{dB}]}(\theta = 90°,\phi)} \quad , \quad N_{ang} = 21 \tag{3.16}$$

Additionally, and specially for lower frequencies, due to track morphology and the longer range at these frequencies, a BS may be placed in an elevation or surrounding vantage point instead of the trackside [Sour13]. Due to this, it is also relevant to compute the average gain for all angles, which consists of using (3.14) with $N_{ang} = 360$.

3.7 Model assessment

Having designed the necessary antennas and the model of the train depicting the two configurations of the grooved surface to test, in this section tests made to assess the validity of the model are presented.

First, the flat roof surface was tested for all the four frequencies to serve as reference for further simulations. The far-field view for the 2.6 GHz antenna with the PEC box flat surface can be seen in Figure 3.11, featuring a gain of 7.7 dBi. The reflection coefficient is acceptable at the central frequency for 2.6 GHz, as can be seen in Figure 3.12.

For the rest of the frequency range in test the results were similar, corresponding to an increase in gain due to the increased PEC surface and higher directivity, which is more subtle in the lower frequencies and shows a bigger impact for the higher ones. In Annex G, it is possible to see the model assessment tests for all frequencies. In Table 3.3, it is possible to see the attained results for all frequencies, with the cutting plane set for $\phi = 90°$, meaning a cut along the train in forward direction. The PEC box used is the same for all four antennas.

The angular width shows a significant decrease in the higher frequencies, with the side lobe level magnitude being higher in the lower end of the frequencies. It is then possible to conclude the higher frequency antennas have a higher directivity, with all systems achieving a similar total efficiency.

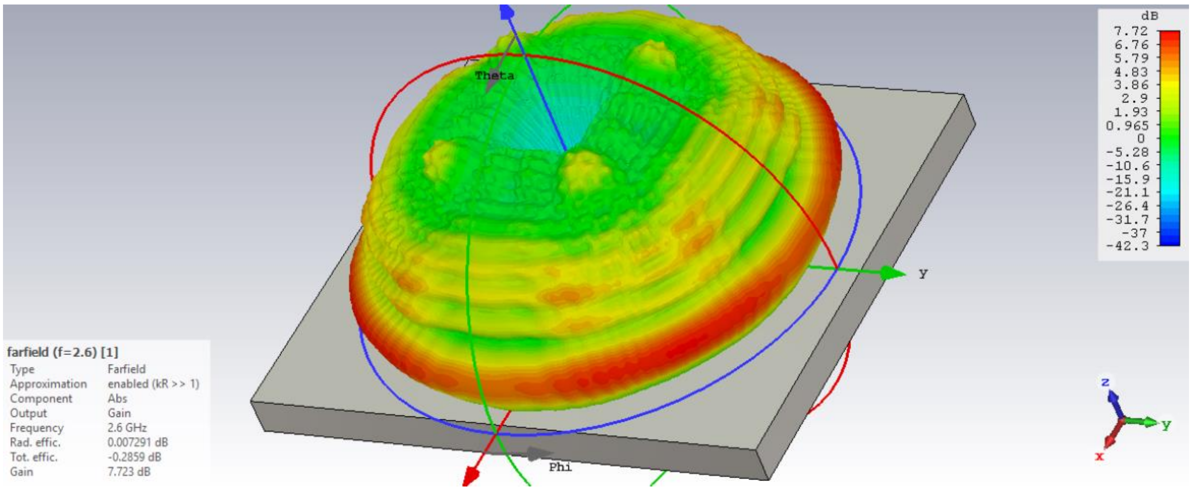

Figure 3.11 Far-field view of the reference flat model with a 2.6 GHz monopole.

Regarding the size of the model, and as mentioned in the previous section, this simplification of the train roof required, for the 5.9 GHz antenna, a mesh with 4.6 million mesh cells, and took 2 hours and 46 minutes. Considering a full-scale train model, even with just one car, would result in more than 336 million mesh cells for the same simulation. With similar settings such a test would take more than 200 hours, while it would not add relevant considerations for the purpose of this work.

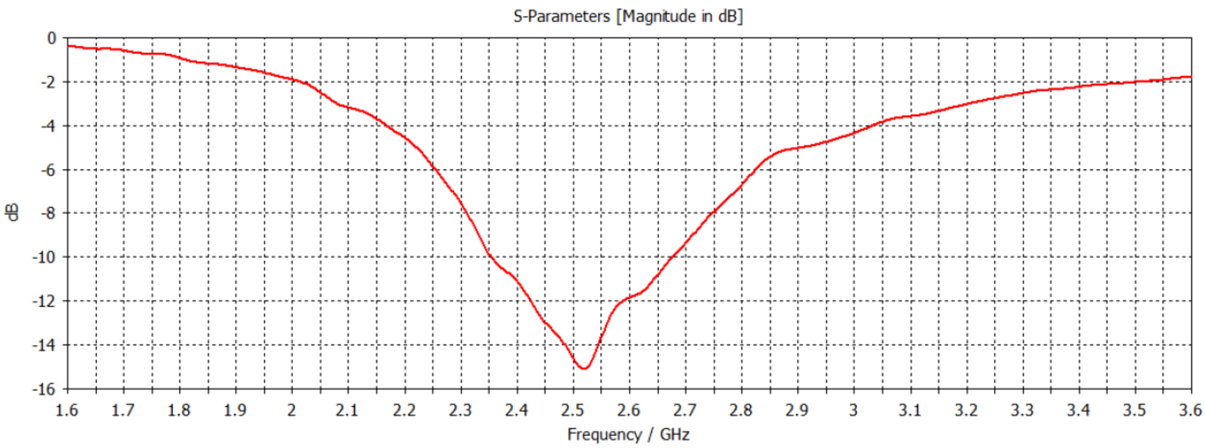

Figure 3.12 Reflection coefficient for reference flat model with a 2.6 GHz monopole.

In Figure 3.13, one can observe the polar radiation pattern for the 2.6 GHz monopole with the reference flat box of PEC, at a fixed azimuth of $\phi = 90°$, as well as the theoretical monopole radiation pattern [Corr18] (gain is expressed in dBi).

The radiation pattern shows the monopole radiates in a manner according to the theoretical literature [Bala16] for grounded monopoles in the presence of PEC, with small differences in the radiation pattern, which are due to the monopole configuration, influence of the PEC box and simulation settings.

Table 3.3 Antenna parameters with a flat surface at 90º azimuth.

Communication technology	TETRA	GSM-R	LTE-R	BBRS
Operating frequency (f) [MHz]	400	900	2600	5900
Simulated gain [dBi]	6.0	6.6	7.7	6.7
Reflection coefficient (S_{11}) [dB]	-13.1	-15.5	-11.9	-18.8
Main lobe magnitude [dB]	5.1	5.8	6.3	6.0
Angular width (α_{3dB}) [º]	31.3	19.8	12.3	13.5
Side lobe level [dB]	-4.7	-2.5	-2.2	-0.9

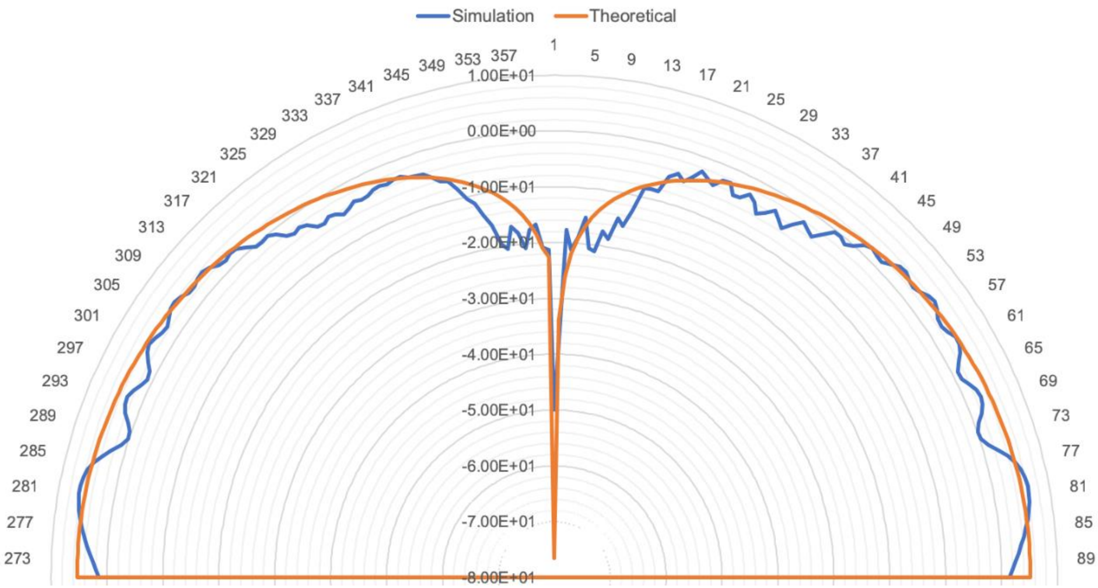

Figure 3.13 Far-field Gain of monopoles operating at 2.6 GHz (theoretical and simulation).

Chapter 4

Results Analysis

In this chapter, the main results from simulations are presented, after defining the simulation scenarios that were considered. Three approaches are addressed: a comparison between flat and grooved surfaces, a comparison of two grooved surfaces with different groove dimensions and an analysis of the influence of the height of the antenna in the performance.

4.1 Scenarios description

Following the KPI definition in Section 3.7, in this section an overview of the scenarios that were simulated and analysed is presented.

First, one defines the reference scenario for the problem under study: this consists of the most realistic approach for the problem, which is a train featuring a curved, grooved roof, with the antenna being placed 1 cm above the surface (h_p=1 cm), supported in a plastic support that is not featured since the dielectric properties of the plastic do not impact propagation. The model for this scenario is the one depicted in Figure 4.1, sized to offer the best trade-off between simulation accuracy and computational resources used, and was fitted with medium-sized grooves with the following dimensions:

- Groove width w_g = 15 mm;
- Groove height h_g = 25 mm;
- Distance between grooves d_g = 15 mm.

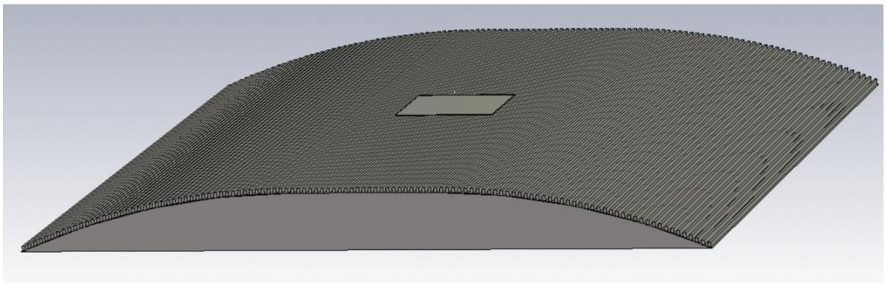

a) Model overview

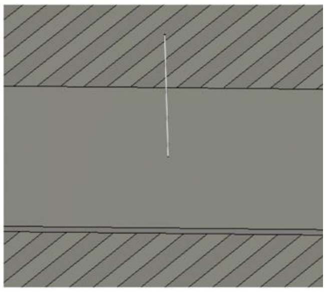

b) Surface detail

Figure 4.1 Reference scenario featuring a 900 MHz antenna.

The first approach addresses the influence of the grooved surface in the performance of the antennas. For that, as explained in detail in Section 3.5, three 3D models are used: a flat box of PEC material, depicting a section of a real train roof; a straight grooved model, with the same dimensions and finally the reference curved grooved model, depicted in Figure 4.1.

For this approach, the procedure consists of testing the antennas for the four frequencies (400, 900, 2600 and 5900 MHz) placed on the three models, to compare the differences introduced by the grooves and the curved surface to the antenna behaviour placed on top of the flat surface. No inputs should be changed for theses simulations comparing to the isolated antennas tests, unless mismatch occurs and additional tuning is required.

For the flat model, the ground plane of the monopoles is placed 1 cm above the top, while for the grooved models the ground plane is placed 1 cm above the highest groove surface (h_p=1 cm). In what concerns the meshing, dedicated meshing groups for the port, the antenna wire, and its ground plane are kept, while the global mesh properties are adjusted, for the different frequencies and 3D models, to always guarantee an adequate number of mesh cells (between 5 and 10 million mesh cells), with the heaviest simulations being the 5.9 GHz ones due to its lowest wavelength.

The results of this first approach are presented in Section 4.2, analysing and comparing the outputs from the different simulations according to the prior KPI definition, comparing, for each frequency, the different attenuations resultant from the introduction of the grooves and the curved surface.

The next approach has the goal of understanding how the groove dimensions impacts the performance, as there is not a common groove size. Hence, the curved grooved model depicted above was changed:

- Wider groove width w_g = 20 mm (instead of 15 mm);
- Smaller groove height h_g = 15 mm (instead of 25 mm);
- Grooves farther from each other with a distance between them d_g = 20 mm (instead of 15 mm).

For this approach, only the position of the antenna ground plane is adjusted, to cope with the decrease in the grooves' height (and to sit 1 cm above its top, as in the reference scenario). The results are then compared with the reference grooved scenario, in Section 4.3.

Finally, as stated before, in order to evaluate the impact of the antenna height in the performance, additional simulations are done, changing the antenna and ground plane height (h_p).

While most of the railway antennas are placed close to the train roof, some are elevated to – supposedly – improve its performance, at a height usually no higher than 20 cm, since one has to take into account the monopole size (the TETRA antenna designed has 16.5 cm, for instance). Previous work [Ribe18] tested several scenarios including air conditioning units with a 45 cm height on the rooftops, hence elevating the top of the monopole to close to 40 cm is quite reasonable. The range of heights is defined in Table 4.1, where a comparison with the wavelengths for the different frequencies is made. It is possible to see that, for the lower frequencies, the range of heights considered is far from the wavelength, whereas for the higher frequencies one has the opposite case. It is therefore expected that the higher frequencies experience more significant impacts from the changes in antenna height.

Table 4.1 Comparison of antenna heights with the wavelength for the four frequencies.

Frequency [MHz]		**400**	**900**	**2600**	**5900**
Wavelength [m]		**0.75**	**0.33**	**0.12**	**0.05**
Antenna height [m]	h_p=0.01	0.01λ	0.03λ	0.09λ	0.20λ
	h_p=0.10	0.13λ	0.30λ	0.87λ	1.97λ
	h_p=0.20	0.27λ	0.60λ	1.73λ	3.93λ

These three measurements were defined having in mind the limited computational resources, since it would be interesting to test additional mid-range values of height. Results are compared in Section 4.4.

For all these scenarios, the gains are compared bearing in mind the relevant angle window, since the impact is only relevant if it changes the performance of the overall system. Therefore, for both azimuth and elevation planes, angles facing forward, the train moving direction, is considered in more detail (the interval of angles was defined in Figure 3.10). Finally, an additional overall gain difference, taking into account the entire angle range for both planes (N_{ang}=360), is computed, due to BS location being some times far from the railway, especially in TETRA and GSM-R systems [Sour13].

4.2 Influence of the grooved surface

In this section, the four antennas are tested for the flat PEC model, the straight grooved model and the reference scenario curved grooved model. It is important to remember the most important KPI is the gain, which will help understanding how the grooved surface impacts the expected performance of the train antenna, and in which directions. The angles in which this is important depend on the technology. For higher frequencies, BS are placed closed to each other and usually directly in front of the train, therefore making the angles in the relevant angle window more critical. For lower frequencies, due to higher range, sometimes the BS is placed far from the train, in its side, not close from the track, and therefore side angles matter more. The 2D far-fields for all tests can be seen in Annex H.

4.2.1 TETRA

The first simulations were performed for 400 MHz, and the comparison is done for the ϕ=90º plane according to the defined angles of interest for the problem. The results can be seen in Table 4.2. One can see the biggest changes occur not for the straight grooved surface but when besides the grooved surface, a curved shape is also added. While the gain does not change significantly, the main lobe direction is lowered from 63º to 73º, closer to the horizon.

Table 4.2 Flat, straight and curved grooved surface performance at 400 MHz.

Surface		Gain [dBi]	Main lobe direction θ [º]	α_{3dB} [º]	Side lobe level [dB]	Main lobe half-power range Θ [º]
Flat	ϕ=90º	6.0	63	31.3	-4.7	[47.4;78.7]
Straight grooved	ϕ=90º	5.8	63	31.0	-0.5	[47.5;78.5]
Curved grooved	ϕ=90º	5.4	73	61.5	-1.1	[42.3;103.8]

The increase in the half-power beamwidth occurs due to the dispersion of electromagnetic performance caused by the curved surface of this model, and is quite significant (nearly doubles the beamwidth from 31.3º to 61.5º), meaning the curved grooved surface radiates a power higher than 2.7 dBi (half of maximum gain for an interval of $\theta \in [42.3; 103.7.8]°$ instead of $\theta \in [47.4; 78.7]°$ for the flat surface (with a slightly higher gain, however). Although this allows the main lobe to cover the relevant window of angles in terms of elevation, it also goes beyond the limits defined, meaning there is significant power being radiated out of the defined boundaries, potentially reducing the overall performance.

The 2D far-fields for the reference, straight grooved and curved groove surface can be seen in Figure 4.2, Figure 4.3 and Figure 4.4, respectively.

It can be clearly seen in the curved surface far-field the dispersion caused by the shape of the surface, which increases the directivity of the antenna since the antenna is no longer quasi-isotropic but features an increased beam directivity, especially for ϕ between 60 and 120 degrees.

On the other hand, the radiation pattern shows a clear decrease in power for the side views (ϕ=0º and ϕ=180º), which is not expected to impact performance of the overall system since the radiation in these angles will only be considered when the train is passing by a BS and, in that situation, due to the proximity of the antennas, the attenuation does not pose a threat to the performance of the system.

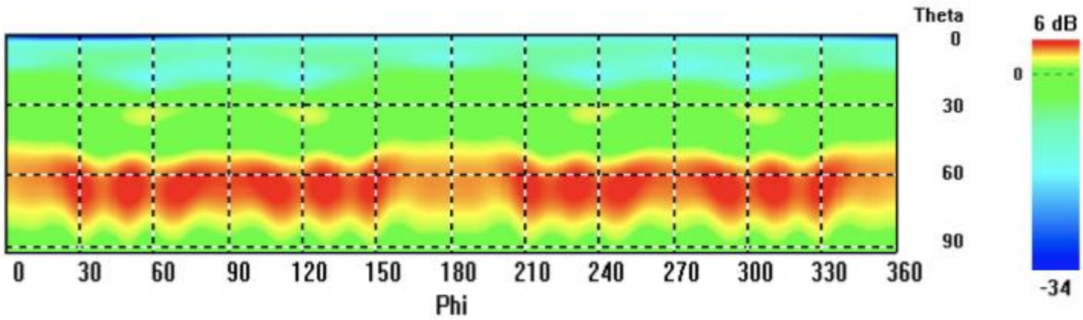

Figure 4.2 Far-field performance of the 400 MHz antenna over the flat surface.

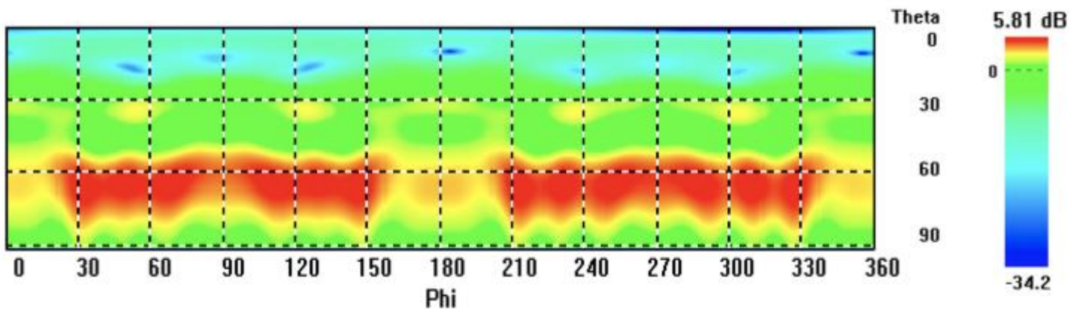

Figure 4.3 Far-field performance of the 400 MHz antenna over the straight grooved surface.

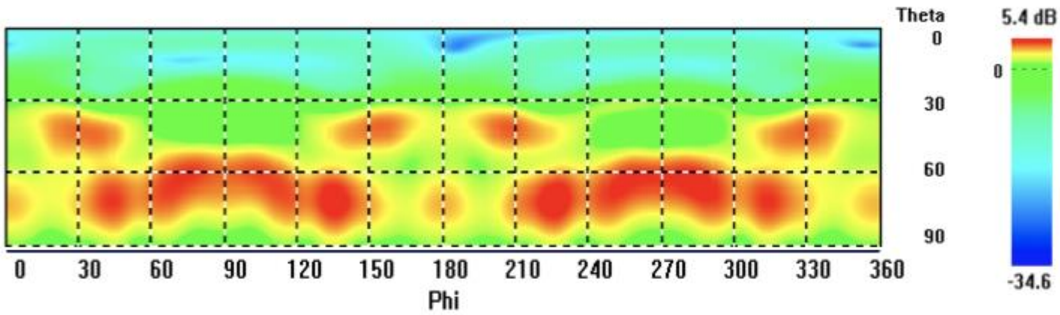

Figure 4.4 Far-field performance of the 400 MHz antenna over the curved grooved surface.

4.2.2 GSM-R

For the 900 MHz antenna, the same procedure was followed, testing the antenna for the three surface models. The results can be seen in Table 4.3.

From the results shown, it is possible to observe a clear increase in the main lobe direction angle for the curved surface, and a significant α_{3dB} increase as well. The tilt of the main lobe should not have a significant influence in the system, since it is now closer from the horizon, but still inside the relevant angle interval. For the straight grooved surface there are no critical changes (1º tilt on the main lobe and a very slight decrease of α_{3dB} and S_{LL} values), which suggests the biggest impacts for the performance of the 900 MHz antenna come from the curved surface rather than the grooves.

Table 4.3 Flat, straight and curved grooved surface performance at 900 MHz.

Surface		**Gain [dBi]**	**Main lobe direction θ [º]**	**α_{3dB} [º]**	**Side lobe level [dB]**	**Main lobe half-power range Θ [º]**
Flat	ϕ=90º	6.6	74	19.8	-2.5	[64.1; 83.9]
Straight grooved	ϕ=90º	7.1	73	19.2	-3.3	[63.4;82.6]
Curved grooved	ϕ=90º	6.6	89	25.7	-1.7	[76.2;101.9]

The 2D far-fields show a behaviour very close to the 400 MHz antenna. The straight grooved surface shows some influence on the propagation, increasing its directivity towards the front and rear of the train (ϕ=90º and ϕ=270º) and decreasing the radiation on side angles. Furthermore, the increase in α_{3dB} is not entirely positive for the relevant angle window, since while the gain does not decrease (compared to the reference flat surface), having α_{3dB}=25.7º and the main lobe direction increased to θ=89º means a gain higher than 3.3 dBi is radiated for an interval of $\theta \in [76.2; 101.9]°$ instead of $\theta \in [64.1; 83.9]°$ for the flat surface. Since the relevant window ends at $\theta = 90°$ it would most likely not be useful to radiate at a higher intensity for an elevation higher than that (lower than the horizon).

4.2.3 LTE-R

Similarly to the lower frequencies, for 2.6 GHz the same procedure was followed, with the antenna tested for the three models depicting the roof of the train. The results can be seen in Table 4.4.

For this frequency it is immediately possible to see how the straight grooved surface changes significantly the main lobe direction from θ=79º to θ=56º, meaning the main lobe is tilted up, and since the half-power beamwidth increases to α_{3dB}=21.4º a gain higher than 3.8 dBi is radiated for an interval of $\theta \in [45.3; 66.7]°$ instead of $\theta \in [72.9; 85.2]°$ for the flat surface (with a lower gain, however). The curved grooved surface further rises the main lobe direction, and in addition to the smaller half-power beamwidth than the straight grooved surface, the resulting beam with gain higher than 4 dBi is radiated for $\theta \in [46.3; 61.8]°$.

Table 4.4 Flat, straight and curved grooved surface performance at 2.6 GHz.

Surface		Gain [dBi]	Main lobe direction θ [º]	α_{3dB} [º]	Side lobe level [dB]	Main lobe half-power range Θ [º]
Flat	ϕ=90º	7.7	79	12.3	-2.2	[72.9; 85.2]
Straight grooved	ϕ=90º	8.8	56	21.4	-0.9	[45.3;66.7]
Curved grooved	ϕ=90º	8.0	54	15.5	-0.7	[46.3;61.8]

The 2D far-field of the flat surface is very similar to the lower frequencies' ones, while the straight grooved and curved grooved, Figure 4.5, surfaces feature a clear decrease of power for the 60-120º (and 240-300º) band in the azimuth plane, slightly stronger in the curved surface. This poses a problem since the angles of interest for this plane are $\phi \in [80; 100]°$ because this represents the front of the train. It is therefore possible to conclude that, for 2.6 GHz, there will probably be a severe impact in the performance of the overall communication system due to the strong attenuation in the propagation in the relevant angles for the link with the trackside BS.

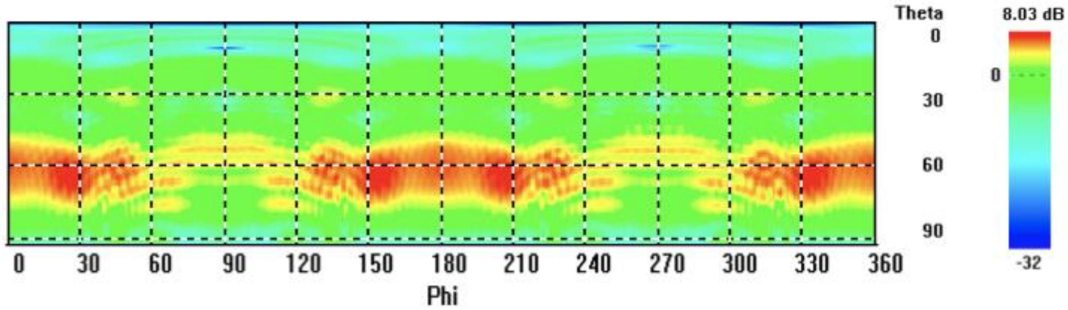

Figure 4.5 Far-field performance of the 2.6 GHz antenna over the curved grooved surface.

Since there is a significant change in the radiation pattern for this frequency, the 2D polar plot was also computed, and seen in Figure 4.6. This plot confirms the biggest gain decrease occurs for ϕ=90º (and, symmetrically, for ϕ=270º), with a relevant reduction for the straight grooved surface and much stronger for the curved grooved surface (almost 10 dB). This impact is higher for 2.6 GHz than for the lower frequencies due to the size of the grooves being close to the wavelength.

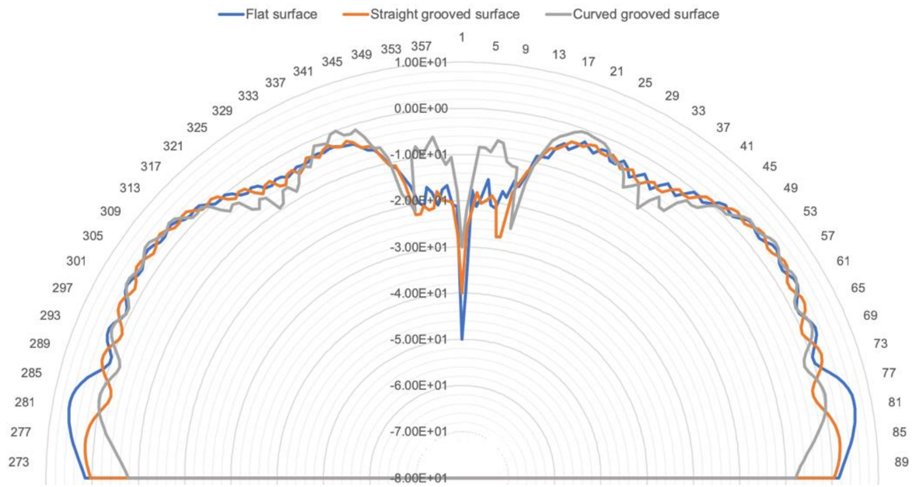

Figure 4.6 Far-field polar plot of the 2.6 GHz antenna over the three surfaces (ϕ=90º).

4.2.4 BBRS

Finally, the 5.9 GHz antenna was tested for the same three scenarios. The results can be seen in Table 4.5. The first challenge was to tune once again the antenna for the new surfaces, since with the flat model the antenna was not operating correctly (S_{11} value increased to higher than -10 dB), hence it was needed to reduce the size of the monopole to h=10 cm.

For this frequency there are no significant changes in the KPIs for the straight grooved compared to the flat surface, while for the curved grooved model one can see a noteworthy increase in the main lobe direction, pulling the main lobe half-power range up, with part of it getting outside the relevant angles. The 2D far-field for the curved groove surface can be seen in Figure 4.7 and shows a significant dispersion. By analysing the three far-fields (Annex H), it is clear the grooved surfaces increase the dispersion of the radiated power, with the gain in the flat surface being more concentrated in the 60º to 75º band, while for the grooved surfaces it is possible to observe there is no consistent band of angles with higher gain, while there are a lot of lobes in all directions.

Table 4.5 Flat, straight and curved grooved surface performance at 5.9 GHz.

Surface		**Gain [dBi]**	**Main lobe direction θ [º]**	**α_{3dB} [º]**	**Side lobe level [dB]**	**Main lobe half-power range Θ [º]**
Flat	ϕ=90º	6.7	75	13.5	-0.9	[68.3;81.8]
Straight grooved	ϕ=90º	5.7	73	16.1	-0.8	[66.0;81.0]
Curved grooved	ϕ=90º	7.6	49	16.7	-1.8	[40.7;57.4]

Furthermore, as observed for the 2.6 GHz case, there is a clear decrease of power for the 60º to 120º band in the grooved surfaces, worst for the curved model. This is a critical issue for the overall performance since this band is the most relevant for communications in railway environment, especially for BBRS where BS spacing is usually no more than 300 m, making front propagation crucial.

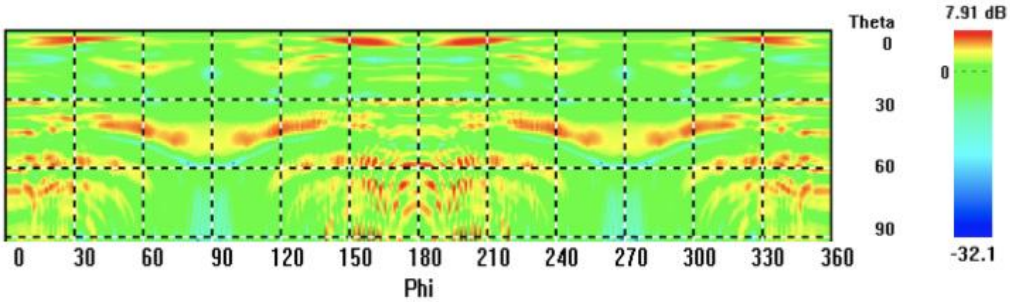

Figure 4.7 Far-field performance of the 5.9 GHz antenna over the curved grooved surface.

4.2.5 Overall gain differences

According to the equations for gain differences calculations presented in Section 3.7, in this section the overall differences for the acquisition angles are presented, for all frequencies.

First, the equations for the straight grooved surface comparing to the flat surface are computed, both for $\phi = 90°$ and $\theta = 90°$ planes, through (3.13) and (3.15) for the average values, the results being shown in Table 4.6 and Table 4.7, respectively. Gain differences are classified by levels:

- Difference lower than 1 dB: marginal impact in the performance of the system;
- Difference higher than 1 dB but lower than 5 dB: considerable impact but still not significant;
- Difference higher than 5 dB: strong impact, may compromise communications.

Analysing the results in the these two tables it is possible to see the biggest impacts are observed for the higher frequencies. In the elevation plane, for the 5.9 GHz frequency, the impacts are positive in the interval of angles of interest, with the grooved surface achieving a gain 1.37 dB higher on average. On the other hand, for 2.6 GHz the gain is lowered on average 1.49 dB in the same window. For the azimuth plane, the results are similar, with a significantly higher positive impact registered for the 5.9 GHz simulation (almost 16 dB average higher gain in the interval of angles of interest), and the 2.6 GHz showing a slight decrease of 1.13 dB on average. The average for the full angle range of the polar plot was also computed (N_{ang}=360) and it was possible to conclude that for this range there are no significant changes that may compromise communications, except for 2.6 GHz once more.

Table 4.6 Gain differences straight grooved surface compared to flat surface (fixed azimuth).

Frequency [MHz]	Angles	Acquisition angles				Average gain difference	
		θ=45º	θ=60º	θ=75º	θ=90º	N_{ang} = 46	N_{ang} = 360
400	ϕ=90º	0.59	-0.42	-0.65	-0.16	**-0.27**	**0.04**
900		-0.13	0.18	0.22	0.34	**-0.07**	**0.09**
2600		0.75	-1.70	-5.20	-0.96	**-1.49**	**-1.61**
5900		-0.07	0.30	-3.22	16.85	**1.37**	**1.33**

Table 4.7 Gain differences straight grooved surface compared to flat surface (fixed elevation).

Frequency [MHz]	Angles	Acquisition angles					Average differences	
		ϕ=80º	ϕ=85º	ϕ=90º	ϕ=95º	ϕ=100º	N_{ang} = 21	N_{ang} = 360
400	θ=90º	-0.51	-0.24	-0.16	-0.18	-0.44	**-0.26**	**0.21**
900		0.13	0.24	0.34	0.30	0.01	**0.24**	**1.93**
2600		-1.21	-1.09	-0.96	-1.16	-1.18	**-1.13**	**-6.16**
5900		19.71	15.42	16.85	15.54	19.61	**15.97**	**5.96**

The equations for the curved grooved surface comparing to the flat surface were computed, both for $\phi = 90°$ and $\theta = 90°$ planes, the results being shown in Table 4.8 and Table 4.9, respectively.

Concerning the curved grooved surface, once again the impacts are more significant in the higher frequencies, with the 5.9 GHz simulations showing a strong negative impact in the elevation plane, with more than 4.5 dB of gain loss on average, while for the azimuth plane a strong increase of more than 6.4 dB is observed. The 2.6 GHz simulations bear the worst results (consistent loss of gain in both planes, on average being 2.77 dB lower in the elevation plane and more than 10 dB lower in the azimuth plane), which should be carefully dealt with since a 10 dB attenuation will most likely cut communications in several sections of the railway if no measures are taken during the sites planning phase.

On both models, it is possible to say the 400 and 900 MHz tests do not show a significant impact in terms of gain in the relevant angle of interest, which can be explained due to the higher difference between the groove dimensions and the wavelength for these frequencies, a difference that is quite lower for the higher frequencies. When the full angle range is considered (N_{ang} = 360) the results are in line to the relevant angle window, with a slight increase in gain (2.83 dB) for the 900 MHz test and a positive impact (5.40 dB) registered for the 5.9 GHz in the elevation cut.

Table 4.8 Gain differences curved grooved surface compared to flat surface (fixed azimuth).

Frequency [MHz]	Angles	Acquisition angles				Average differences	
		θ=45º	θ=60º	θ=75º	θ=90º	N_{ang} = 46	N_{ang} = 360
400	ϕ=90º	0.58	-0.64	-0.65	-0.26	**-0.39**	**0.55**
900		-0.26	0.29	0.19	0.12	**-0.23**	**-0.76**
2600		0.79	-0.04	-4.17	-9.37	**-2.77**	**-1.29**
5900		1.76	-11.32	-13.82	11.95	**-4.56**	**5.40**

Table 4.9 Gain differences curved grooved surface compared to flat surface (fixed elevation).

Frequency [MHz]	Angles	Acquisition angles					Average differences	
		ϕ=80º	ϕ=85º	ϕ=90º	ϕ=95º	ϕ=100º	N_{ang} = 21	N_{ang} = 360
400	θ=90º	0.58	-0.01	-0.26	0.05	0.54	**0.09**	**0.80**
900		-0.13	0.03	0.12	0.10	-0.21	**-0.02**	**2.83**
2600		-11.22	-9.59	-9.37	-10.14	-10.80	**-10.08**	**-8.25**
5900		15.78	9.80	11.95	9.86	15.12	**6.41**	**4.84**

Summarising, the results shown above allow to draw some conclusions on the impacts generated by both the curved surface and the grooved surfaces:

- The lower frequencies (400 and 900 MHz) are the less impacted by the grooves, due to the wavelengths being far from the groove dimensions (the maximum relative size is h_g that is equal to 0.75λ for 900 MHz), and the computed average gain differences show a less than 1 dB gain reduction, hence no difficulties are expected for TETRA and GSM-R;
- The higher frequencies (2.6 and 5.9 GHz) show the introduction of the grooves causes a significant impact, especially in the angles around ϕ=90º, where the power decreases, an effect that is worse for the 2.6 GHz case, where average gain differences show an impact up to -14 dB

in some angles. Strong impacts are expected and therefore, if an average approach is preferred, a 10 dB safety margin should be considered for LTE-R systems with grooved roof designs. Should the system support critical functions, then a worst approach safety margin should be used, considering a 14 dB safety margin;

- The 5.9 GHz simulations show a very disperse radiation pattern with a lot of lobes, and while on average the groove introduction do not worsen the gain, in some angles the gain was almost -14 dB lower for the grooved surface, which suggests a safety margin of communications should also be considered for BBRS. Although 5 dB would probably be enough to use as average approach safety margin, the worst approach should consider the same 14 dB.

4.3 Influence of the grooves' dimensions

In this section, one presents the results of the antennas tested with the modified curved grooved model, featuring wider grooves (w_g = 20 mm) with a smaller height (h_g = 15 mm) and a bigger distance between them (d_g = 20 mm). The 2D far-fields from CST can be seen in Annex I.

4.3.1 TETRA

Starting with the 400 MHz simulation, the comparison is done for the ϕ=90º plane according to the defined angles of interest for the problem. The results can be seen in Table 4.10.

The results show a slight decrease of the main lobe direction, which is for the wider grooved model now pointing upper, but a significant reduction of the half-power beamwidth, resulting in a narrower main lobe half-power range, that keeps, however, within the relevant angle window.

Table 4.10 Reference and the wider grooved surface performance at 400 MHz.

Surface		**Gain [dBi]**	**Main lobe direction θ [º]**	**α_{3dB} [º]**	**Side lobe level [dB]**	**Main lobe half-power range Θ [º]**
Reference	ϕ=90º	5.4	73	61.5	-1.1	[42.3;103.8]
Wider grooves	ϕ=90º	5.3	62	29.7	0.5	[47.2;76.9]

The 2D far-fields in Annex I show there are no significant changes in the pattern, except for the slight attenuation in the gain for the side views, that becomes stronger than the one observed for the reference grooved model. It is possible to say the wider grooves impact more the side view, mostly due to higher reflection, but in an extension that shall not compromise the link to the BS (3-4 dB reduction).

4.3.2 GSM-R

For the 900 MHz simulation, the results can be seen in Table 4.11. The results show a slight decrease of the main lobe direction, which is for the wider grooved model now pointing upper, with an also slight reduction of the half-power beam width. These two effects combined, while reducing the size of the main lobe half-power interval Θ, result that this range is now completely in the relevant angle window. This might be a positive impact, depending on BS location, since as seen before for systems operating at lower frequencies (such as 900 MHz) the BS sites are sometimes far from the trackside.

Table 4.11 Reference and wider grooved surface performance at 900 MHz.

Surface		Gain [dBi]	Main lobe direction θ [º]	α_{3dB} [º]	Side lobe level [dB]	Main lobe half-power range Θ [º]
Reference	ϕ=90º	6.6	89	25.7	-1.7	[76.2;101.9]
Wider grooves	ϕ=90º	6.4	73	19.5	-0.6	[63.3;82.8]

The pattern shows a slight reduction in the dispersion, while maintaining the same profile that was observed for the reference scenario. There are no significant changes since the groove dimensions are far from the wavelength (λ=0.33 m) for both models. The wider grooved surface suggests a higher gain should be expected for the 30 to $\phi \in [30; 140]°$ meaning it most likely improves the link to the BS.

4.3.3 LTE-R

For the 2.6 GHz antenna the same procedure was followed, with the antenna tested for the model with wider grooves. The results can be seen in Table 4.12.

Table 4.12 Comparison of reference and the wider grooved surface performance at 2.6 GHz.

Surface		Gain [dBi]	Main lobe direction θ [º]	α_{3dB} [º]	Side lobe level [dB]	Main lobe half-power range Θ [º]
Reference	ϕ=90º	8.0	54	15.5	-0.7	[46.3;61.8]
Wider grooves	ϕ=90º	7.8	54	15.1	-0.6	[46.5;61.6]

The change in the groove dimensions do not impact significantly the pattern neither the KPI results.

4.3.4 BBRS

Finally, the wider grooves model was tested for the 5.9 GHz antenna. Results are shown in Table 4.13, being possible to see a very strong reduction of the main lobe direction angle, together with a reduction to one third of the half power beamwidth, meaning the main lobe is for the wider grooved model now pointing upward and is quite thinner, being now completely out of the relevant angle window. The far-field patterns show a very scattered gain for both surfaces, with a slight reduction of the dispersion of the wider grooved model. In both models one can see that at ϕ=90º the gain is very low, which is very critical for the communications, since BBRS systems typically feature BS 300 m apart from each other and is therefore very likely these will be directly forward facing the train.

Table 4.13 Reference and wider grooved surface performance at 5.9 GHz.

Surface		Gain [dBi]	Main lobe direction θ [º]	α_{3dB} [º]	Side lobe level [dB]	Main lobe half-power range Θ [º]
Reference	ϕ=90º	7.6	49	16.7	-1.8	[40.7;57.4]
Wider grooves	ϕ=90º	9.9	4.8	5	-0.9	[3.5;8.5]

The significant impacts observed come from the fact that, at 5.9 GHz, the wavelength is 0.05 m which is exactly in the range of the groove dimensions' changes, so it was expected changes in the groove size would impact severely the KPI in analysis.

4.3.5 Overall gain differences

Similarly to what was done for the comparison of surface types, for this chapter's groove dimension comparison, gain differences were computed in order to have a quantitative overview of the impacts. The equations and colour scheme used are the same as in Section 4.2.5. In Table 4.14, it is possible to see the gain differences for the ϕ=90º cut, while Table 4.15 shows the results for the θ=90º cut.

Table 4.14 Gain differences wider grooved model compared to reference (fixed azimuth).

Frequency [MHz]	Angles	Acquisition angles				Average differences	
		θ=45º	θ=60º	θ=75º	θ=90º	N_{ang} = 46	N_{ang} = 360
400	ϕ=90º	0.09	0.38	0.24	0.09	**0.28**	**0.10**
900		0.54	0.50	0.57	0.45	**0.45**	**0.36**
2600		-0.17	0.30	-0.25	0.86	**0.08**	**1.57**
5900		-0.08	-5.43	2.25	-1.40	**-0.61**	**-0.09**

In both tables it is possible to see that, generally, the change in the groove dimensions does not affect significantly the lower frequencies, in neither of the cut planes, and not even when N_{ang} is increased to 360 the impacts became relevant. For the 2.6 GHz simulations, some impacts in the fixed elevation cut can be observed (1.32 dB gain increase, average), but again these are not expected to cause problems to the communication between the train and the BS network, since on average the gain in the relevant angle window increased, and only in specific angles it decreases. The biggest changes are observed for the 5.9 GHz simulations. This can be explained by the fact that, at this frequency, the wavelength is close to the groove dimensions (λ=0.05 m) and the changes in the grooves' parameters have triggered additional reflections in this wavelength. However, even though at 5.9 GHz some acquisition angles show relevant decrease of gain, on average the gain increases for the relevant angle window. As seen in Section 4.3.4, at this frequency the radiation is quite scattered on top of the model, and changing the grooves changes this scatter pattern a little bit, but overall the changes in groove dimensions are not negative for the frequencies tested.

Table 4.15 Gain differences wider grooved model compared to reference (fixed elevation).

Frequency [MHz]	Angles	Acquisition angles					Average differences	
		ϕ=80º	ϕ=85º	ϕ=90º	ϕ=95º	ϕ=100º	N_{ang} = 21	N_{ang} = 360
400	θ=90º	0.12	0.10	0.09	0.12	0.13	**0.11**	**-0.03**
900		0.56	0.52	0.45	0.51	0.54	**0.50**	**-0.86**
2600		-1.23	0.37	0.86	1.39	-1.49	**0.59**	**1.32**
5900		-8.89	-4.26	-1.40	-3.12	-6.02	**1.73**	**0.44**

From the results shown it is possible to conclude:

- The lower frequencies (400 and 900 MHz) show a slight power decrease for the side view on the wider grooved surface, but not very significant (3 to 4 dB), while for 2.6 GHz no changes occur when the grooves are widened, therefore no further safety margins are recommended for this frequencies in case a train roof with wider grooves is present;
- The 5.9 GHz simulation continues to show a very disperse radiation pattern, being the frequency for which more changes happened, namely the decrease in the main lobe direction (from 49º to 5º) making it point almost vertically, but again, the pattern shows a lot of lobes, and the average gain differences show the impacts are under 1 dB on average. Since some specific angles feature gain losses of almost 9 dB comparing to the reference scenario, it is recommended that the 5 dB safety margin of communications is applied to any grooved roof train type, however the worst case approach should be now 23 dB to cope with the maximum gain decrease comparing to the flat scenario.

4.4 Influence of the antenna & ground plane height

Last but not least, in this section the impact of the antenna height in the performance is evaluated, with the results of the additional simulations performed shown. In addition to the reference scenario with the ground plane at 1 cm from the grooved surface top, further simulations with h_p=10 and h_p=20 cm were done, according to the scenarios' description in Section 4.1. The far-fields can be seen in Annex J.

4.4.1 TETRA

The first simulations were performed for 400 MHz, and the simulation results were analysed according to the ϕ=90º cut. The results can be seen in Table 4.16.

The increase in the antenna and ground plane height has a significant impact on the KPIs for this frequency. Table 4.16 shows that the raise to h_p=10 cm improves the antenna gain while reducing the main lobe direction and the half-power beamwidth, meaning the main lobe points upwards and is thinner, with the Θ range out of the relevant angle window. The additional raise to h_p=20 cm further increases the gain, although not as strongly as with h_p=10 cm. On the other hand, the half-power beamwidth raises along with an improvement in the main lobe direction, which pushes the main lobe half-power range further down to be inside the relevant angle window, however only partially.

Table 4.16 Performance at 400 MHz for three antenna heights.

Surface		Gain [dBi]	Main lobe direction θ [º]	α_{3dB} [º]	Side lobe level [dB]	Main lobe half-power range Θ [º]
Reference (h_p=1 cm)	ϕ=90º	5.4	73	61.5	-1.1	[42.3;103.8]
h_p=10 cm	ϕ=90º	7.7	33	18.6	-3.5	[23.7;42.3]
h_p=20 cm	ϕ=90º	7.9	44	46.7	-1.6	[20.7;67.4]

The 2D far-field for h_p =10 cm can be seen in Figure 4.8, where the impact of the height increase in the radiation patter is clear. With the increase of the antenna and ground plane height, the radiation stops "following" the curved surface to be more directional for specific angles. The gain increase observed in the table above results from a lower dispersion of the radiation. However, one can see that, for the relevant angles (around ϕ=90º) there is a clear decrease in radiated power for the higher placement scenarios, and therefore it is possible to conclude this increase in height is not positive for this frequency.

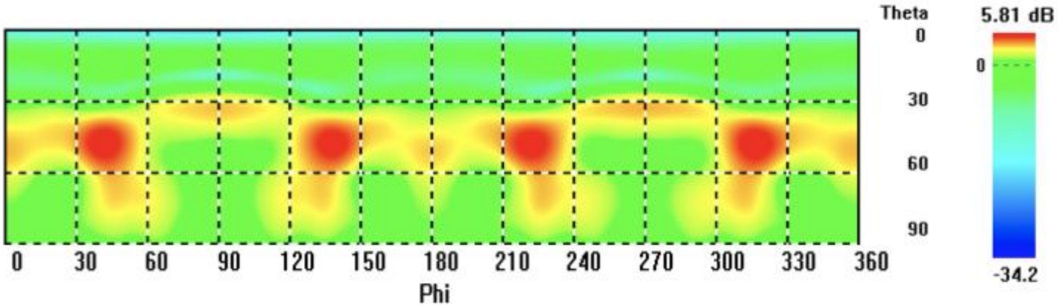

Figure 4.8 Far-field performance of the 400 MHz antenna at h_p =10 cm.

4.4.2 GSM-R

For the 900 MHz antenna, the same procedure was followed, testing the antenna for the three surface models. The results can be seen in Table 4.17. It is possible to see a consistent decrease of the main lobe direction, along with a reduction of the half-power beamwidth, both these leading to a thinner, more elevated main lobe half-power interval. However, this tilting up might be considered beneficial since for h_p =1 cm part of this range was outside the relevant angle window, which does not happen for the two higher placement settings.

Table 4.17 Performance at 900 MHz for three antenna heights.

Surface		Gain [dBi]	Main lobe direction θ [º]	α_{3dB} [º]	Side lobe level [dB]	Main lobe half-power range Θ [º]
Reference (h_p=1 cm)	ϕ=90º	6.6	89	25.7	-1.7	[76.2;101.9]
h_p =10 cm	ϕ=90º	6.4	79	18.9	-0.5	[69.9;88.1]
h_p =20 cm	ϕ=90º	6.6	59	12.1	-2.4	[53.0;65.1]

The 2D far-fields show the increase of the antenna height results in significant changes in the radiation patterns, especially for the intermediate height where a strong power dispersion can be observed.

For the proximities of ϕ=90º, there is lower radiation intensity. In the elevation plane, both scenarios (h_p=10 and h_p=20 cm) tilt the higher gains up, moving them to the range of θ=60º, which is still in the relevant angle window.

4.4.3 LTE-R

Similarly to the lower frequencies, for 2.6 GHz the same procedure was followed, with the antenna tested for the three models with the three different heights. The results can be seen in Table 4.18. The 2D far-field for a height of h_p=20 cm can be seen in Figure 4.9.

Knowing the height changes are in the same order of magnitude than the wavelength for this frequency, significant changes were to be expected, a priori. By analysing Table 4.18 it is possible to see that a tilt down of the main lobe occurs strongly for the highest placement of the antenna, however all the three placements feature the main lobe half-power range within the relevant angle window. The half-power beamwidth reduces for the biggest h_p, while the side lobe level only shows slight changes.

The 2D far-fields show that the radiation power is more isotropically distributed as the height of the antenna increases, which is beneficial for the 60-120º (and 240-300º) band in the azimuth plane, which has now more power, and this is a very important band for the link to the BS as seen before. One can conclude the increase in height will probably improve performance of the overall system for this frequency, which is important since this frequency shows the worst impacts due to the introduction of the curved and grooved surfaces (see Section 4.2).

Table 4.18 Performance at 2.6 GHz for three antenna heights.

Surface		Gain [dBi]	Main lobe direction θ [º]	α_{3dB} [º]	Side lobe level [dB]	Main lobe half-power range Θ [º]
Reference (h_p=1 cm)	ϕ=90º	8.0	54	15.5	-0.7	[46.3;61.8]
h_p =10 cm	ϕ=90º	6.9	56	15.9	-0.5	[48.1;64.0]
h_p =20 cm	ϕ=90º	6.6	73	6.2	-0.7	[69.9;76.1]

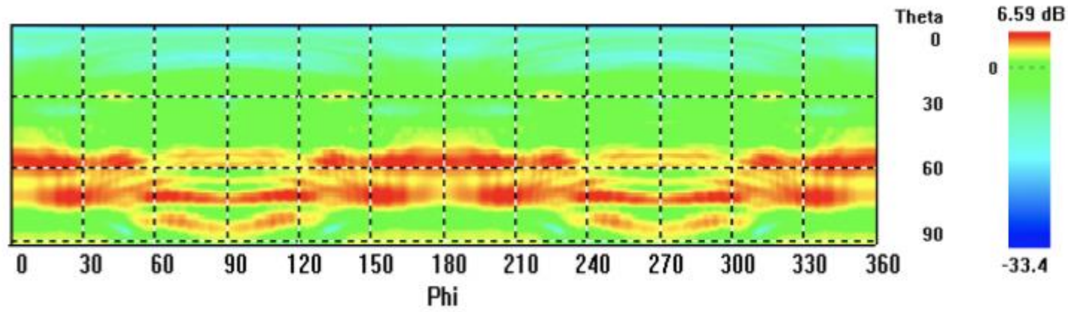

Figure 4.9 Far-field performance of the 2.6 GHz antenna at h_p=20 cm.

4.4.4 BBRS

In this section the results for the 5.9 GHz antenna with the three different heights are presented. The results can be seen in Table 4.19. As with the 2.6 GHz simulations, strong impacts in the radiation patterns were expected from the height changes, since they are in the range of the wavelength for 5.9 GHz.

Table 4.19 Performance at 5.9 GHz for three antenna heights.

Surface		**Gain [dBi]**	**Main lobe direction θ [º]**	**α_{3dB} [º]**	**Side lobe level [dB]**	**Main lobe half-power range Θ [º]**
Reference (h_p =1 cm)	ϕ=90º	7.6	49	16.7	-1.8	[40.7;57.4]
h_p =10 cm	ϕ=90º	10.1	39	6.3	-1.2	[35.9;42.2]
h_p =20 cm	ϕ=90º	12.0	18	2.2	-1.6	[16.9;19.1]

The 2D polar plot was computed, overlapping the results from the three heights, and it can be seen in Figure 4.10. It is possible to see the significant dispersion at 5.9 GHz.

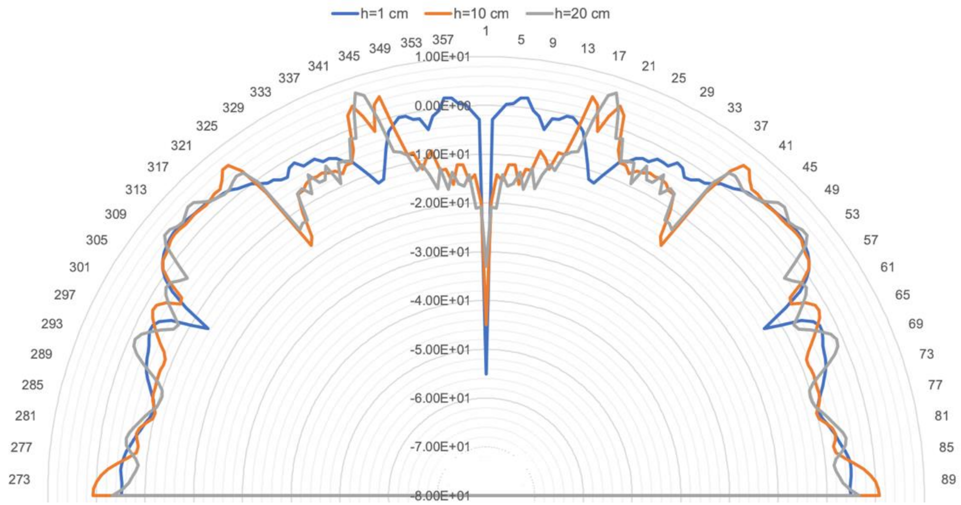

Figure 4.10 Far-field polar plot of the 5.9 GHz antenna at three different heights (ϕ=90º).

Looking at the results it is possible to see an increase in gain with the increase in height of the antenna, but along with a strong reduction of the half-power beam width, meaning the higher the antenna, the more scattered is the power in the radiation pattern. With a 2.2º α_{3dB} it is not relevant to talk about main lobe. The 2D far-fields confirm what was possible to infer from the KPIs in Table 4.19: at 5.9 GHz the radiation is quite scattered, and although the increase in height makes some changes in the pattern, it does not seem to impact strongly enough the relevant angle window.

4.4.5 Overall gain differences

Finally, the overall gain differences for this section are presented. The post-processing calculations were again made using (3.13) and (3.15) for the average values concerning the comparison between h_p= 10 cm and the reference, and results are shown in Table 4.20 and

Table 4.21, respectively.

Looking at the two tables it is clear the increase in height is generally positive, with an increase in gain for all frequencies and angles in the azimuth plane, while in the elevation plane the lower frequencies show, on average, a decrease of gain in the relevant window of angles. When N_{ang} is increased to 360, simulations show there is almost no change in gain, on average.

Table 4.20 Gain differences of antenna h_p =10 cm compared to h_p =1 cm (fixed azimuth).

Frequency [MHz]	Angles	Acquisition angles				Average differences	
		θ=45º	θ=60º	θ=75º	θ=90º	N_{ang} = 46	N_{ang} = 360
400	ϕ=90º	2.04	-5.03	-1.54	-0.38	**-2.32**	**-0.05**
900		3.40	-1.76	-2.47	0.46	**-2.86**	**0.42**
2600		-2.10	-1.68	-0.29	8.16	**1.48**	**0.21**
5900		-0.16	8.34	0.05	5.79	**0.27**	**-1.50**

Table 4.21 Gain differences of antenna h_p =10 cm compared to h_p =1 cm (fixed elevation).

Frequency [MHz]	Angles	Acquisition angles					Average differences	
		ϕ=80º	ϕ=85º	ϕ=90º	ϕ=95º	ϕ=100º	N_{ang} = 21	N_{ang} = 360
400	θ=90º	-0.48	-0.45	-0.38	-0.34	-0.38	**-0.40**	**-0.60**
900		0.62	0.21	0.46	0.19	0.61	**0.35**	**-1.62**
2600		8.90	8.29	8.16	8.81	8.43	**8.50**	**5.75**
5900		3.08	5.97	5.79	6.19	4.04	**4.49**	**1.79**

Concerning the comparison between the simulations with antenna height h_p =20 cm and the reference, (3.13) and (3.16) were used and the results can be seen in Table 4.22 and Table 4.23 for the $\phi = 90°$ and $\theta = 90°$ cut planes, respectively.

The fixed azimuth cut shows almost no impact in the increase of height for the 400 MHz antenna, with slight reductions in gain observed, something that happens also in the fixed elevation result. The 900 MHz antenna shows a decrease in gain for the relevant angle window while for N_{ang}=360 a subtle increase is observed in the fixed azimuth, while in the fixed elevation cut for both average differences one gets a reduction in the gain compared to the reference scenario (h_p =1 cm).

Table 4.22 Gain differences of antenna h_p =20 cm compared to h_p =1 cm (fixed azimuth).

Frequency [MHz]	Angles	Acquisition angles				Average differences	
		θ=45º	θ=60º	θ=75º	θ=90º	N_{ang} = 46	N_{ang} = 360
400	ϕ=90º	4.27	-1.65	-0.54	-0.17	**-0.26**	**-0.34**
900		4.14	5.59	-7.69	0.05	**-1.52**	**0.74**
2600		-3.11	-0.62	3.86	9.99	**-4.30**	**3.73**
5900		1.80	4.19	-0.45	1.74	**3.69**	**3.37**

The 2.6 GHz antenna shows a decrease of more than 4 dB on average, for ϕ=90º, while for θ=90º a strong increase of gain (more than 10 dB) is observed, suggesting lifting the antenna may increase the gain in the relevant angle window but only for specific angles, as seen in the 2D far-fields before. Finally, the 5.9 GHz antenna shows positive gain differences (around 4 dB increase in gain) in both planes for the increase in height to h_p =20 cm.

Table 4.23 Gain differences of antenna h_p =20 cm compared to h_p =1 cm (fixed elevation).

Frequency [MHz]	Angles	Acquisition angles					Average differences	
		ϕ=80º	ϕ=85º	ϕ=90º	ϕ=95º	ϕ=100º	N_{ang} = 21	N_{ang} = 360
400	θ=90º	-0.72	-0.36	-0.17	-0.19	-0.53	**-0.33**	**-1.01**
900		0.23	-0.34	0.05	-0.36	0.23	**-0.13**	**-3.55**
2600		11.31	10.29	9.99	10.75	10.66	**10.55**	**7.54**
5900		1.83	-2.32	-3.76	-0.50	3.52	**3.95**	**1.02**

Finally, to conclude the analysis, a graph showing the different gains for the three heights is shown for the four frequencies, in Figure 4.11, being possible to conclude the increase in height is generally positive for the 400 MHz and 5.9 GHz antennas, while it impacts negatively the gain for the two centre frequencies, 900 MHz and 2.6 GHz. However, one should note a lower gain but pointing in the correct direction may improve the link between the train and the BS. Only with a clear understanding of the system requirements and the BS placement is possible to understand if these gain differences impact the system performance in a positive or negative way.

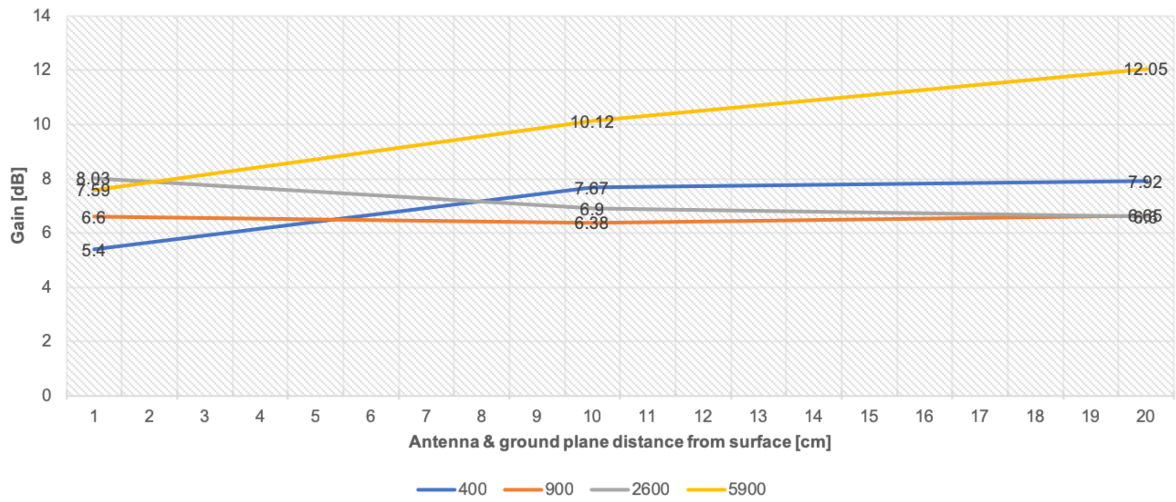

Figure 4.11 Antenna gain vs antenna height.

Finally, from the results of the tests with different heights, it is possible to conclude as follows:

- At 400 MHz, the impacts are mostly negative or neutral, with the increase in height consistently increasing the gain, but with a strong directivity for a range outside the relevant angle window. Gain differences computed show slight reductions or no changes in gain for both the relevant window and N_{ang}=360, therefore the recommendation for 400 MHz systems is to place the antenna closer to roof;
- At 900 MHz, it is possible to see a gain penalty in the pattern for ϕ angles between 60º and 120º for h_p =10 cm while the further increase to 20 cm created a consistent lobe facing forward, tilted up to θ=60º, which might very positive for BS placements far from trackside, depending on system requirements, suggesting 900 MHz systems should place the antenna the highest possible, closer to 20 cm to benefit the forward-facing propagation;
- This effect is similar for 2600 MHz, although in this case both increases in height were positive, with average strong gain improvements for almost all angles and windows, reaching more than 10 dB. Antennas for this system placed higher can reduce significantly the impacts caused by the grooved surface, as this frequency was the most affected by them. Since the negative impacts are reduced with the increase in height, it is hence recommended to, with an average safety approach, add no margin of communications, while for a worst case approach a 7 dB margin should be considered;
- The 5.9 GHz simulations show a strong increase in gain, with a reduction of the half-power beamwidth, and a tilt up of the main lobe direction. Nevertheless, and since the radiation patterns for this frequency are quite disperse, the gain differences show a positive impact of around 4 dB for both heights, but the pattern still shows most gain is radiated for the side views. For this frequency it is, then, generally positive to increase the height of the antenna. The safety margin for the average approach can be avoided with the increase in height, while for the worst case approach a 10 dB margin should be used.

Chapter 5

Conclusions

In this chapter, the final conclusions of this work are presented, featuring a synthesis of the results obtained, recommendations on antenna placement in grooved surfaces, and aspects that may be developed in future works.

The goal of this work was to analyse the performance of antennas mounted on trains for mobile communications, evaluating the influence of their position on the train roof and the roof surface, more specifically two particular issues: the influence of a grooved surface in the antenna performance, and the influence of the antenna height. To assess this goal, a study on the train roof parameters was conducted, followed by the development of a general model. This model is considered to depict the train roof scenario in a reliable way, with dimensions that would allow the simulations to be accurate enough. The frequencies chosen were defined through the industry link. A wide range of simulations were executed through the CST Microwave Studio software, with parameters chosen to be the best trade-off between computational resources and simulation accuracy. The outcomes from simulations allow both quantitative and qualitative approaches to the result analysis, and post-processing functions were developed to extract relevant KPIs.

The thesis starts with Chapter 1, focusing on mobile communications evolution, as well as an overview of the railway industry and what future developments may be, and how mobile communications may be used in the future of rail transportation. The motivations for this work are defined and a thesis structure and contents definition are presented.

Chapter 2 follows, starting with the fundamental concepts for the comprehension of the technical aspects, with a theoretical background on the technologies studied (TETRA, GSM-R, LTE-R and BBRS), concerning the network architecture and radio interface for each of them, and at the end a comparison of services and technical features is presented. Then, the requirements for railway communications are set, with the definition of the different ECTS level standards, system requirements, and quality of service parameters. The different environment scenarios and path loss metrics are shown, as well as the performance parameters that can be analysed, followed by a technical section on antennas, with special focus to the devices most commonly installed on trains. An overview of the CST simulation software is also presented, with a mention to the different solvers and meshing techniques supported. The chapter finishes with the state of the art, where several works on antenna performance and influence of conduction environments are referenced.

In Chapter 3, a model for the work developed is presented, containing the input and output parameters to be considered. On the input side, there are two classes of inputs: antenna parameters, such as the gain, polarisation or the antenna dimensions; and the environment parameters, in this case the longitudinal grooves and the higher placement of the antenna and ground plane, the ones that will be changed to assess the results. Regarding the outputs, these come from the simulation results from CST: 2D and 3D radiation patterns, and other antenna metrics that would help to assess the performance of the system, such as the antenna gain, the half-power beamwidth, the main lobe direction, the reflection coefficient, and the first side lobe level. In this chapter, analytic models for the problem are also presented, with an antenna theory explanation, since this is the theoretical approach for the monopole over a conduction plane scenario, as well as an analysis of the literature on the specific topics addressed, in which it was possible to find several references to the elevated ground plane topic, detailing the minimum and ideal ground plane sizing for optimal performance, however for the irregular surface topic it was not possible to find much literature.

In this chapter the use of the CST tool is also explained in further detail, and the first simulations, performed to evaluate the isolated antennas performance (antennas previously developed by [Ribe18]), are also shown. For these tests, the frequencies for each technology are defined (TETRA – 400 MHz, GSM-R – 900 MHz, LTE-R – 2.6 GHz, BBRS – 5.9 GHz) and the antennas are tested according to the set of parameters defined. The antenna is a quarter-wave monopole, with its height tuned for correct performance. The ground plane size is set according to the minimum size defined in the datasheets of the commercial antennas considered for each of the frequencies (50x50 cm^2), except for the lower frequency, where a bigger ground plane is needed to achieve an acceptable reflection coefficient. The theoretical gain for $\lambda/4$ monopoles over an infinite ground plane is 5.19 dB, and the four antennas show a behaviour according to the theory, with gains less than 1 dB different from the theoretical value, and acceptable reflection coefficients.

The train model is also presented, and an explanation of how it was obtained is given: due to difficulties in finding information on groove size, measurements were made for two types of rolling stock in Portugal, and 3D models were developed in AutoCAD to depict 3.5 per 4 m sections of the train roof. To assess the impact of the grooves, three different models were developed: a flat box of PEC to simulate a flat roof with no irregular surface, a straight roof featuring grooves, and a curved roof featuring grooves, these last two to simulate irregular roof surfaces, both in straight and curved configurations. Groove parameters are also defined since their size and spacing varies for different manufacturers and types of trains. Next, an assessment of the model validity is presented, with the simulated pattern and results being close to what was expected: an increase in the directivity of the antennas, close to the surface of the PEC flat surface, due to its metallic properties. These results validate the model for further use in the following sections.

To the end of Chapter 3, the KPIs for this problem are defined, and they bare basically outputs from CST such as the 2D and 3D radiation patterns, the half-power beamwidth, the main lobe direction and the side lobe level for two different cuts (θ=90º and ϕ=90º). Additionally, post-processing calculations with these metrics offer new KPIs such as the interval in which at least half of the gain is radiated, the gain differences and average gain differences. The equations to compute these additional post-processing KPIs are also defined. For the quantitative analysis, the relevant angle window and acquisition angles for both fixed elevation and fixed azimuth cuts are defined: in the elevation plane (fixed azimuth of ϕ=90º), angles of θ between 45º and 90º are considered the most relevant, while in the azimuth plane (fixed elevation of θ=90º), angles of ϕ between 80º and 100º are set as the most relevant. These angles were defined through a discussion with the industry link, since most train mounted antennas are on the top of the head unit of train compositions, and its link is with a BS that is located in front of it. Since BS placements is mostly done near the railway track, the antennas' relevant angle window are the angles facing forward. Nevertheless, since for lower frequencies the antenna range is higher, the BS placement is sometimes done in surrounding buildings or elevations that can cover a wider region, and for that matter side angles are also important, leading to the average gain differences being calculated also for the full angle range to provide information on the overall impact.

Chapter 4 begins with an overview of the scenarios simulated, first presenting the reference scenario, the one that meets more closely the reality: model of a train featuring a curved, grooved roof, with the antenna and ground plane placed 1 cm above the surface. The grooves for the reference scenario are medium-sized, according to the measurements (w_g=15 mm, h_g=25 mm, d_g=15 mm). Next, the three different approaches for the problem are presented: the first tests the antennas for all the frequencies placed on a flat surface model, on a grooved model with a straight profile, and finally the reference scenario of a curved grooved model; the second, which addresses the impact caused by the groove dimensions, and compares the reference scenario with simulations featuring a new model with wider grooves (w_g=25 mm, h_g=15 mm, d_g=20 mm); and the third, which consists of changing the height of the antenna and ground place in the reference curved groove scenario, in the interval $h_p \in [1; 20]\ \mathrm{cm}$, for which two additional heights were tested after the reference scenario (h_p=10 cm and h_pd=20 cm).

For the first approach, changing the surface in which the antenna is placed has led to strong impacts. The 400 MHz antenna increases its directivity for ϕ between 60º and 120º (relevant angle window), while showing a clear decrease in power for the side view (ϕ=0º and ϕ=180º), which is not expected to impact performance of the overall system. The 2D patterns show significant dispersion caused by the curved surface, along with a wider half-power beam width. The calculated gain differences show, however, the gain does not change significantly neither in the relevant angle window or with N_{ang}=360 degrees, with average gain differences lower than 1 dB. The 900 MHz antenna results again show an increase of the half-power beamwidth, with increased directivity towards the front and rear of the train (ϕ=90º and ϕ=270º) which generally can be considered positive. The 2D far-fields also feature increased dispersion and a strong reduction (3 to 4 dB) of radiated power for the side views (ϕ=0º and ϕ=180º), which might be negative, depending on system requirements and BS placement. The quantitative analysis shows marginal impacts in both cuts (less than 1 dB), with only the curved grooved surface presenting an average increase in gain for the θ=90º of almost 3 dB with N_{ang}=360 compared to the flat surface, hence one can conclude the addition of the grooves and curved surface has, in general, a positive impact for this frequency.

Concerning the 2.6 GHz simulations for this first scenario, it is possible to see the addition of the grooves rises the main lobe direction (from θ=79º for the flat to θ=56º), and the curved surface further increases this metric (to θ=54º), with the main lobe being significantly titled up. For this frequency, the half-power beamwidth increases for both surfaces but shows a stronger increase for the straight grooved model (doubles to 21.4º). The 2D far-fields show a significant reduction of gain (4 to 6 dB) in the 60º to 120º range of the ϕ angle, which might severely impact the propagation, since this range is coincident with the relevant angle window. The dispersion effects can be seen, as for the previous frequencies, with the pattern following the curved surface. Gain differences for the 2.6 GHz simulations show this is the most penalised frequency, which is explained by the fact that the wavelength for this frequency is 11 cm and the groove dimensions are exactly of this order of magnitude. The gain differences were on average -1 to -1.5 dB for the straight grooved surface, increasing to -2.77 dB for the elevation cut of the curved grooved surface, and for -10 dB for the azimuth cut of the same model. A gain reduction of this magnitude is expected to impact severely communications, and should be addressed during the project phase in order to be mitigated.

Finally, the 5.9 GHz simulations show once more a decrease of power for the 60º to 120º range of the ϕ angle, which is quite negative for the overall system performance, along with a strong tilt up of the main lobe direction. The quantitative analysis shows a positive impact of the addition of the grooves for both cuts, with an increase on average of almost 16 dB for the fixed elevation cut. The curved grooved surface has a decrease of almost 5 dB for the fixed azimuth cut, but a gain increase of more than 6 dB. For some angles there is a gain decrease of almost 14 dB in the grooved surface.

Moving on to the second approach, the antennas are tested with the modified curved grooved model, and the results are compared with the reference scenario. For the 400 and 900 MHz antennas, there are no significant changes, other than a slight reduction of power for the side view (3 to 4 dB). This was already expected since these frequencies' wavelengths are λ=75cm and λ=33cm, respectively for the 400 and 900 MHz antennas, and the groove dimensions are far from this. The gain differences' calculations show a slightly higher gain was achieved for the wider grooved model, for both frequencies and both cuts, but noting significant (improvement lower than 0.5 dB).

The 2.6 GHz simulation of the wider grooved model shows no significant changes, with the KPIs having almost the same values compared to the reference scenario. The gain differences show an average modest increase for both cuts (around 1 dB), therefore one can conclude the change in groove dimensions does not impact the performance for the 2.6 GHz antenna. It is worth mentioning this frequency is the most strongly impacted by the grooved surface, as seen in earlier test conclusions, and therefore this test only shows there is no further decline of gain with the groove widening.

For 5.9 GHz, an increase in gain was observed, but since both models show significant dispersion, this might be inconclusive. The wider grooved model shows, however, a very strong reduction of the main lobe direction (from 49º to 5º) together with a reduction to one third of the half-power beamwidth (from 17 dB to 5 dB), meaning the main lobe points upwards and is quite thinner, which is not positive for propagation. On the other hand, the average differences show the gain increases on average for both cuts, even with the increase in dispersion. It was expected the tests for this frequency would show a significant impact since the wavelength for this frequency is 0.05 m which is exactly the dimension changes made to the grooves.

Looking at the results from the third approach, it is important to note this parameter is the one that is more easily managed by the operators and/or the company installing the communication system in the train, since while it might be impossible to change the roof surface morphology, the antenna can be in most cases placed higher at little or no extra cost.

Increasing the height for the 400 MHz antenna has mostly negative or neutral impacts, with a consistent increase in gain (2 dB) but also with the appearance of a strongly directive lobe for a range outside the relevant angle window (ϕ=135º), and the gain differences computed show slight reductions (maximum of 2.32 dB) or no changes in gain for both N_{ang} ranges considered.

In the 900 MHz patterns, there is a significant gain penalty in the relevant angle window for h_p=10 cm while the further increase to 20 cm creates a consistent lobe facing forward, tilted up to θ=60º which is very positive for environments where the BS placement is far from the trackside.

The 2.6 GHz tests show results similar to the 900 MHz, although for this case both increases in height are positive, with average strong gain improvements for almost all angles, reaching more than 10 dB. Antennas for 2.6 GHz systems are therefore recommended to be placed higher, at least with h_p=10 cm (or 0.9λ) but better with h_p=20 cm (or 1.7λ) since at this frequency the higher placement can eliminate or at least mitigate the strong impacts of the grooves in the propagation.

Last but not least, the 5.9 GHz simulations show a strong increase in gain (from 7.6 dB up to 12 dB with the increases in height), with a reduction of the half-power beamwidth to 2.2º, and a tilt up of the main lobe direction, but as with the other approaches, the radiation patterns show a very disperse radiation. Although the gain differences computed for this frequency show a positive impact of around 4 dB for both heights, the pattern still shows most gain is being radiated for the side views. In spite of this, it is generally positive to increase the height of the antenna.

In order to guarantee the link between the train-mounted antenna and the BS, some recommendations are drawn according to the results presented in Chapter 4:

- For 400 MHz systems the grooves do not impact significantly, but communications can be improved keeping the antenna close to the train roof;
- For 900 MHz systems, the addition of the grooves does not cause a gain loss, however increasing its height for h_p=20 cm improves the gain, hence doing so is recommended;
- For 2.6 GHz systems the strong impacts due to the grooved surface lead to the recommendation of adding a safety communications margin of 10 dB if an average approach is used, or 14 dB for the worst-case approach (i.e. if vital systems depend on this link and the communication needs to be assured at any cost). It is, however, possible to reduce these margins if the antenna height is increased to 20 cm, and doing so the recommendation is to add a 7 dB safety margin only for the worst case approach;
- For 5.9 GHz systems grooved surfaces are also expected to generate strong impacts, and therefore a 5 dB safety margin should be considered as average approach, with 14 dB for the worst case approach. Being possible to increase the height of the antenna to 20 cm, then it is recommended to add a 10 dB safety margin only for the worst case approach.

Finally, this work could be enhanced with the study of additional train roof features, such as other degrees of curvature or extra groove dimensions. Other antenna types could be considered, such as microstrip antennas (patch antennas) or arrays of antennas, or else the position of the antenna could be changed for underneath the metallic train roof, for example in the front cabin window, to address train classes where due to gauge limitations it is not possible to place the antenna on top of the roof. Additionally, some trains featuring fibreglass and composite materials do not help in providing a suitable ground plane for the antenna, and therefore it would be worth to address this issue, testing antennas on top of non-metallic train roof models. The use of diversity could also be interesting to test. Finally, performing measurements in real train scenarios would also be very positive to the understand the validity of the conclusions presented here.

Annex A

Technologies comparison

In this table, a brief comparison of GSM-R, TETRA, BBRS and LTE-R technologies is presented. Infrastructure, Radio Interface and Performance issues are mentioned, as well as the Services provided by each technology and the specific solutions for those services.

Table A.1 Railway communications using GSM-R, TETRA, BBRS and LTE-R technologies.

Infrastructure	**GSM-R**	**TETRA**	**BBRS**	**LTE-R**
ETSI standard availability	1997	1996	Not yet	Not yet
Network scalability	No small network capacity	Scalable from single site to nationwide	Scalable but not suitable for big scale	No small network capacity
Infrastructure cost	Higher than GSM (standard GSM architecture + rail-specific elements)	Requires no commercial architectural elements	Low (less expensive equipment)	Higher than LTE (standard LTE plus rail specific elements)
Maintenance cost	Higher (more sites to maintain)	Cheaper (less sites to maintain)	Low (cheaper to maintain per site)	Higher (more sites to maintain)
Radio Interface				
Modulation	GMSK	$\pi/4$ DQPSK	BPSK/QPSK/ 16-64-QAM	QPSK/16-QAM
Bandwidth (MHz)	4	0.025	20-40	1.4-20
Frequency bands (MHz)	873-880 918-925	380-400 410-430 450-470 800	2405-2495 5150-5825 5825-5925	400 800 1800 2600
Guard bands (MHz)	0.3	0.025	4	0.14-2
Performance				
Receiver sensitivity (dBm)	-104	-103	-104	-103
Maximum MT speed (km/h)	500	500	250	500
Maximum propagation distance (km)	40	58	1	35
Common propagation distance (km)	5-10	10-25	0.3	4-12
Cell handover time (ms)	≈ 0	≈ 0	<100	≈ 0
Call access time (s)	5-8.5	0.5	NA	1.5-2
Group, individual and broadcast call setup time (s)	5	0.5	NA	1.5
Priority/emergency call (s)	2	0.5	NA	0.1
DL peak data rate (Mbps)	0.172	0.029	125	50
UL peak data rate (Mbps)	0.172	0.029	125	10

Services				
Full duplex voice	Yes	Yes	No	No
Call queuing	No	Yes	No	No
Status messaging	Yes	Yes	Yes	Yes
Short data messaging	Yes	Yes	Yes (IP)	Yes (IP)
Circuit mode data	Yes	Yes	No	No
Simultaneous voice and data	Yes	Yes	Yes	Yes (VoLTE)
Packet data	No	Yes	Yes	Yes
Direct Mode Operation	No	Yes	No	No
Specific railway services				
Addressing modes	Location-dependent addressing (LDA)	Short Subscriber Identity (SSI) addressing	NA	LTE positioning protocol (LPP)
Signalling	Functional addressing (FA)	Session Initiation Protocol (SIP)	NA	Session Initiation Protocol (SIP)
Broadcast calls	Voice broadcast calls (VBS)	TMO broadcast calls	NA	Evolved Multimedia Broadcast Multicast Services (eMBMS)
Group calls	Voice group call services (VGCS)	TMO and DMO group calls	NA	Push-to-talk over Cellular (PoC)
Emergency calls	Railway emergency calls (REC, e-REC)	Red-button emergency call (works in DMOl)	NA	IMS emergency calls
Queuing	Priority and Pre-emption (eMLPP)	Pre-emptive Priority Call (PPC)	NA	Allocation and Retention Priority (ARP)
Call set up	Fast call set up	Fast call set up	NA	Very low latency; access class barring
Messaging services	SMS services	Short Data Service (SDS)	NA	IMS-based SMS

Information shown is based on data from [3GPP17], [ETSI97], [GSMR15b], [SEPU17], [THAL18] as well as [HAWG16], taking into account the most common options for railway communication systems.

Annex B

Train Antenna K702021 datasheet

Datasheet of a common broadband antenna used in the railway industry, featuring a fiberglass radome and suitable to high-speed rail operation, but most commonly used in tramways and light rail networks. Operates frequencies between 410-470 MHz. It is commonly used in TETRA and other PMR systems. Extracted from [Kath18c].

Train Antenna 410 – 470 MHz K702021

KATHREIN

• Low profile broadband antenna in fiberglass radome.

Type No.	**K702021** 601118
Input	N female
Frequency range	410 – 470 MHz
VSWR	< 1.5
Gain	0 dB (ref. to the quarter-wave antenna)
Impedance	50 Ω
Polarisation	Vertical
Max. power	170 W (at 50° C ambient temperature)
Radome weight	159 g [0.4 lb]
Total weight	500 g [1.1 lb]
Packing size (outside)	151 x 87 x 210 mm [5.9 x 3.4 x 8.3 inches]

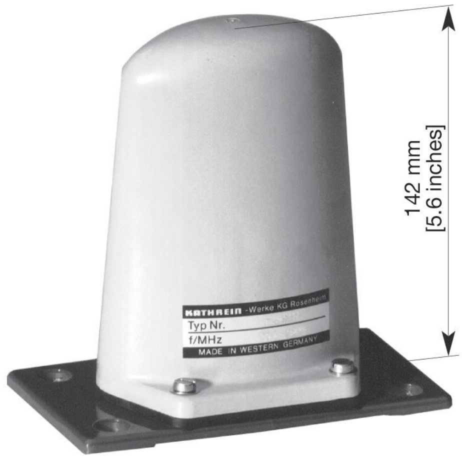

Material:	Radiator and Flange: Aluminum. Radome: Fiberglass, color: Light grey. All screws and nuts: Stainless steel. Sealing: Neoprene and rubber. **Note:** Don’t use detergents that might harm the sealing.
Mounting:	On a conductive surface with a minimum size of 50 x 50 cm [19.7 x 19.7 inches] by means of existing M10 studs.
Grounding and high voltage protection:	This antenna approved by the “Deutsche Bahn AG” is DC grounded to protect against lightning and high-tension lines.

Mounting flange:

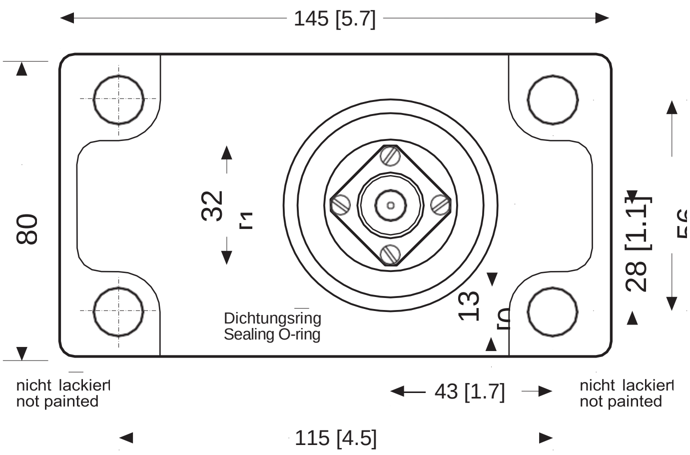

All dimensions in mm and [inches]

Mounting hole for the connector: 33 (max. 35) mm diameter.

Note: Keep mounting surface clear of paint for electrical contact.

Subject to alteration.

936.005/d

Fire prevention:	UL94 (HB) DIN 5510 T2 DIN EN 45545-2: 2013
IP class:	IP 66 (when product is mounted properly)
Standards:	EN 50122-1 EN 50125 EN 50155 EN 60068-2-1 EN 60068-2-2 EN 60068-2-6 EN 60068-2-27 EN 60068-2-30 EN 61373 ETS 300 019-1-2 class 2.2 ETS 300 019-1-1 T 1.2 ETS 300 019-1-5 T 5.2 ETS 300 019-2-2 T 2.2 ETS 300 019-1-2 T 1.2

Annex C

Train Antenna K741009 datasheet

Datasheet of a common broadband antenna used in the railway industry, featuring a fiberglass radome and suitable to high-speed rail operation. Operates frequencies between 870-960 MHz. It is commonly used in GSM-R systems. Extracted from [Kath18a].

KATHREIN SE • P.O. Box 10 04 44 • 83004 Rosenheim • Germany

Rosenheim, 01.05.2018

KATHREIN-Werke KG ist jetzt KATHREIN SE
KATHREIN-Werke KG is now KATHREIN SE

Zum 1. Mai 2018 ist die KATHREIN-Werke KG auf die KATHREIN SE, einer Europäischen Aktiengesellschaft (Societas Europaea), übergegangen.

Die neuen Firmendaten lauten seither wie folgt:
KATHREIN SE
Anton-Kathrein-Str. 1-3
83022 Rosenheim, Deutschland
Steuer-Nr.: 156/117/30745
UST-Ident-Nr.: DE 131 558 540
Registergericht: Traunstein, HRB 24848

On 1st May 2018, KATHREIN-Werke KG has been transferred to KATHREIN SE, a European stock corporation (Societas Europaea).

Since then the company data is as follows:
KATHREIN SE
Anton-Kathrein-Str. 1-3
83022 Rosenheim, Deutschland
Tax ID No.: 156/117/30745
VAT Reg. No.: DE 131 558 540
Commercial Register: Traunstein, HRB 24848

KATHREIN SE

Anton-Kathrein-Straße 1-3
83022 Rosenheim
Germany
Phone: +49 8031 184-0
Fax: +49 8031 184-306
www.kathrein.com

936.00002

Train Antenna 870 – 960 MHz 741009

KATHREIN

- Broadband antenna of very low profile in fiberglass radome.
- Special radome suitable for high-speed trains.
- The antenna fulfils the requirements according to EN 50155.

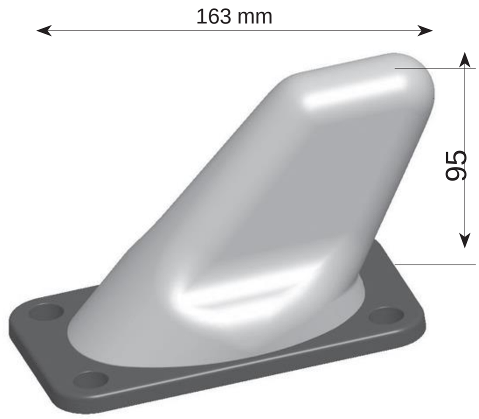

Type No.	741009
Input	N female
Frequency range	870 – 960 MHz
VSWR	< 1.5
Gain	0 dB (ref. to quarter-wave antenna)
Impedance	50 Ω
Polarisation	Vertical
Max. power	100 W (at 50 °C ambient temperature)
Radome weight	166 g
Total weight	500 g
Packing size (outside)	137 x 92 x 174 mm

Material:	Radiator: Brass. Flange: Aluminum. Radome: Fiberglass; Colour: Light grey. All screws and nuts: Stainless steel. Sealing: Neoprene and nitrile rubber. **Note:** Don't use detergents that might harm the sealing
Mounting:	On a conductive surface of a minimum size of 50 x 50 cm by means of 4 existing M10 studs.
Grounding and high voltage protection:	This antenna, which is approved by the "Deutsche Bahn AG", is DC grounded to protect against lightning and high-tension lines.

Mounting flange:

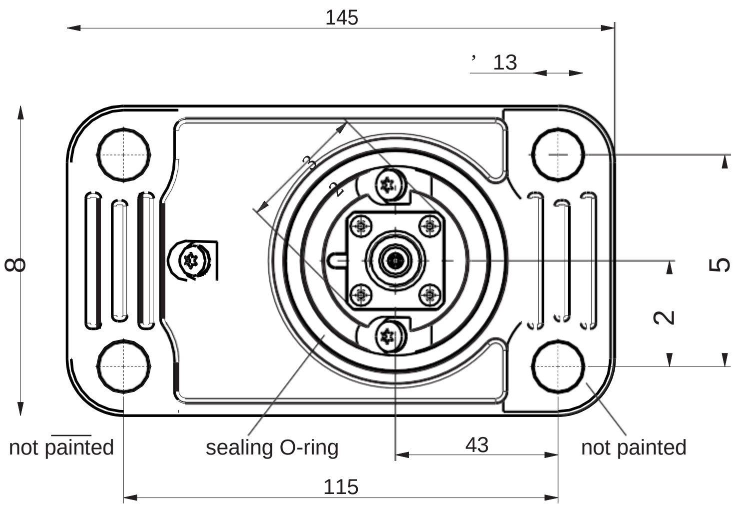

936.1443/b Subject to alteration.

Mounting hole for the connector: 33 (max. 35) mm diameter.

Note: Keep mounting surface clear of paint for electrical contact.

All dimensions in mm.

Train Antenna 870 – 960 MHz

KATHREIN

741009

Fire prevention:	UL94 (HB) DIN 5510 T2 DIN EN 45545-2: 2013
IP class:	IP 66 (when product is mounted properly)
Standards:	EN 50122-1 EN 50125 EN 50155 EN 60068-2-1 EN 60068-2-2 EN 60068-2-6 EN 60068-2-27 EN 60068-2-30 EN 61373 ETS 300 019-1-2 class 2.2 ETS 300 019-1-1 T 1.2 ETS 300 019-1-5 T 5.2 ETS 300 019-2-2 T 2.2 ETS 300 019-1-2 T 1.2

Any previous data sheet issues have now become invalid.

Annex D

Train Antenna K87010010 datasheet

Datasheet of a common broadband antenna used in the railway industry, featuring a fiberglass radome and suitable to high-speed rail operation. Operates frequencies between 1710-3800 MHz. Designed for LTE-R systems, it works also with UMTS, W-LAN and WiMAX technologies. Extracted from [Kath18b].

KATHREIN SE • P.O. Box 10 04 44 • 83004 Rosenheim • Germany

KATHREIN SE

Anton-Kathrein-Straße 1–3
83022 Rosenheim
Germany

Phone: +49 8031 184-0
Fax: +49 8031 184-306
www.kathrein.com

Rosenheim, 01.05.2018

KATHREIN-Werke KG ist jetzt KATHREIN SE
KATHREIN-Werke KG is now KATHREIN SE

Zum 1. Mai 2018 ist die KATHREIN-Werke KG auf die KATHREIN SE, einer Europäischen Aktiengesellschaft (Societas Europaea), übergegangen.

Die neuen Firmendaten lauten seither wie folgt:
KATHREIN SE
Anton-Kathrein-Str. 1-3
83022 Rosenheim, Deutschland
Steuer-Nr.: 156/117/30745
UST-Ident-Nr.: DE 131 558 540
Registergericht: Traunstein, HRB 24848

On 1st May 2018, KATHREIN-Werke KG has been transferred to KATHREIN SE, a European stock corporation (Societas Europaea).

Since then the company data is as follows:
KATHREIN SE
Anton-Kathrein-Str. 1-3
83022 Rosenheim, Deutschland
Tax ID No.: 156/117/30745
VAT Reg. No.: DE 131 558 540
Commercial Register: Traunstein, HRB 24848

936.00002

Train Antenna 1710 – 3800 MHz 87010010

- Multi-band antenna: 1800/1900/UMTS/LTE/W-LAN/WiMAX.
- The antenna can be operated in all frequency ranges simultaneously.
- Low profile antenna in fiberglass radome.
- The antenna fulfils the requirements according to EN 50155.

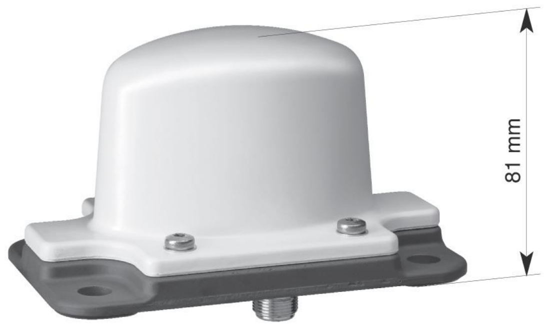

Type No.	87010010
Antenna multi-band	
Input	N female
Frequency range	1710 – 3800 MHz
VSWR	1710 – 1920 MHz: < 1.6 1920 – 3800 MHz: < 1.5
Gain	0 dB (ref. to the quarter-wave antenna)
Impedance	50 Ω
Polarisation	Vertical
Max. power	100 W (at 50° C ambient temperature)
Inner conductor	DC grounded
Radome weight	115 g
Total weight	450 g
Packing sia, L x W x H	152 x 91 x 125 mm
Height	81 mm

Material: Radiator: Copper and brass.
Flange: Aluminum. Radome: Fiberglass.
All screws and nuts: Stainless steel.
Colour: Grey.
Sealing: Neoprene and silicon. **Note:** Don’t use detergents that might harm the sealing.

Mounting: On a conductive surface with a minimum size of 50 x 50 cm.

Grounding and high voltage protection: This antenna, tested by an independent institute and approved by the “Deutsche Bahn AG”, is DC grounded to protect against lightning and high-tension lines.

Mounting flange:

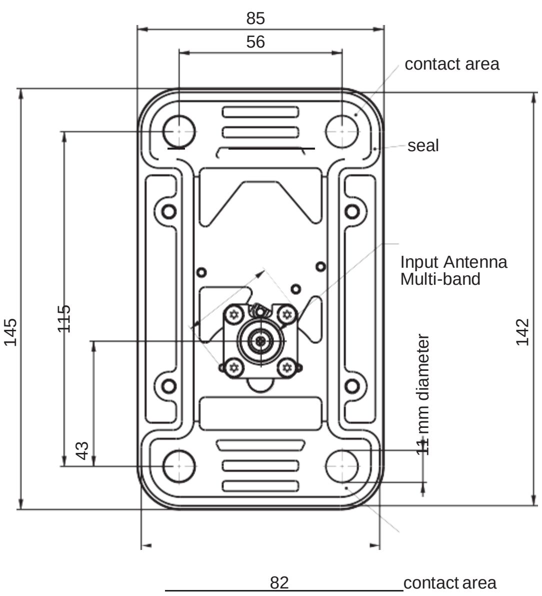

Mounting hole for the connector: 33 (max. 35) mm diameter.

Note: Keep mounting surface clear of paint for electrical contact.

Evenness of opposite surface 0.2 mm.

Use a cap nut or hex-head screw plus the enclosed sealing washer.

Subject to alteration.

Fire prevention:	UL94 (HB) DIN 5510 T2 DIN EN 45545-2: 2013
IP class:	IP 66 (when product is mounted properly)
Standards:	EN 50122-1 EN 50125 EN 50155 EN 60068-2-1 EN 60068-2-2 EN 60068-2-6 EN 60068-2-27 EN 60068-2-30 EN 61373 ETS 300 019-1-2 class 2.2 ETS 300 019-1-1 T 1.2 ETS 300 019-1-5 T 5.2 ETS 300 019-2-2 T 2.2 ETS 300 019-1-2 T 1.2

Annex E

Train Antenna K87010022 datasheet

Datasheet of a multi-band antenna used in the railway industry, featuring a fiberglass radome and suitable to high-speed rail operation, but most commonly used in tramways and light rail networks. Operates frequencies between 694-6000 MHz, being commonly used in BBRS and other Wi-Fi based systems, as it features WLAN 5.8. Extracted from [Kath18d].

Train Antenna 694 – 6000 MHz

KATHREIN

and GNSS (GPS, GLONASS, BEIDOU, GALILEO) 87010022

- Multi-band antenna: 700/800/900/1800/1900/UMTS/2600/3500/5000/ LTE/W-LAN and GNSS.
- The antenna can be operated in all frequency ranges simultaneously.
- Low profile antenna in fiberglass radome.
- The antenna fulfils the requirements according to EN 50155.

Type No.		87010022
Antenna multi-band		
Input		**N female**
Frequency range	**MHz**	**694 – 6000**
VSWR		**694 – 960 MHz: < 1.5** **1350 – 4920 MHz: < 1.8** **4920 – 6000 MHz: < 2.0**
Gain	**dB**	**0 (ref. to the quarter-wave antenna)**
Impedance	**Ω**	**50**
Polarisation		**Vertical**
Max. power	**W**	**40 (at 50° C ambient temperature)**
Operating temperature	**°C**	**−40 – +85**
Inner conductor		**DC grounded**
Antenna GPS / Galileo / GLONASS / BEIDOU		
Center frequency	**MHz**	**1581 ± 5**
Bandwidth in 10 dB	**MHz**	**49**
Polarisation		**Right hand circular**
Peak gain at Fc	**dBic**	**3**
Integrated LNA		
Frequency range	**MHz**	**1550 – 1610**
VSWR		**< 2.0**
Impedance	**Ω**	**50**
Gain	**dB**	**23 ± 3**
Noise figure	**dB**	**typ. 2.0, max. 2.5**
Operation voltage	**V**	**2.5 ... 5.5**
Operation current	**mA**	**typ. 7, max. 10**
Input		**N female, 110 mm | 4.3 inches cable length**
Radome weight	**g | lb**	**180 | 0.4**
Total weight	**g | lb**	**630 | 1.4**
Packing size	**mm** **inches**	**170 x 120 x 100** **6.7 x 4.7 x 3.9**
Height	**mm** **inches**	**93** **3.7**

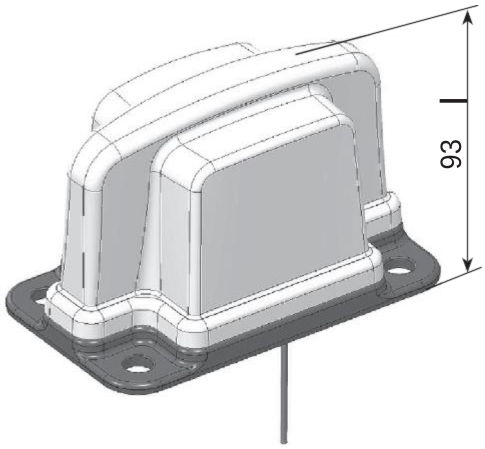

Mounting flange:

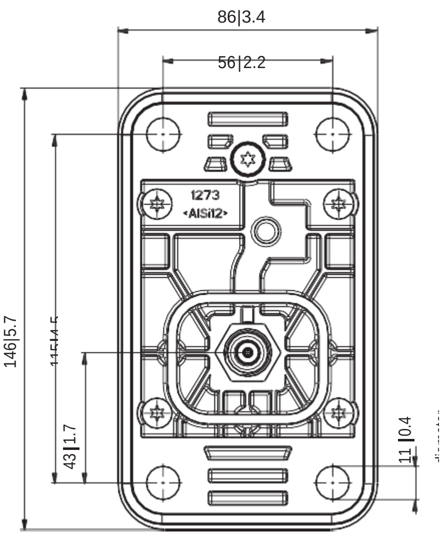

Material: Radiator: Aluminum
Flange: Aluminum. Radome: Fiberglass. All screws and nuts: Stainless steel.

Colour: Grey.
Sealing: Polyurethan and silicone. **Note:** Don't use detergents that might harm the sealing.

Mounting: On a conductive surface with a minimum size of 50 x 50 cm | 19.7 x 19.7 inches using 4 M10 bolts.

Mounting hole for the connector: 33 (max. 35) mm |

1.3 (max. 1.4) inches diameter.

Note: Keep mounting surface clear of paint for electrical contact.

Evenness of opposite surface 0.2 mm | 0.008 inches. Surface roughness of opposite surface max. R_z40

Annex F

Far-field views of $\lambda/4$ monopoles

Far-field views of the $\lambda/4$ monopole based on [Ribe18] design and modified to work with each system according to the specific parameters of each antenna (datasheets in Annexes B-E).

TETRA

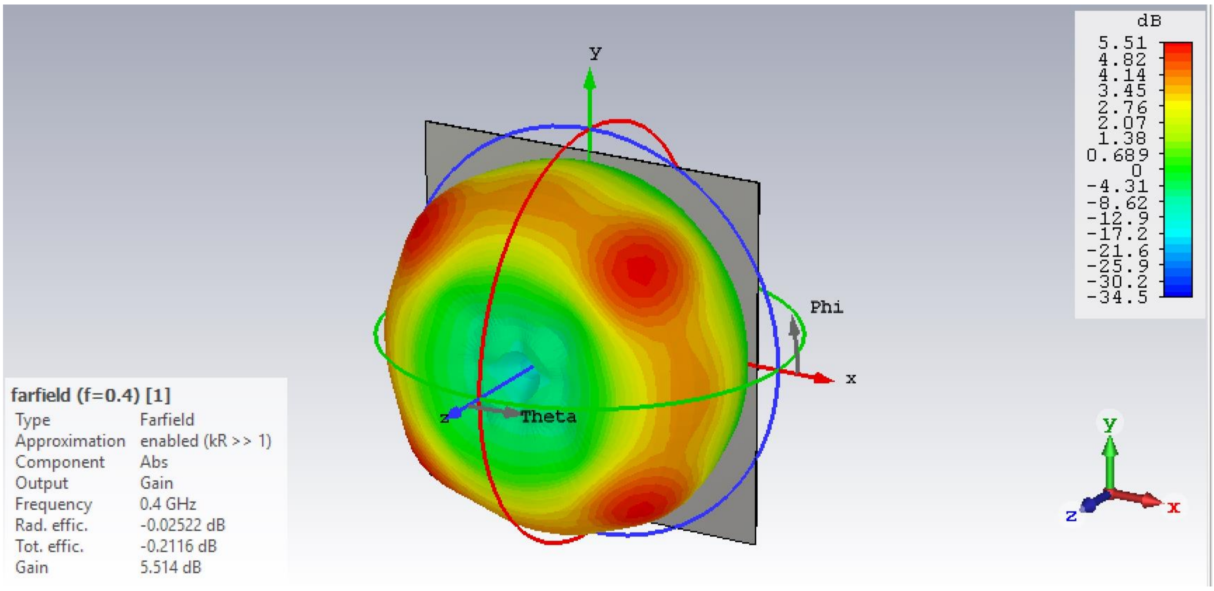

Figure F.1 Far-field view of a λ/4 monopole operating at 400 MHz.

GSM-R

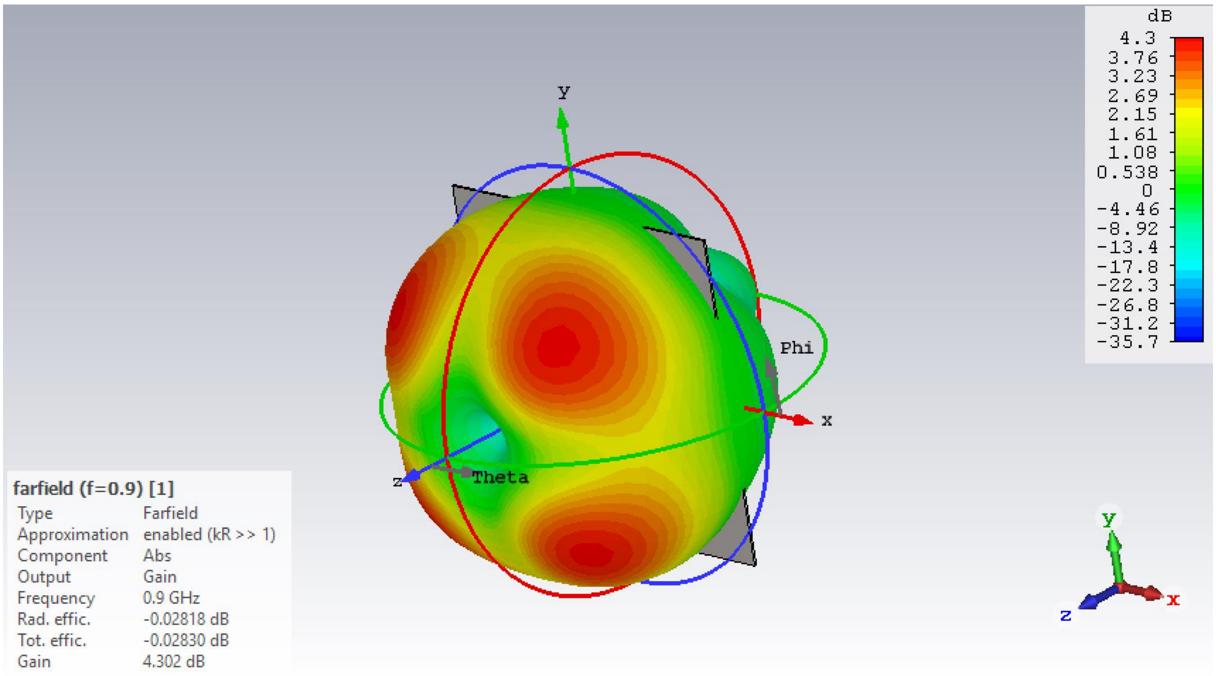

Figure F.2 Far-field view of a λ/4 monopole operating at 900 MHz.

LTE-R

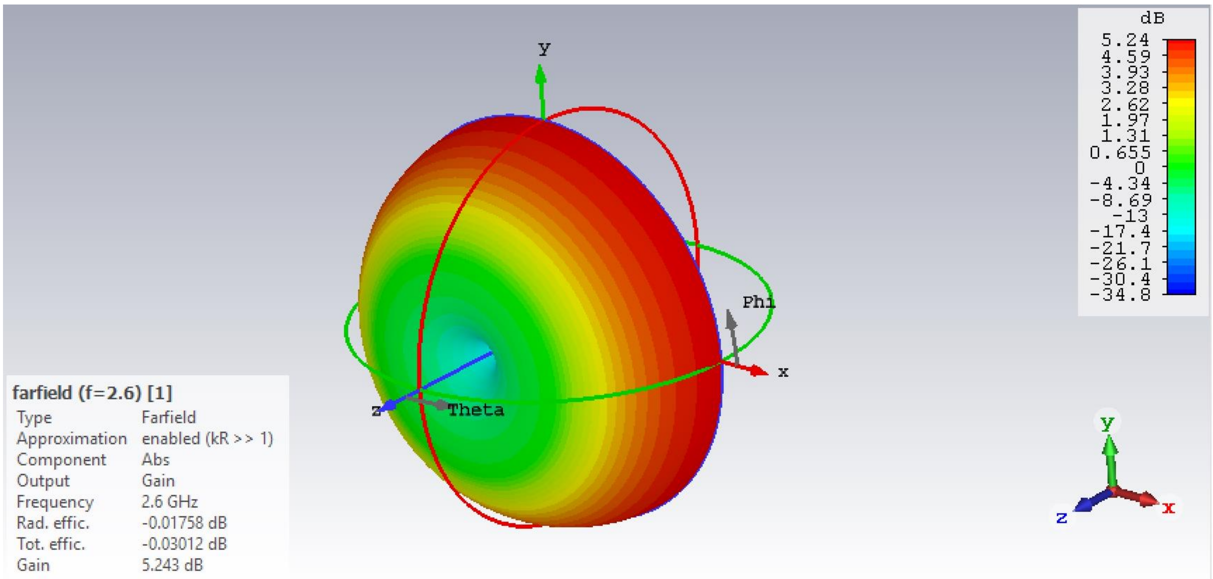

Figure F.3 Far-field view of a λ/4 monopole operating at 2.6 GHz.

BBRS

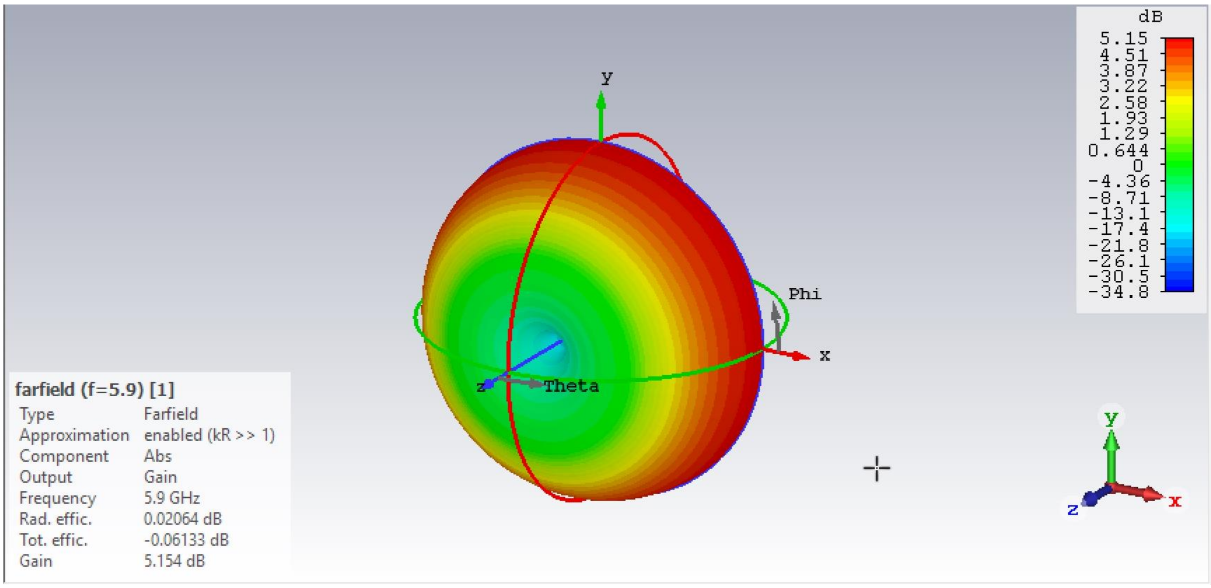

Figure F.4 Far-field view of a λ/4 monopole operating at 5.9 GHz.

Annex G

Far-field views of test antennas with flat surface

Using the antennas whose tests can be found in Annex F, here are presented the far-field views of the antennas 1 cm over the flat surface (rectangle box of PEC).

TETRA

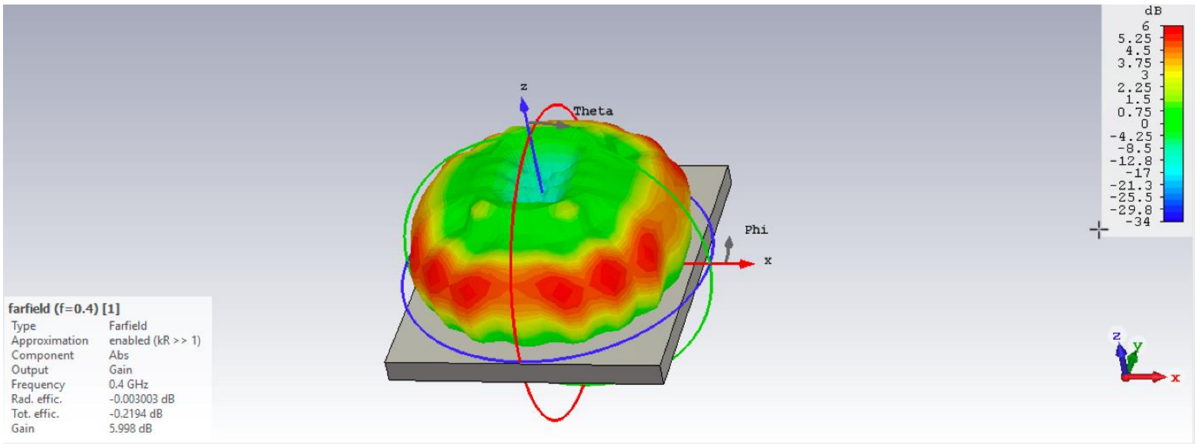

Figure G.1 3D far-field flat surface with a 400 MHz antenna.

GSM-R

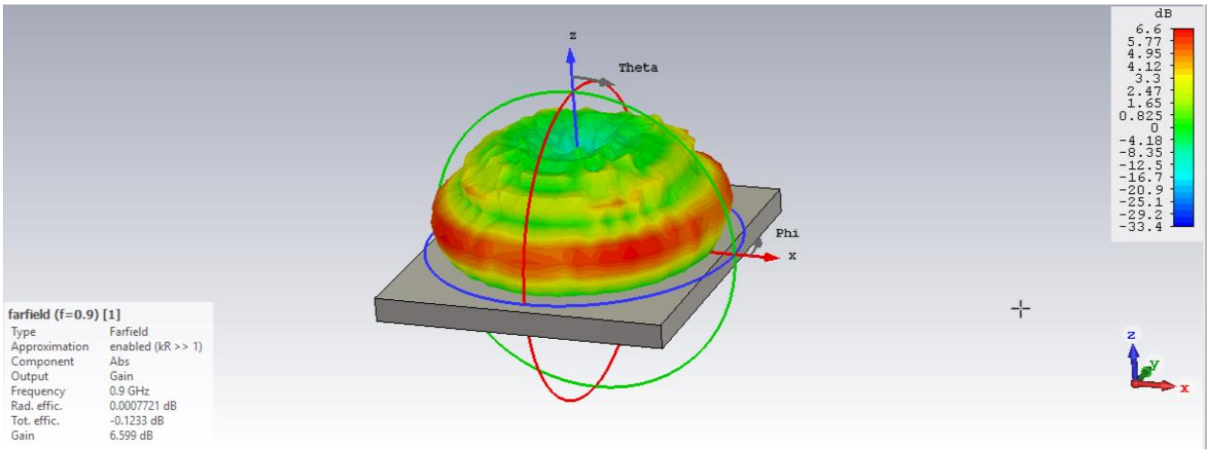

Figure G.2 3D far-field flat surface with a 900 MHz antenna.

LTE-R

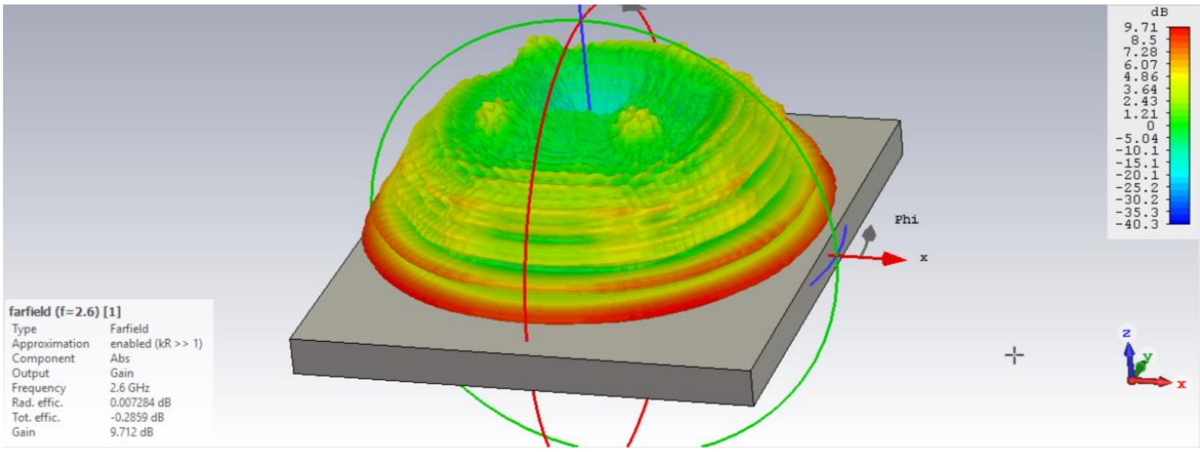

Figure G.3 3D far-field flat surface with a 2.6 GHz antenna.

BBRS

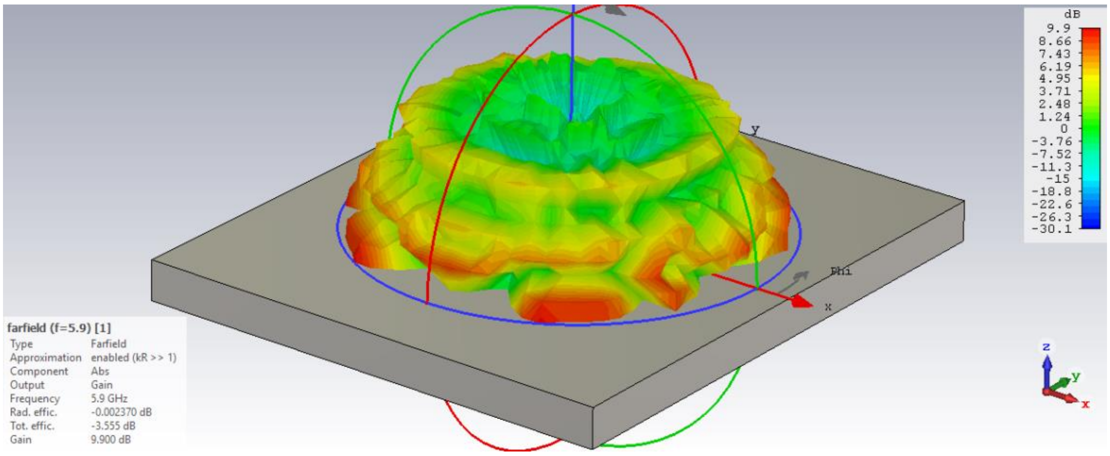

Figure G.4 3D far-field flat surface with a 5.9 GHz antenna.

Annex H

Influence of the grooved surface: 2D far-field results

Far-field views of the antennas for the four systems comparing the radiation patterns for the different 3D models: flat surface, straight grooved surface, curved grooved surface.

TETRA (400 MHz)

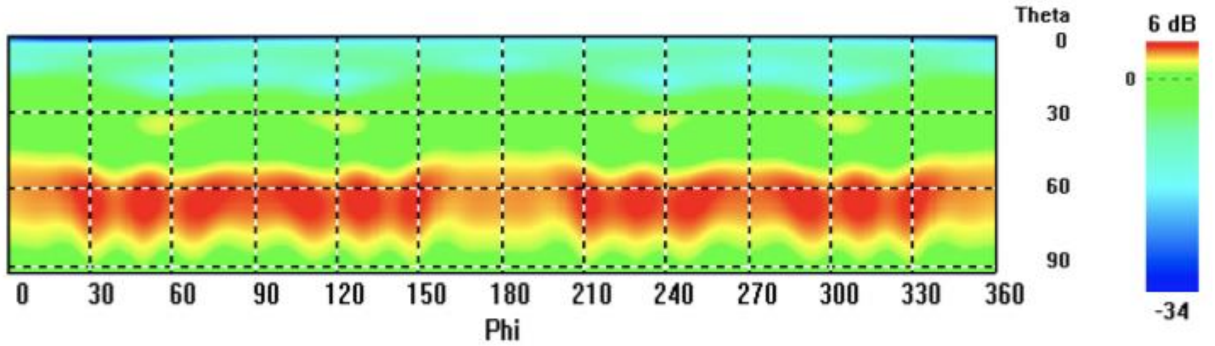

Figure H.1 Far-field performance of the 400 MHz antenna over the flat surface.

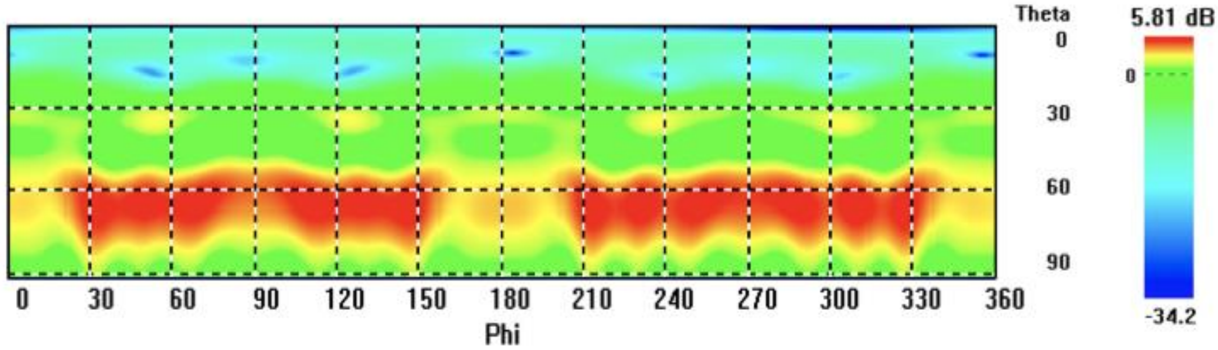

Figure H.2 Far-field performance of the 400 MHz antenna over the straight grooved surface.

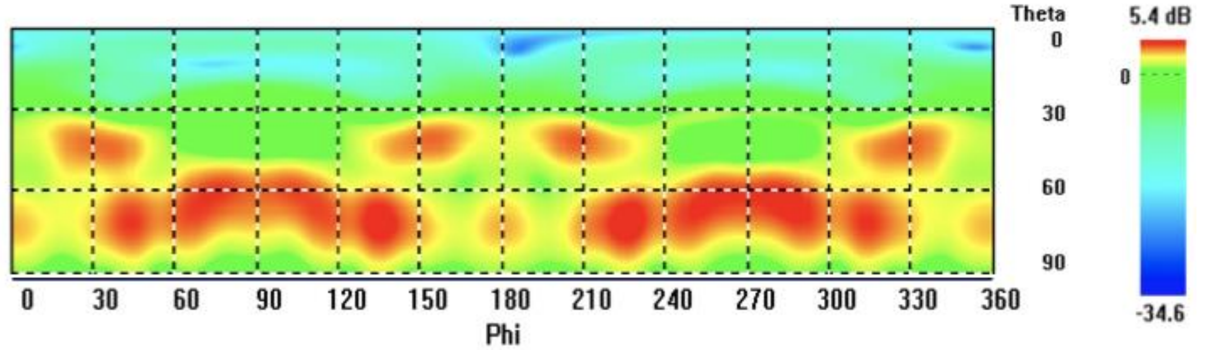

Figure H.3 Far-field performance of the 400 MHz antenna over the curved grooved surface.

GSM-R (900 MHz)

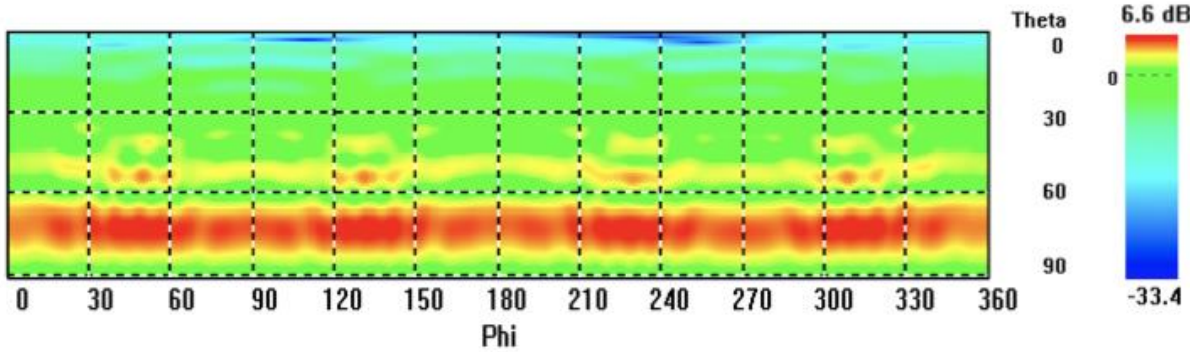

Figure H.4 Far-field performance of the 900 MHz antenna over the flat surface.

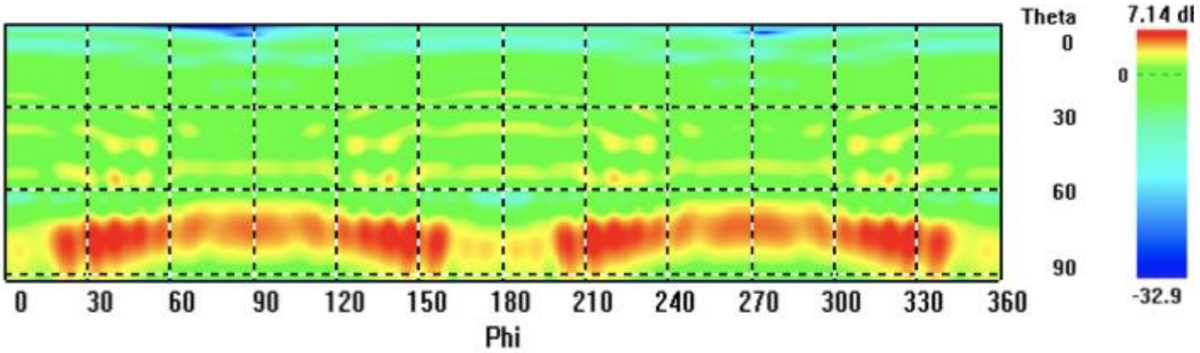

Figure H.5 Far-field performance of the 900 MHz antenna over the straight grooved surface.

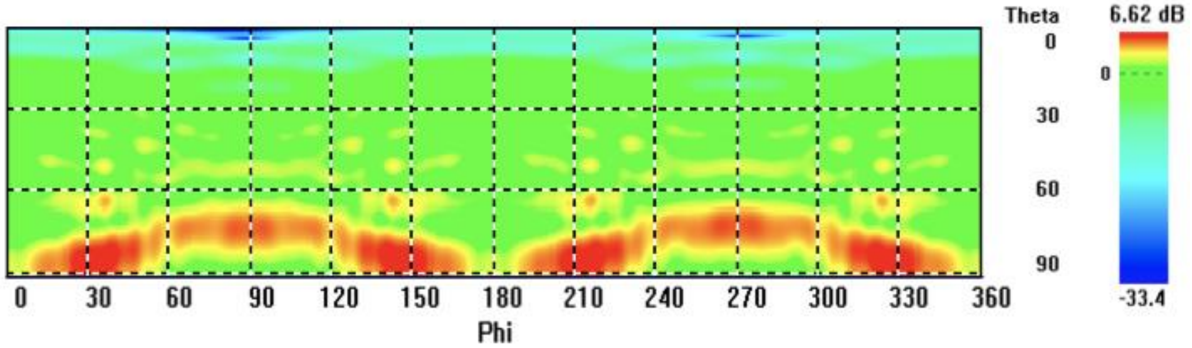

Figure H.6 Far-field performance of the 900 MHz antenna over the curved grooved surface.

LTE-R (2.6 GHz)

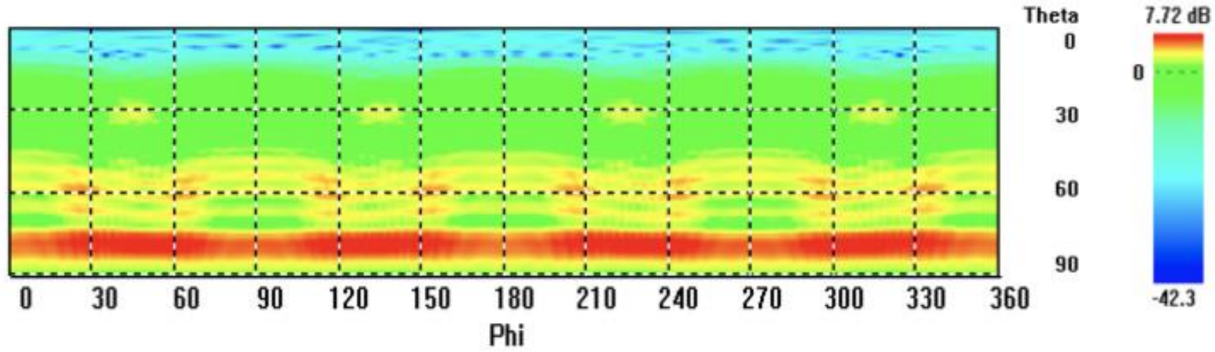

Figure H.7 Far-field performance of the 2.6 GHz antenna over the flat surface.

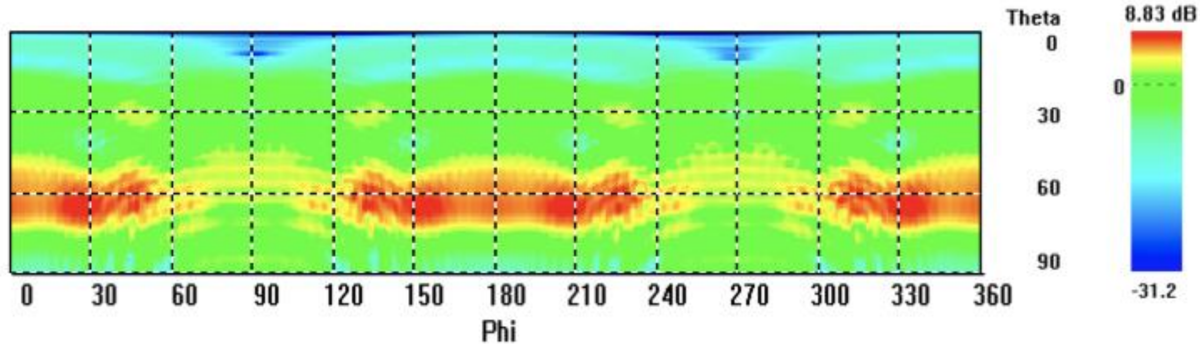

Figure H.8 Far-field performance of the 2.6 GHz antenna over the straight grooved surface.

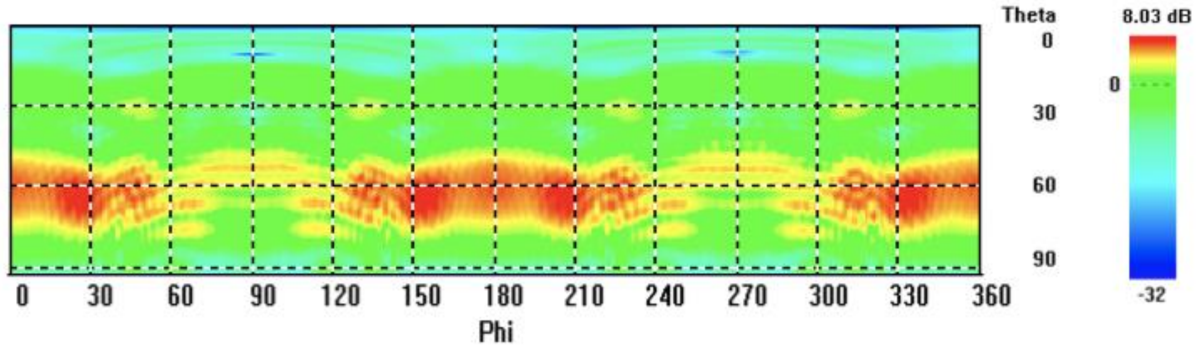

Figure H.9 Far-field performance of the 2.6 GHz antenna over the curved grooved surface.

BBRS (5.9 GHz)

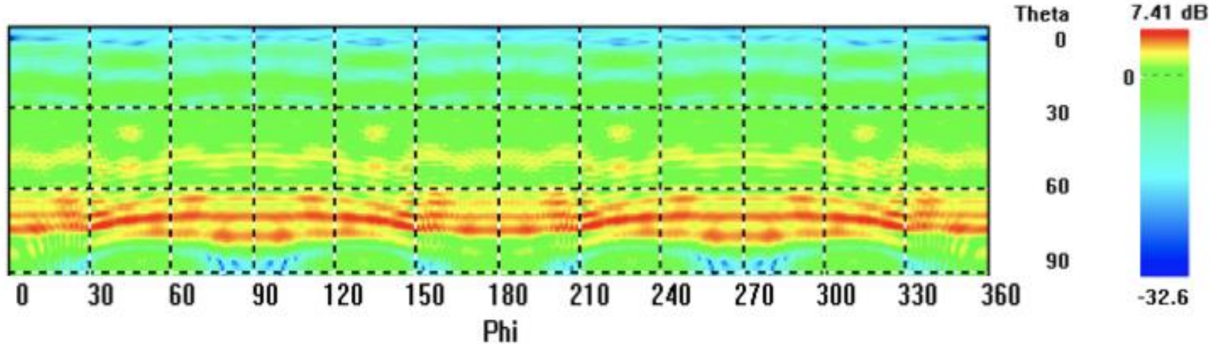

Figure H.10 Far-field performance of the 5.9 GHz antenna over the flat surface.

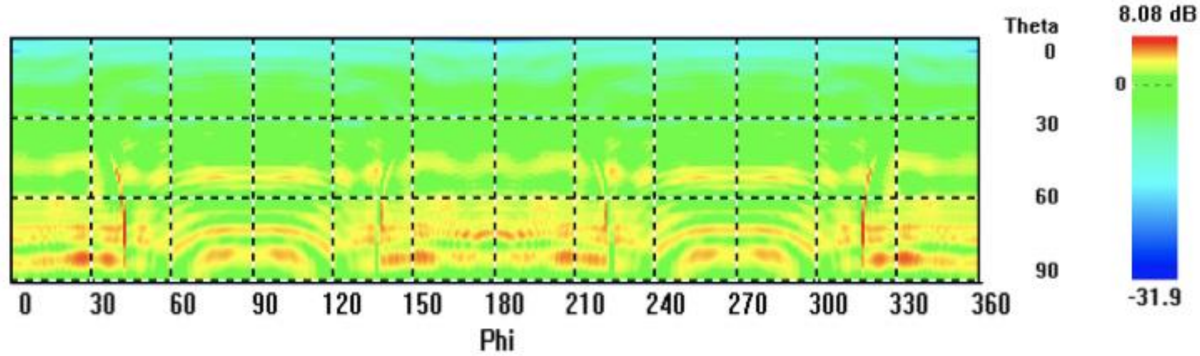

Figure H.11 Far-field performance of the 5.9 GHz antenna over the straight grooved surface.

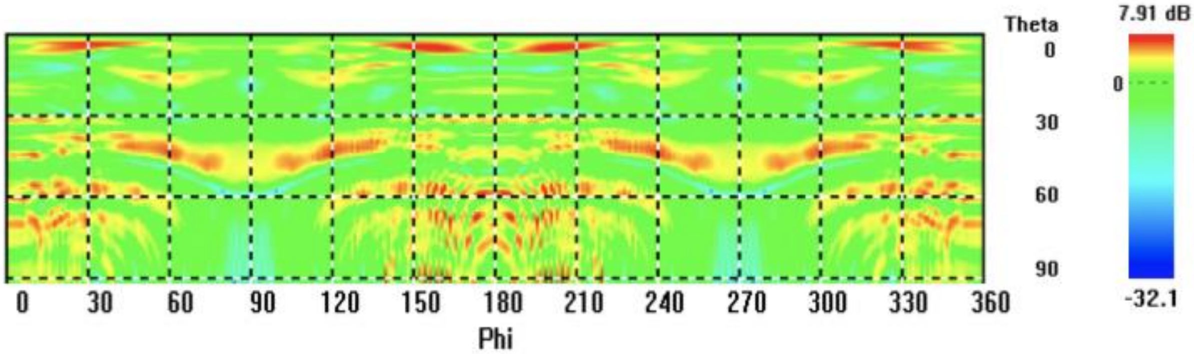

Figure H.12 Far-field performance of the 5.9 GHz antenna over the curved grooved surface.

Annex I

Influence of the grooves dimensions: 2D far-field results

Far-field views of the antennas for the four systems comparing the radiation patterns for the reference curved grooved scenario and the wider grooved model.

TETRA (400 MHz)

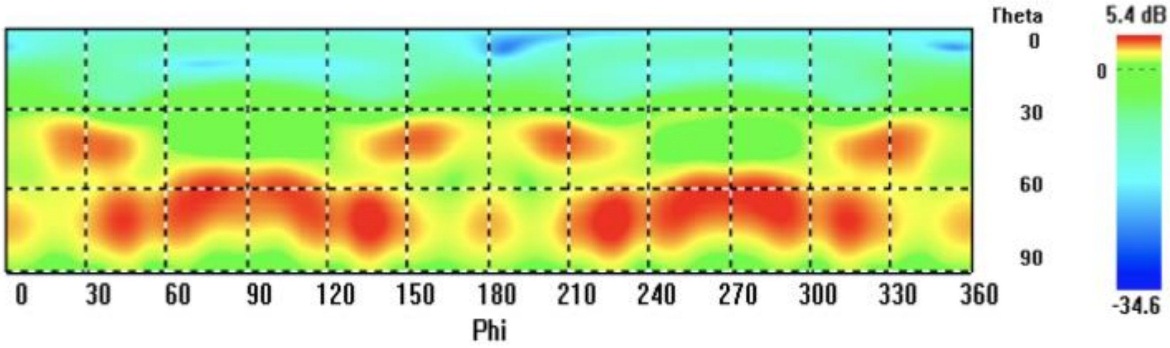

Figure I.1 Far-field performance of the 400 MHz antenna over the reference grooved surface.

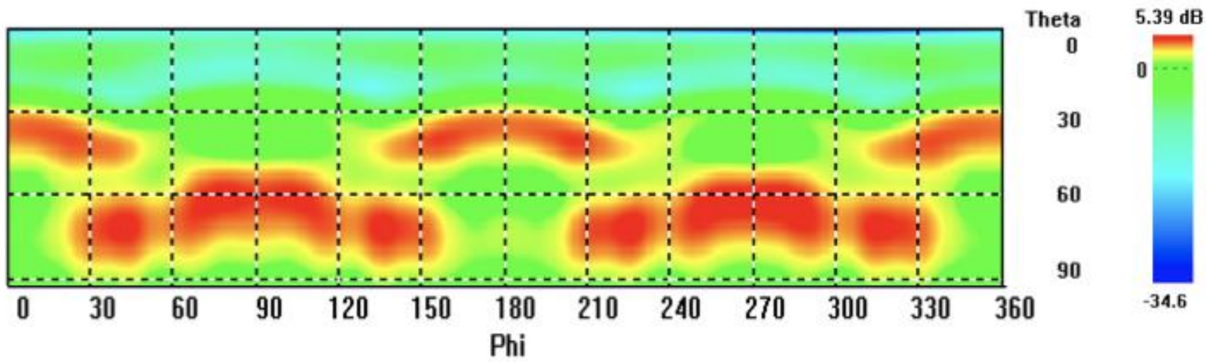

Figure I.2 Far-field performance of the 400 MHz antenna over the wider grooved surface.

GSM-R (900 MHz)

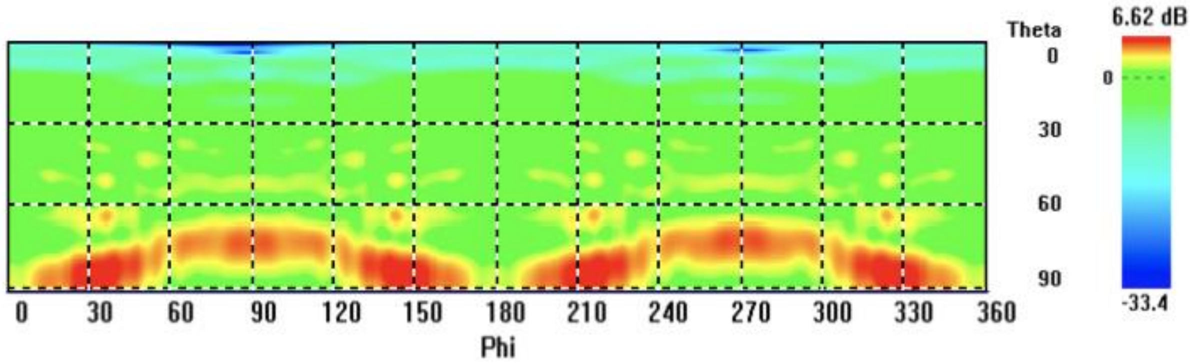

Figure I.3 Far-field performance of the 900 MHz antenna over the reference grooved surface.

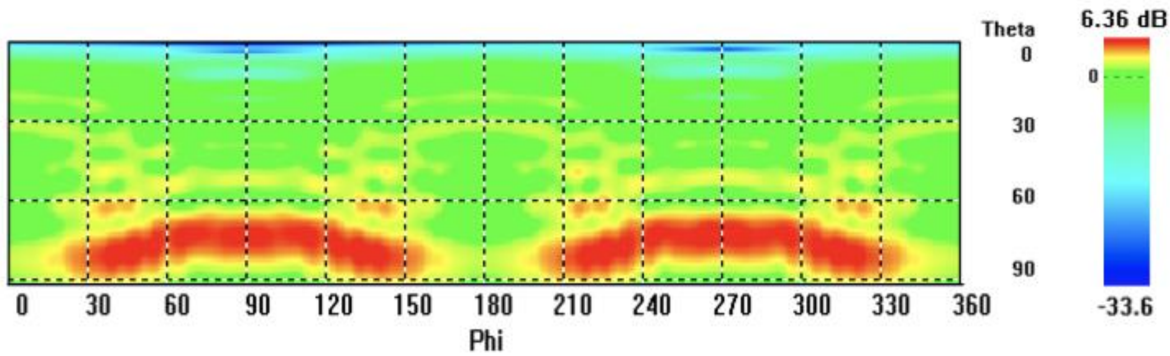

Figure I.4 Far-field performance of the 900 MHz antenna over the wider grooved surface.

LTE-R (2.6 GHz)

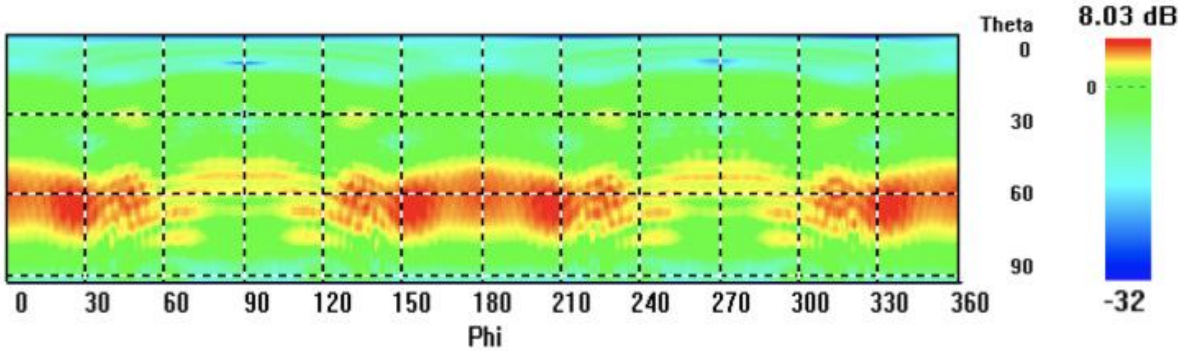

Figure I.5 Far-field performance of the 2.6 GHz antenna over the reference grooved surface.

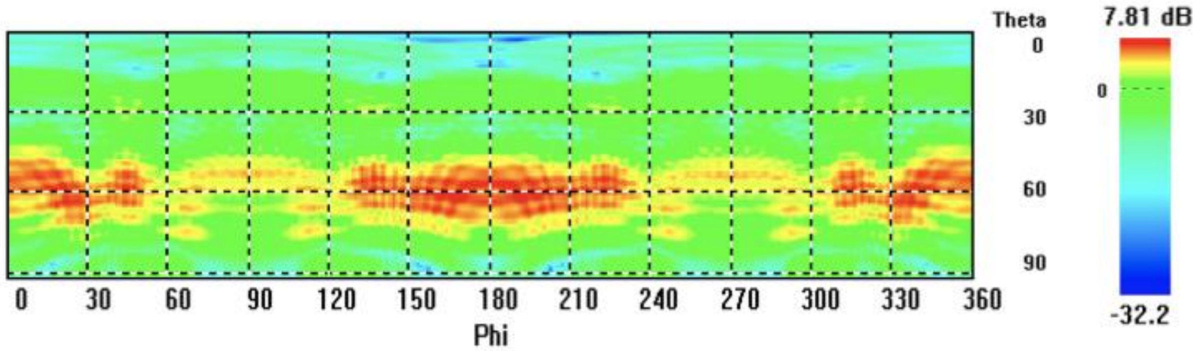

Figure I.6 Far-field performance of the 2.6 GHz antenna over the wider grooved surface.

BBRS (5.9 GHz)

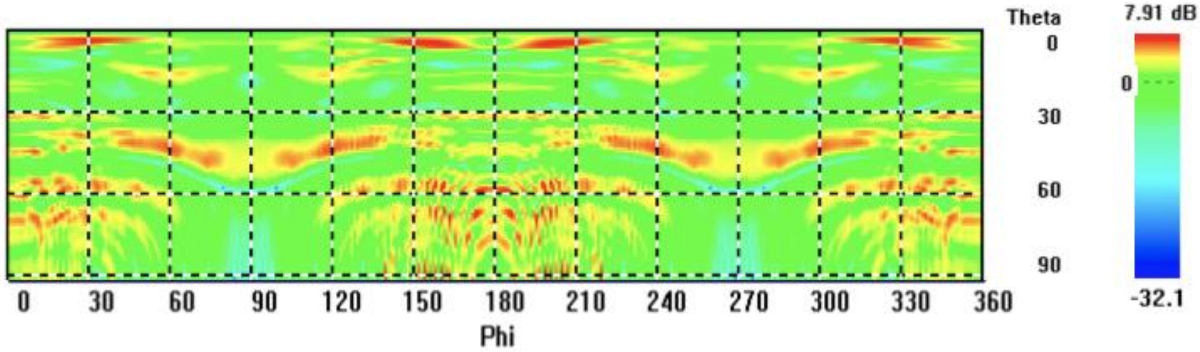

Figure I.7 Far-field performance of the 5.9 GHz antenna over the reference grooved surface.

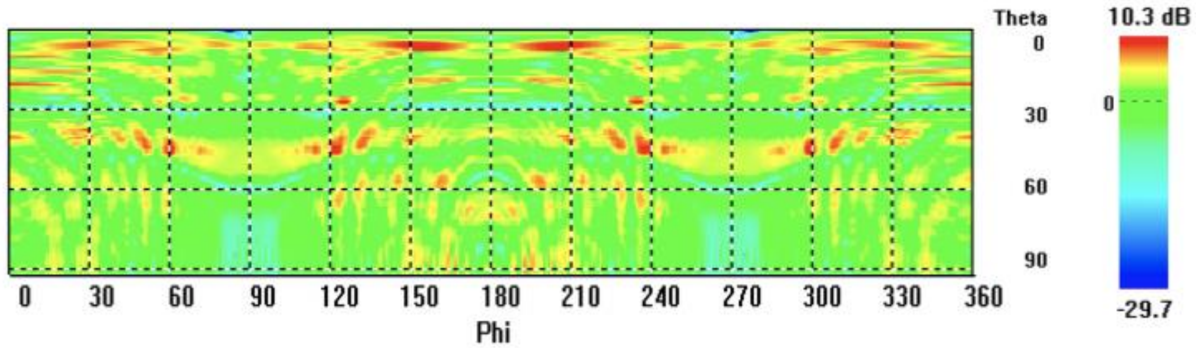

Figure I.8 Far-field performance of the 5.9 GHz antenna over the wider grooved surface.

Annex J

Influence of the antenna & ground plane height: 2D far-field results

Far-field views of the antennas for the four systems comparing the radiation patterns for the different 3D models: flat surface, straight grooved surface, curved grooved surface.

TETRA (400 MHz)

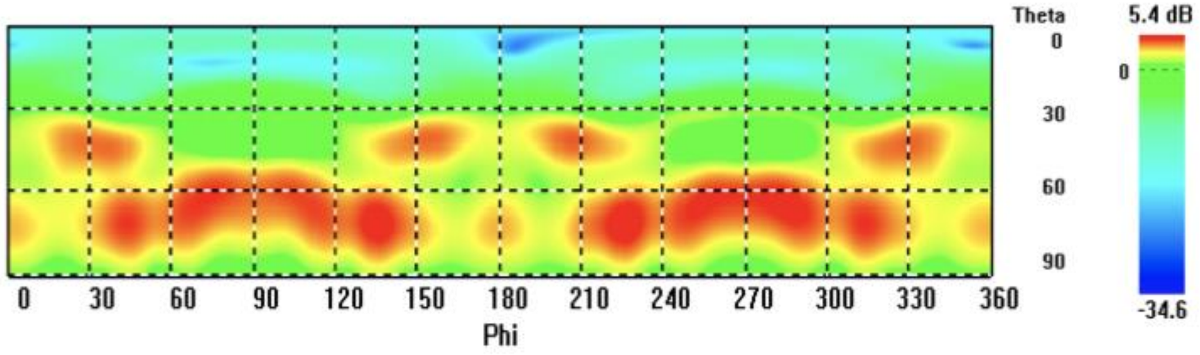

Figure J.1 Far-field performance of the 400 MHz antenna at h_p=1 cm.

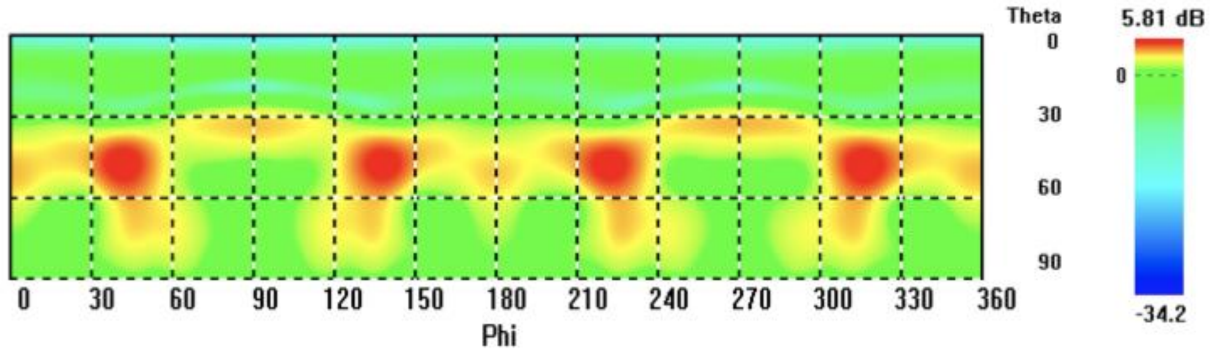

Figure J.2 Far-field performance of the 400 MHz antenna at h_p=10 cm.

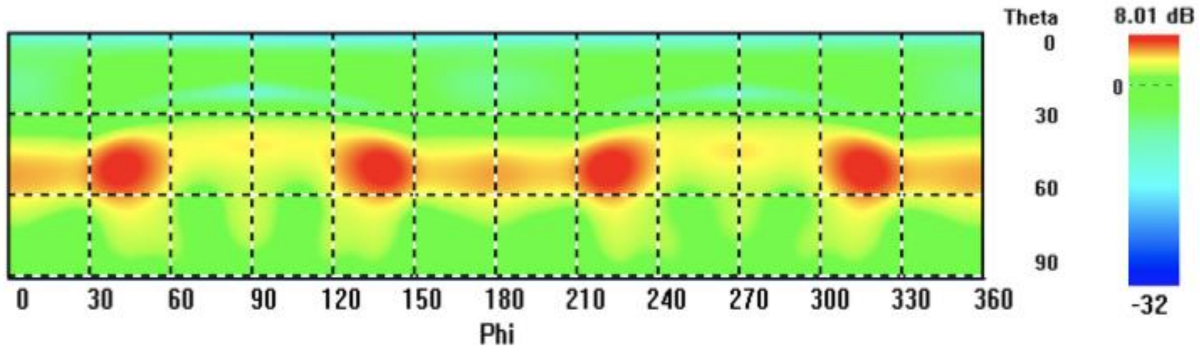

Figure J.3 Far-field performance of the 400 MHz antenna at h_p=20 cm.

GSM-R (900 MHz)

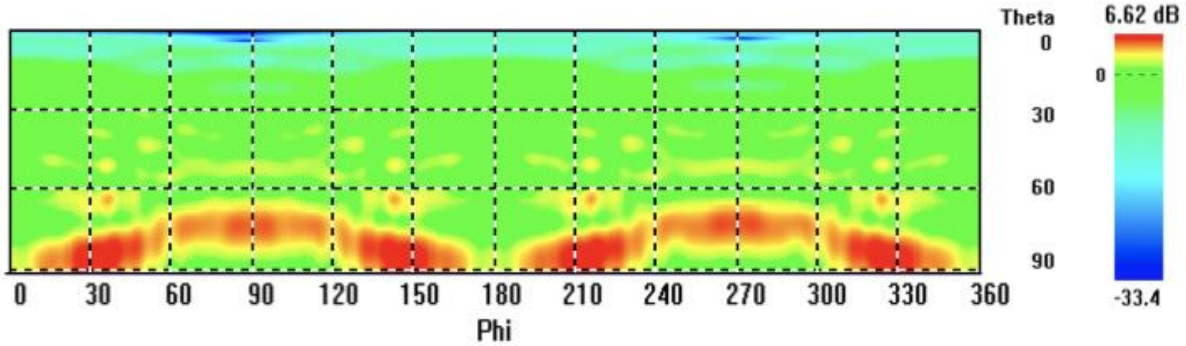

Figure J.4 Far-field performance of the 900 MHz antenna at h_p=1 cm.

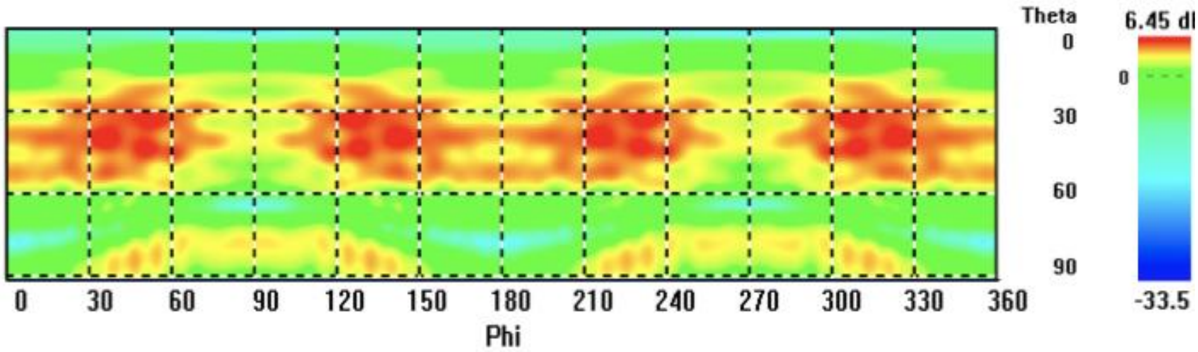

Figure J.5 Far-field performance of the 900 MHz antenna at h_p=10 cm.

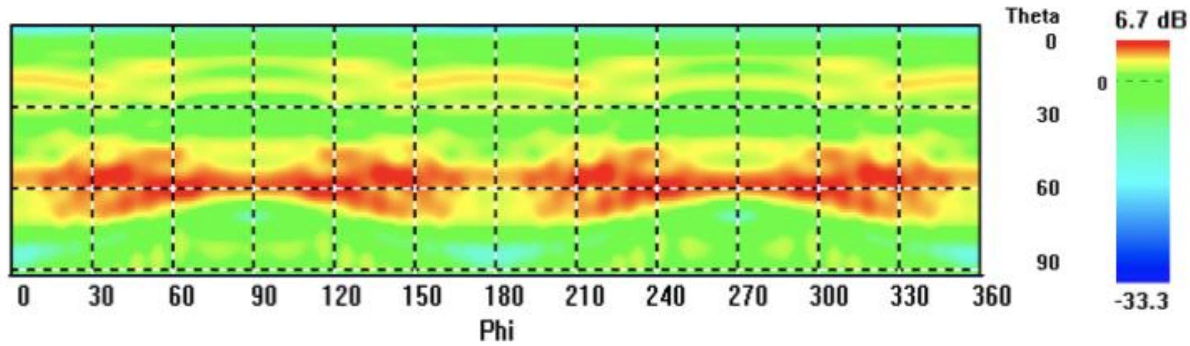

Figure J.6 Far-field performance of the 900 MHz antenna at h_p=20 cm.

LTE-R (2.6 GHz)

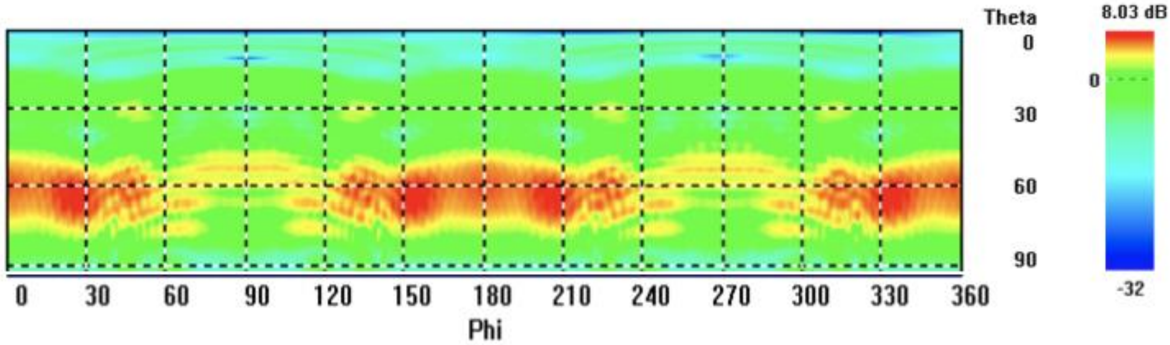

Figure J.7 Far-field performance of the 2.6 GHz antenna at h_p=1 cm.

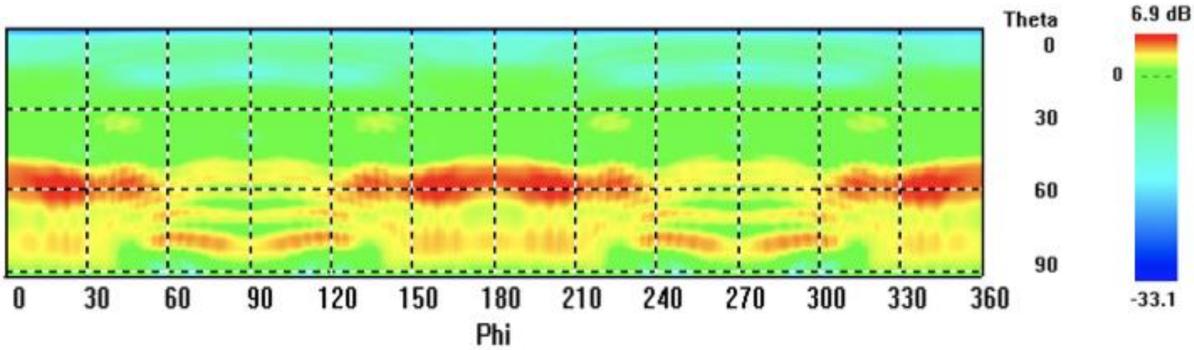

Figure J.8 Far-field performance of the 2.6 GHz antenna at h_p=10 cm.

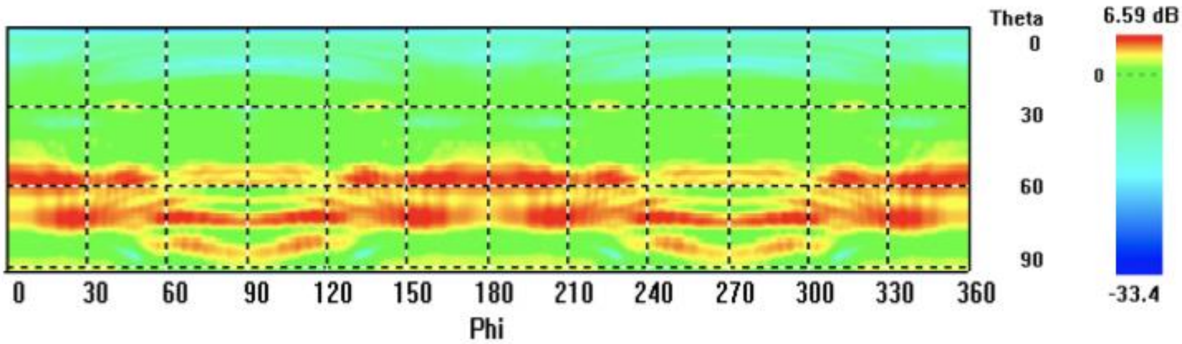

Figure J.9 Far-field performance of the 2.6 GHz antenna at h_p=20 cm.

BBRS (5.9 GHz)

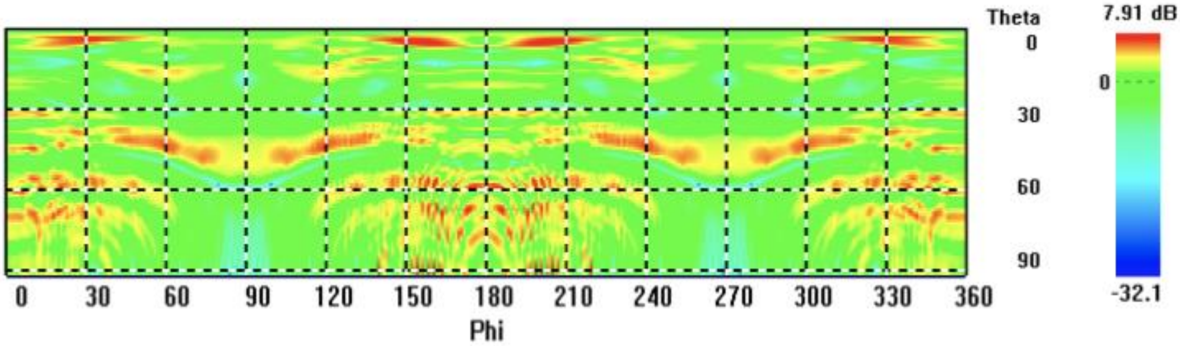

Figure J.10 Far-field performance of the 5.9 GHz antenna at h_p=1 cm.

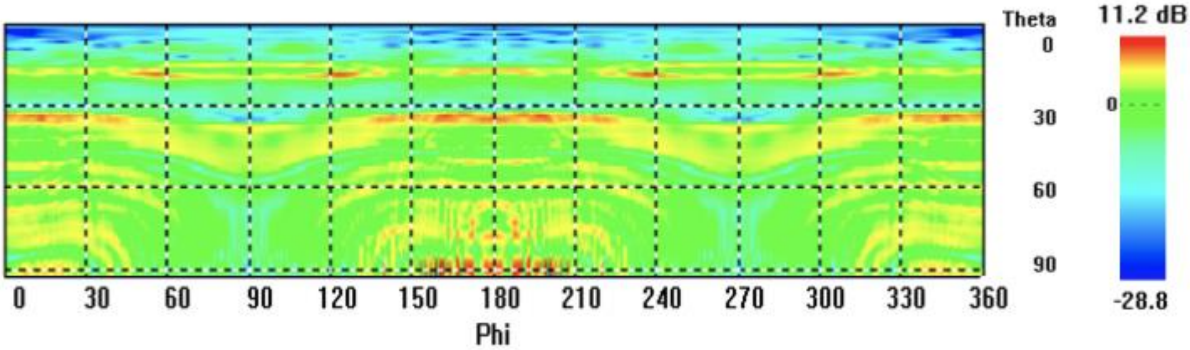

Figure J.11 Far-field performance of the 5.9 GHz antenna at h_p=10 cm.

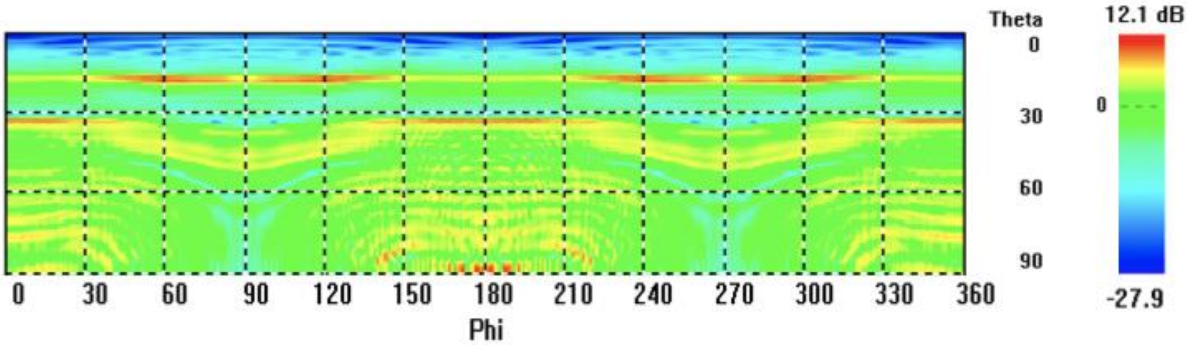

Figure J.12 Far-field performance of the 5.9 GHz antenna at h_p=20 cm.

References

[3GPP01] *Technical Specification Group Core Network - eMLPP,* 3rd Generation Partnership Project, Sophia, France, June 2001. [Online] Available in: (http://www.arib.or.jp/english/html/overview/doc/STD-T63v9_20/5_Appendix/R99/23/23067-330.pdf).

[3GPP15] *Release 12,* 3rd Generation Partnership Project, Sophia, France, March 2015. [Online] Available in: (http://www.3gpp.org/specifications/releases/68-release-12).

[3GPP17] *Release 14, LTE – Evolved Universal Terrrestrial Radio Access (E-UTRA) – User Equipment (UE) radio transmission and reception*, Report ETSI TS 36.101, V14.3.0, Release 2017, 3rd Generation Partnership Project, Sophia, France. [Online] Available in: (https://www.etsi.org/deliver/etsi_ts/136100_136199/136101/14.03.00_60/ts_136101v140300p.pdf).

[AARO18] *Frequency Usage Plan Germany*, Aaronia AG, Euscheid, Germany. [Online] Available in: (https://www.aaronia.com/basics/frequency-tables/frequency-usage-plan/) [Accessed in December 2018].

[AHZG12] B. Ai, R. He, Z. Zhong, K. Guan, B. Chen, P. Liu and Y. Li, "Radio Wave Propagation Scene Partitioning for High-Speed Rails", *International Journal of Antennas and Propagation*, Vol. 2012, September 2012. [Online] Available in: (https://www.hindawi.com/journals-/ijap/2012/815232/).

[ANAC18] *Spectrum Management – Frequencies of the Terrestrial Mobile Communications System* (in Portuguese), Autoridade Nacional de Comunicações, Lisboa, Portugal. [Online] Available in: (https://www.anacom.pt/render.jsp?categoryId=382989) [Accessed in December 2018].

[Anto18] *Installation instruction for train and bus antennas (outdoor)*, Technical Guide, Antonics-ICP GmbH, Velten, Germany. [Online] Available in: (https://www.antonics.com/fileadmin/antonics/img/Bilder/technische-Informationen/Installation_instruction_train_and_bus_antennas_EN.pdf) [Accessed in December 2018].

[Bala16] C. Balanis, *Antenna Theory – analysis and design*, 4th edition, John Wiley and Sons, New Jersey, United States of America, 2016.

[Corr18] L.M. Correia, *Mobile Communication Systems*, Slides, Instituto Superior Técnico, Lisboa, Portugal, 2018.

[CSTS19] *CST Studio Suite*, SIMULIA – Dassault Systèmes, Vélizy-Villacoublay, France. [Online] Available in: (https://www.cst.com/products/cstemcs) [Accessed in January 2019].

[Darl17] P. Darlington, *Train Antennas*, article, Rail Engineer UK, 2017. [Online] Available in: (https://www.railengineer.uk/2017/09/28/train-antennas/).

[Debe19] K. Debe, *What is Finite Integration Technique (FIT)?,* article, Microwaves101.com. [Online] Available in: (https://www.microwaves101.com/encyclopedias/finite-integration-technique) [Accessed in January 2019].

[DFHR13] V. Deniau, H. Fridhi, M. Heddebaut, J. Rioult, I. Adin, et al., *Analysis and Modelling of the EM Interferences produced above a Train associated with the contact between the catenary and the pantograph,* article, Université of Lille, Lille, France, 2013.

[DNXi08] A. Dutta, D. Norton and J. Xiao, *3GPP Long Term Evolution*, project, University of Colorado Boulder, Boulder, United States of America, August 2008. [Online] Available in: (http://ecee.colorado.edu/~ecen4242/LTE–/e_utran.html) [Accessed in November 2018].

[ECMT11] *White Paper on transport;* European Commission – Directorate-General for Mobility and Transport, Brussels, Belgium, March 2011. [Online] Available in: (https://ec.europa.eu/transport/sites/transport/files/themes/strategies/doc/2011_white_paper/white-paper-illustrated-brochure_en.pdf).

[ERTM18a] *ERTMS history*, Factsheet, Association of the European Rail Industry, UNIFE, Brussels, Belgium, September 2018. [Online] Available in: (http://www.ertms.net/wp-content/uploads/2018/10/8-UNISIG1.pdf).

[ERTM18b] *ERTMS levels*, Factsheet, Association of the European Rail Industry, UNIFE, Brussels, Belgium, September 2018. [Online] Available in: (http://www.ertms.net/wp-content/uploads/2018/10/3-ERTMS-Levels1.pdf).

[ETSI07] *Terrestrial Trunked Radio (TETRA) Release 2*, Technical Report, European Telecommunications Standards Institute, Sophia, France, October 2007. [Online] Available in: (https://www.etsi.org/deliver/etsi_tr/102500_102599/102580/01.01.01_60/tr_102580v010101p.pdf).

[ETSI96] *Digital Telecommunications Systems: Network architecture*, GSM Technical Specifications, European Telecommunications Standards Institute, Sophia, France, 1996. [Online] Available in: (https://www.etsi.org/deliver/etsi_gts/03/0302/05.01.00_60/gsmts_0302v050100p.pdf).

[ETSI97] *Terrestrial Trunked Radio (TETRA) Voice plus Data (V+D)*, Overview, technical description and radio aspects, European Telecommunications Standards Institute, Sophia, France, May 1997. [Online] Available in: (https://www.etsi.org/deliver/etsi_etr/300_399/30001/01_60/etr_30001e01p.pdf).

[Fern18] C. Fernandes, *Radio Wave Propagation – Scattering from Rough Ground* (in Portuguese), slides, Instituto Superior Técnico, Lisboa, Portugal, 2018.

[FFCa16] P. Fraga-Lamas, T. Fernández-Caramés and L. Castedo, "Towards the Internet of Smart Trains: A Review on Industrial IoT-Connected Railways" in *Sensors*, Vol.17, No. 6, October

2016. [Online] Available in: (https://www.ncbi.nlm.nih.gov/pmc/articles/PMC5492363/).

[GGBS09] D. Gerstenberger, F. Gunnarsson, J. Bergman, S. Strom, *Continued HSPA Evolution of mobile broadband*, Report, Ericsson AB, 2009. [Online] Available in: (https://www.ericsson.com/res/thecompany/docs/publications/ericsson_review/2009/issue1/hspa.pdf).

[GSMA17] *Global Mobile Trends 2017 Report,* GSMA Intelligence, September 2017. [Online] Available in: (https://www.gsma.com/globalmobiletrends/index.html).

[GSMR15a] GSM-R Operators Group, *Functional Requirements Specification Version 8.0.0,* European Integrated Railway Radio Enhanced Network, Paris, France, December 2015. [Online] Available in: (https://www.-cept.org/files/18286/SRS-16.0.0%20UIC%20951-0.0.2.pdf).

[GSMR15b] GSM-R Operators Group, *Functional Requirements Specification Version 16.0.0,* European Integrated Railway Radio Enhanced Network, Paris, France, December 2015. [Online] Available in: (https://www.cept.org/files/18286/SRS-16.0.0%20UIC%20951-0.0.2.pdf).

[GSMR18] GSM-R, Willtek Technologies. [Online] Available in: (https://web.archive.org/web/20140111232042/http://www.willtek.com/english/technologies/gsmr/) [Accessed in November 2018].

[HAWG16] R. He, B. Ai, G. Wang and K. Guan, “High-Speed Railway Communications: From GSM-R to LTE-R”, *IIEEE Vehicular Technology Magazine*, Vol. 11, No. 3, September 2016, pp. 49-58.

[HUAW15] *The Future of GSM-R, TETRA with LTE in the Railway Sector,* Huawei Technologies, Shenzhen, China, 2015. [Online] Available in: (https://e.huawei.com/uk/news/uk/2015/201512030948).

[HYTE18] What is TETRA and who uses it, Hytera Communications Co. Ltd. [Online] Available in: (https://hytera.co.uk/news/what-is-tetra-and-who-uses-it) [Accessed in December 2018].

[ITUT11] *About mobile technology and IMT-2000*, International Telecommunications Union, Geneva, Switzerland, 2011. [Online] Available in: (https://www.itu.int/osg/spu/imt-2000/technology.html).

[ITUT16] *Radio Regulations*, Articles, International Telecommunications Union, Geneva, Switzerland, 2016. [Online] Available in: (http://search.itu.int/history/HistoryDigitalCollectionDocLibrary/1.43.48.en.101.pdf).

[Kath02] *Installation Guidelines for Train and Bus Antennas*, Technical Guide, Version 1.0, Kathrein SE, Rosenheim, Germany, 2002. [Online] Available in: (http://www.kathrein.fr/media/installation_guide_for_train_antennas.pdf).

[Kath18a] *Train Antenna 870-960 MHz 741009*, Data Sheet, Version 1.0, Kathrein SE, Rosenheim, Germany, 2018. [Online] Available in: (https://www.kathrein.com/en/solutions/mobile-communication-/products/antennas-accessories/train-antennas/?tx_solr%5Bpage%-5D=1).

[Kath18b] *Train Antenna 1710-3800 MHz 87010010*, Data Sheet, Version 1.0, Kathrein SE, Rosenheim, Germany, 2018. [Online] Available in: (https://www.kathrein.com/en/solutions/mobile-communication-/products/antennas-accessories/train-antennas/?tx_-solr%5Bpage%5D=1).

[Kath18c] *Train Antenna 410-470 MHz K702021*, Data Sheet, Version 1.0, Kathrein SE, Rosenheim, Germany, 2018. [Online] Available in: (https://www.kathrein.com/en/solutions/mobile-communication-/products/antennas-accessories/train-antennas/?tx_solr%5Bpage%5-D=1).

[Kath18d] *Train Antenna 694-6000 MHz 87010022*, Data Sheet, Version 1.0, Kathrein Electronics, 2018. [Online] Available in: (https://www.kathrein.com/en/solutions/mobile-communication-/products/antennas-accessories/train-antennas/?tx_solr%5Bpage%5D=1).

[KiCh06] D. Kim, J. Choi, “Design of a Multiband Frequency Selective Surface”, *ETRI Journal*, Vol. 23, No. 4, 2006, pp. 506-508.

[Kraf17] C. Kraft, *The Digital Train Communication Network*, Article, Global Railway Review, 2017. [Online] Available in: (https://www.globalrailwayreview.com/article/34640/etcs-db-kommunikatio–nstechnik/).

[KRNA18] *The World’s First LTE-R for 250km/h High-Speed Railway in Republic of Korea*, Project Presentation, Korea Rail Network Authority, Daejeon, Korea, 2018. [Online] Available in: (https://www.itu.int/dms_pub/itu-r/oth/0a/0E/R0A0E0000C40001PDFE.pdf).

[Leit09] M. Leitão, *Mobile Communication Systems: TETRA – Terrestrial Trunked Radio System*, Technical Presentation, Faculdade de Engenharia da Universidade do Porto, Porto, Portugal 2009. [Online] Available in: (https://web.fe.up.pt/~mleitao/CMOV/Teoricas/CMOV_TETRA.pdf).

[LiRL05] S. Lim, R. L. Rogers, H. Ling, “Ground plane size reduction in monopole antennas for Ground Wave transmission” in *Antennas and Propagation Society International Symposium*, Washington, D.C., United States of America, July 2005. [Online] Available in: (https://www.researchgate.net/publication/4198932_Ground_plane_size_reduction_in_monopole_antennas_for_ground_wave_transmission).

[LTEM07] *Long Term Evolution (LTE): A Technical Overview*, Technical White Paper, Motorola Solutions Inc., Chicago, United States of America, 2007. [Online] Available in: (https://www.motorolasolutions.com/en_xu.–html?geo=redirect).

[Mich14] G. Michaildis, *Train-borne Antennas – A business case study*, M.Sc. Thesis, KTH Information and Communication Technology, Stockholm, Sweden, October 2014. [Online] Available at: (http://www.diva-portal.se/smash/get/diva2:862169/FULLTEXT01.pdf);

[MiKu15] M. Mir and S. Kumar, “Evolution of Mobile Wireless Technology from 0G to 5G”, *International Journal of Computer Science and Information Technologies*, Vol. 6, No. 3, 2015, pp. 2545-2551.

[MiZh00] L. Min and Z. Zhangdui, "Location dependent addressing using GSM-R cellular positioning" in the preceedings of *IEEE International Conference on Communication Technology*, Beijing, China, August 2000.

[MPAN15] *How Antennas Support Rail and Transit Safety*, White Paper, MP Antenna Limited, Ohio, United States of America, 2015. [Online] Available in: (http://www.mpantenna.com/transit-and-rail-wireless-communications-challenges-ptc/).

[MPAN17] *Bi-Directional 5GHz Antenna 08-ANT-0974*, Data Sheet, MP Antenna Limited, Ohio, United States of America, 2017. [Online] Available in: (http://www.mpantenna.com/downloads/08-ANT-0974_data.pdf).

[NKOM14] *National Frequency Plan*, Norwegian Communications Authority, Norway, 2014. [Online] Available in: (https://eng.nkom.no/technical/frequency-management/strategy-and-plan/national-frequency-plan).

[Nohr18] M. Nohrborg, *LTE*, Article, 3rd Generation Partnership Project, Sophia, France. [Online] Available in: (http://www.3gpp.org/technologies/keywords-acronyms/98-lte) [Accessed in December 2018].

[Nord13] T. Nordam, *Scattering of light from weakly rough surfaces*, Ph.D. thesis, Norwegian University of Science and Technology, Trondheim, Norway, 2013.

[Pool18] I. Poole, *LTE OFDM, OFDMA SC-FDMA & Modulation*, Radio-Electronics.com. [Online] Available in: (https://www.radio-electronics.com/info/cellulartelecomms/lte-long-term-evolution/lte-ofdm-ofdma-scfdma.php). [Accessed in November 2018]

[PRRB11] R. Parameswar, P. Rao, K. Ray, N. Balakrishnan, "Analysis of distributed conformal antennas on a moving platform", SAMEER – Centre for Electromagnetics, Indian Institute of Science, Bengaluru, India, 2011. [Online] Available in: (https://ieeexplore.ieee.org /stamp-/stamp.jsp?arnumber=6256843).

[PuWa09] S. Pu, J. Wang, "Research on the Receiving and Radiating Characteristics of Antennas on High-Speed Train Using Integrative Modelling Technique", Institute of Ligthwave Technology, Beijing Jiaotong University, Beijing, China, 2009. [Online] Available in: (https://ieeexplore.ieee.org/stamp/stamp.jsp?arnumber=5384374).

[Ribe18] A. Ribeiro, *Analysis of Antenna's Locations on Trains for Mobile Communications*, M.Sc. Thesis, Instituto Superior Técnico, Lisbon, Portugal, 2018.

[RuTa17] M. Rütschlin, D. Tallini, "Simulation for Antenna Design and Placement in Vehicles" in *Antennas, Propagation & RF Technology for Transport and Autonomous Platforms Conference*, Institution of Engineering and Technology, Birmingham, February 2017. [Online] Available in: (https://www.researchgate.net/search.Search.html?type=publication-&query=Simulation%20for%20antenna%20design%20and%20placement%20in%20vehic

les).

[Salk06] A. K. Salkintzis, "Evolving Public Safety Communication Systems by Integrating WLAN and TETRA networks", *IEEE Communications Magazine*, Vol. 44, Issue 1, January 2006, pp. 38 – 46.

[SDey11] S. Dey, *Five performance metrics for wireless device networking*, Article, Electronic Communication News, 2011. [Online] Available in: (https://www.ecnmag.com/article/2011/09/five-performance-metrics-wireless-device-networking).

[SEPU17] *A comparison of TETRA and GSM-R for railway communications*, White Paper, Sepura Systems GmbH, 2017. [Online]. Available in: (https://www.teltronic.es/wp content/uploads/2017/06/MKT-170418_eng_1.2_A-comparison-of-TETRA-and-GSM-R-for-railway-communication.pdf).

[SHum19] S. Hum, *Image Theory / Monopoles,* University of Toronto, Toronto, Canada. [Online] Available in: (http://www.waves.utoronto.ca/prof/svhum/ece422/notes/14-monopole.pdf) [Accessed in February 2019].

[SIMU19] *Antenna Magus – Antenna Design Software,* Dassault Systèmes Simulia, Paris, France. [Online] Available in: (https://www.3ds.com/products-services/simulia/products/antenna-magus/?utm_source=promotional&utm_medium=web&utm_content=cst&utm_campaign=cst-migration) [Accessed in February 2019].

[Sour13] J. Soure, *GSM-R system implementation in the Portuguese Railway Network - pilot* (in Portuguese), M.Sc. Thesis, Instituto Superior de Engenharia de Coimbra, Coimbra, Portugal, 2013. [Online] Available in: (https://comum.rcaap.pt/handle/10400.26/13547).

[TCCA18] *The TETRA standard*, The Critical Communications Association. [Online] Available in: (https://tcca.info/tetra/tetra-standard/) [Accessed in December 2018].

[TELC18] *5G technology introduction*, Telcoma. [Online] Available in: (https://telcomaglobal.com/blog/17780/5g-technology-introduction) [Accessed in December 2018].

[Teoh09] E. Teoh, *Train roof*, Malaysia, 2009. [Online] Available in: (https://www.flickr.com/photos/monkey-ed/4120777067).

[THAL18] *Broad Band Radio System (BBRS)*, Thales Group, Oeiras, Portugal, 2018.

[VoLo17] I. Volpi, L. Lochman, *The value in satisfying the passenger,* article, Global Railway Review, Community of European Railway and Infrastructure (CER), Brussels, Belgium, 2017. [Online] Available in: (https://www.globalrailwayreview.com/article–/61604/satisfying-passenger/).

[WeCY10] Y. F. Weng, S. W. Cheung and T. I. Yuk, "Effects of ground-plane size on planar UWB monopole antenna", in *TENCON 2010 conference*, Fukuoka, Japan, Nov 2010.

[Will09] D. Williams, *Train Roof Antenna Positioning Issue Study,* T739 Project, Rail Safety and Standards Board (RSSB), Siemens Mobility UK, United Kingdom, July 2009. [Online]

Available in: (https://www.rssb.co.uk/research-development-and-innovation/research-project-catalogue/t739).

[WILL18] GSM-R Global Standard Mobile Communications Rail, Willtek Technologies. [Online] Available in: (https://web.archive.org/web/20040923073451/http:/www.willtek.com:80/english/technologies/gsmr) [Accessed in November 2018].